DC Collection Systems for Offshore Wind Farms

Gayan Abeynayake

School of Engineering

A thesis submitted to the Cardiff University
in partial fulfillment of the requirements for the degree of
Doctor of Philosophy

October 2021

"If I had one hour to save the world, I would spend 55 minutes defining the problem and only five minutes finding the solution."

—Einstein, Albert

To my loving family and beloved teachers
Ammi, Appachchi, Aruni, and Lisari

Acknowledgements

I would like to express my sincere gratitude to my supervisors Prof Jun Liang and Dr Wenlong Ming for their guidance and support throughout the duration of my PhD studies. Especially, to Prof Jun Liang for allowing me the opportunity to be a part of the international InnoDC consortium and his guidance through my studies. Special thanks to Dr Gen Li for the time, pieces of advice and encouragement I received throughout my PhD journey. I would like to thank Dr Tom Van Acker for his time, and feedback provided during the later stage of my work.

In addition, I would like to acknowledge the financial support provided by the European Commission through the Marie Curie ITN InnoDC project, which gave me the opportunity to explore and develop my career with different training and dissemination activities. In particular, my special thanks to InnoDC colleagues for the interesting and useful discussions we shared during this project and also to our project manager, Ms Manon Davies for her patience in dealing with all our issues.

I would like to extend my gratitude and thankfulness to the members of the CIREGS research group of Cardiff University for their valuable advice and instructive discussions. Especially to Wei, Tibin, Muditha, Sathsara, and Davide for the laughter and the wonderful times we shared during the past years. A special note of thanks to Dr Tom Van Acker, for the fruitful discussions and interesting time we had during the remote collaboration, which eventually resulted in a journal publication.

I would like to thank my parents and family for their love, support and understanding throughout my candidacy. Specially, to my loving mother from whom I first heard the word 'Engineer' and taught me the right path from my early childhood. Although she is no more with us to see my success so far, I know her blessings are always with me. *"Ammi, hope I fulfilled your dreams and well above!".* The scarification of my father to make me a person where I am standing now is unimaginable.

This acknowledgement would not be completed without thanking my beloved wife Aruni Herath (*Attorney-at-law*) for her love, commitment, patience and understanding in what was a very challenging past few years dealing with our little one and taking care of me.

Abstract

Power generation through natural resources has found to be one of the best options to minimise climate change and global warming concerns. Among the naturally replenish sources, power generation from offshore wind accounts for a larger share. This has been showcased by the rapid development of offshore wind farms (OWF)s especial in the North sea. At the OWF collection system level, only alternating current (ac) technology is being used at present. Conversely, the use of direct current (dc) technology could provide additional benefits in terms of control flexibility, minimising system losses, and increasing power density of components. However, there are still a number of technical challenges that require addressing. One of the major aspects is the reliability of this concept as a whole.

The research work presented in this thesis is aimed to address the existing challenges, in particular, from the component level to the system level from the perspective of reliability. The main contributions of this research work comprise of four parts, namely, (1) reliability analysis of semiconductors of dc-wind turbine machine side converter, (2) propose a new selection guideline based on reliability and costs to identify the most suitable multi-level converter topology for offshore wind power dc collection systems at different voltage levels and power levels, (3) identification of the most suitable dc collection system topology in terms of reliability and other economic factors, and (4) development of an analytical methodology to asses the availability of offshore wind farms considering the cable network dependency.

One of the key building blocks of a dc collection system is the dc wind turbine (dcWT). The lifespan of a wind power system is highly influenced by the reliable operation of its power converter. A mission-profile based reliability assessment technique considering long-term and short-term thermal cycles are used to evaluate the lifetime of power electronic components of a dual active bridge based dcWT. Further, to ensure an effective lifetime evaluation of the entire converter system, a Monte Carlo method is used to generate the lifetime distributions and entire unreliability functions for power semiconductors.

To utilise the full capacity of the dc technology in the context of the OWF collection system, the selection of a suitable power electronic converter topology is a key aspect.

A selection criterion based on the optimal redundancy level with the consideration of the converter reliability, preventive maintenance interval, operational efficiency, the total cost of ownership and return on investment is proposed. The primary motivation of this work is to investigate the feasibility of utilising suitable multi-level voltage source converter topologies at different medium voltage dc levels and power levels.

To select a suitable dc collection system topology, a comprehensive analytical reliability evaluation method based on Universal Generating Function (UGF) is proposed with associated economic factors. This strategy combines the stochasticity of wind with multiple power output states of a single wind turbine (WT). Subsequently, the relationship between the output states and corresponding state probabilities of WTs are combined using the UGF technique considering the network structure. To identify the best topology, the investment- and operating- costs (which includes network losses) are incorporated.

The OWF collection system is made up of a considerable number of inter-array cables. The effectiveness of the OWF to export energy to the grid depends on the availability of that network. Therefore, it is imperative to include the reliability of the collection system in the overall availability assessment. However, this increases the number of components significantly, introducing the dimension curse. This combined with wind turbine output dependence makes the inclusion of the collection system in OWF availability assessment computationally intractable. An analytical reliability model based on the UGF technique is proposed accounting for the cable network dependency. Further, the impact of modelling wind farm components using a binary Markov model rather than a multi-state one is also investigated.

Contents

Acknowledgements ii

Abstract iii

List of Figures ix

List of Tables xii

Abbreviations and Symbols xiii

1 Introduction 1
- 1.1 Background . . . 1
- 1.2 Offshore Wind Farm Collection Systems . . . 3
- 1.3 The Requirement to Assess Reliability of Offshore Wind Farm Collection Systems . . . 5
- 1.4 Research Objectives . . . 5
- 1.5 Thesis Structure . . . 6

2 Literature Review 8
- 2.1 Introduction . . . 8
- 2.2 State-of-the-art Offshore Wind Turbine Technology . . . 8
  - 2.2.1 Control of a Full-scale Wind Turbine . . . 11
  - 2.2.2 Emerging Wind Turbine Technologies . . . 12
    - 2.2.2.1 Super Conducting Wind Generators . . . 13
    - 2.2.2.2 Multi-rotor Wind Turbines . . . 13
  - 2.2.3 DC Wind Turbine Technology . . . 15
    - 2.2.3.1 Candidate dc-Wind Turbine Topologies . . . 15
  - 2.2.4 Selection of a Suitable DC/DC Converter Topology for dc-Wind Turbine . . . 17
- 2.3 Offshore Wind Power Collection Systems . . . 19
  - 2.3.1 DC Collection System Options . . . 21
  - 2.3.2 Economies of scale of DC Collection System Concept . . . 24
  - 2.3.3 Technology Readiness Level of the DC Collection System Concept 25
- 2.4 State-of-the-art Reliability Evaluation Techniques . . . 27
- 2.5 Reliability Requirements of Offshore Wind DC Collection System Concept 29
  - 2.5.1 Reliability Estimation of Components . . . 30

2.5.2 Mission Profile based Reliability Assessment of Semiconductor Devices and Power Converters . . . 31
2.5.3 Component-Level Lifetime Assessment of dc-Wind Turbines . . . 32
2.5.4 Medium Voltage dc Converters and Reliability Requirements . . . 33
2.5.5 The Reliability of DC Collection System Configurations . . . 35
2.6 Overall Offshore Wind Farm Reliability Assessment including the Medium Voltage Cable Network . . . 36
2.6.1 Multi-State System Modelling of Offshore Wind Plants . . . 38
2.7 Summary . . . 39

3 Lifetime Estimation of dc-Wind Turbines 40
3.1 Introduction . . . 40
3.2 Methodology . . . 41
3.2.1 Long- and Short- term Thermal Cycles under a Mission Profile . . . 41
3.2.2 Reliability evaluation of semiconductors of a dcWT with long-term thermal cycles . . . 42
3.2.3 Control of a DAB based dcWT . . . 43
3.2.4 B_{10} Lifetime Estimation under Long-term Thermal Cycles . . . 44
3.2.5 B_{10} Lifetime Estimation under Short-term Thermal Cycles . . . 46
3.2.6 Assumptions made when estimating the lifetime . . . 47
3.3 Results . . . 47
3.3.1 Long-term thermal cycles . . . 48
3.3.2 Calculation of Accumulated Damage . . . 50
3.3.3 Variances in Parameters . . . 51
3.3.4 Impact of Switching Frequency . . . 53
3.4 Summary . . . 54

4 Selection of Multi-Level MVdc Converters for Offshore DC Collection Systems based on Reliability and Cost 55
4.1 Introduction . . . 55
4.2 Methodology . . . 57
4.2.1 Reliability of MVdc Converter Topologies . . . 57
4.2.1.1 Two-level and Three level-NPC . . . 57
4.2.1.2 Cascaded 3L-NPC . . . 58
4.2.1.3 MMC . . . 59
4.2.2 Reliability Modelling . . . 60
4.3 Availability and Maintenance Requirements of MVdc Converters . . . 62
4.3.1 VSC Availability and Redundancy Analysis with Different Maintenance Intervals for ± 27 kV . . . 63
4.4 Analysis of operational efficiency, total cost of ownership and return on investment . . . 67
4.4.1 Operational Efficiency . . . 67
4.4.2 Annual Energy Production . . . 69
4.4.3 Total Cost of Ownership (TCO) . . . 71
4.4.4 Return on Investment (ROI) . . . 72
4.5 Impact of Rated dc Voltage and Current on Topology Selection . . . 73
4.5.1 Impact of dc Voltage Level . . . 73

4.5.2 Impact of Rated Current . . . 75
4.6 Summary . . . 77

5 Selection of Offshore Wind Power DC Collection Systems based on Reliability and Economic Factors 78
5.1 Introduction . . . 78
5.2 Network Topologies for DC Collection Systems . . . 79
5.2.1 Radial-1 Topology (R-1) . . . 79
5.2.2 Radial-2 Topology (R-2) . . . 80
5.2.3 Radial-3 Topology (R-3) . . . 80
5.2.4 Series-Parallel Topology (SP) . . . 81
5.3 Methodology . . . 82
5.3.1 Clustering of Wind Turbine Power Output . . . 82
5.3.2 Reliability Modelling . . . 83
5.3.2.1 Failure Rate Calculation of dcWT . . . 83
5.3.2.2 The Universal Generating Function . . . 84
5.3.2.3 The UGF Model for Radial Topology . . . 85
5.3.2.4 The UGF Model for Series–Parallel Topology . . . 86
5.3.2.5 Reliability Indices . . . 87
5.3.3 Lifetime Cost Estimation . . . 88
5.3.3.1 Capital Investment . . . 88
5.3.3.2 Costs Associated with Energy Losses . . . 89
5.4 Case Study . . . 91
5.4.1 Obtaining Optimal Number of Wind Power Output Clusters and Other Parameters . . . 91
5.4.2 Reliability of DC Collection Systems . . . 94
5.4.3 Economic Evaluation of Candidate DC Collection Systems . . . 97
5.4.4 Overall Assessment of DC Collection System Options . . . 98
5.4.5 Impact of the DC Voltage Level for the Reliability of Series-Parallel Topology . . . 99
5.5 Summary . . . 100

6 Availability Assessment of Large-Scale Offshore Wind Farms including their Collector Systems 101
6.1 Introduction . . . 101
6.2 Methodology . . . 102
6.2.1 Mathematical Framework . . . 102
6.2.2 Time-Homogeneous Markov Process . . . 102
6.2.3 Stochastic Behaviour of Wind Farm Components . . . 103
6.2.3.1 Wind Turbine Output . . . 103
6.2.3.2 Wind Turbine Reliability . . . 104
6.2.3.3 Cable Section Reliability . . . 105
6.2.4 Universal Generating Function Strategy . . . 106
6.2.5 Reliability Indices . . . 109
6.3 Case Study . . . 109
6.3.1 Anholt Wind Farm . . . 110

6.3.2 Impact of Collector System Reliability . . . 112
6.3.3 Multi-State vs. Binary System Reliability . . . 114
6.4 Summary . . . 116

7 Conclusions **117**
7.1 Conclusions . . . 117
7.1.1 The Reliability of dc-Wind Turbine . . . 117
7.1.2 The Selection of a Suitable MVdc Converter Topology . . . 118
7.1.3 Topology Selection of Offshore Wind Power DC Collection Systems . . . 118
7.1.4 Impact of Cable Network Reliability on Availability Assessment of Offshore Wind Farms . . . 119
7.2 Thesis Contributions . . . 120
7.3 Future Work . . . 121
7.3.1 Identification of optimum preventive maintenance intervals of converters considering the wear-out phase failure of semiconductor devices . . . 121
7.3.2 Reliability of closed-loop radial topology . . . 121
7.3.3 Availability assessment of offshore wind farms under non-Markovian context . . . 122

List of Publications and Awards **123**

A Proof of UGFs for Radial Topologies **125**
A.1 Radial-1 Topology . . . 125
A.2 Radial-2 Topology . . . 126
A.3 Radial-3 Topology . . . 127

B Proofs of point of common coupling and feeder UGF **128**
B.1 Proof of UGF at the PCC . . . 128
B.2 Proof of feeder UGF . . . 129

Bibliography **130**

List of Figures

1.1 Global offshore wind development by 2020. 2
1.2 Typical layout of an offshore wind farm. 3
1.3 Wind turbines throughout the decades. 4

2.1 Different drive train configurations with different gearbox, generator and converter types. 9
2.2 Drivetrain choice for some large wind turbines, specified by speed and torque conversion, generator type and rating of power converter. 11
2.3 Control scheme of a PMSG based full-scale acWT. 12
2.4 Vestas multi-rotor wind turbine. 14
2.5 A typical block diagram of a dc-wind turbine 15
2.6 Different dcWT configurations: (a) active rectified based dcWT; (b) non-isolated dc/dc converter based dcWT; (c) ac transformer and passive rectifier based dcWT; (d) matrix converter, medium frequency transformer and passive rectifier based dcWT; (e) active rectifier and galvanic isolated dc/dc converter based dcWT; (f) boost converter between the active rectifier and galvanic isolated dc/dc converter based dcWT. 16
2.7 Different dc/dc converter configurations; (a) single active bridge, (b) dual active bridge. 17
2.8 Different OWPP collection system options: (a) MVac collection with HVac transmission; (b) MVac collection with HVdc transmission; (c) MVdc collection with HVdc transmission; (d) low frequency MVac collection and HVac transmission. 19
2.9 DC radial configuration-1. 22
2.10 DC radial configuration-2. 22
2.11 DC radial configuration-3. 23
2.12 DC radial configuration-4. 23
2.13 DC series-parallel configuration. 24
2.14 Reliability bathtub curve. 30
2.15 Timescale of mechanical and electrical components in a dc-wind turbine system. 32

3.1 The long- and short- term thermal cycles under a mission profile. 41
3.2 Dual active bridge based dc wind turbine system. 42
3.3 Control of a DAB based dc wind turbine. 43
3.4 Flowchart to calculate B_{10} lifetime of IGBT and diode under real-time wind speed and ambient temperature under long-term thermal cycles. . . 44

3.5 Flowchart to calculate B_{10} lifetime of IGBT and diode under real-time wind speed and ambient temperature under short-term thermal cycles. . . 46
3.6 Results of the long-term thermal cycle based lifetime estimation: (a) Wind speed and ambient temperature; (b) Turbine output power; (c) Total loss for IGBT; (d) Total loss for diode; (e) Junction temperature for IGBT and diode. 48
3.7 Rainflow counting results for IGBT. 49
3.8 Rainflow counting results for diode. 49
3.9 Normal PDFs for coefficients in Bayerer's lifetime model (a) A, (b) β_1, (c) β_2, (d) β_3. 51
3.10 Normal PDFs for thermal stress related parameters in Bayerer's lifetime model (a) mean junction temperature for IGBT, (b) junction temperature fluctuation for IGBT, (c) mean junction temperature for diode, (d) junction temperature fluctuation for diode. 52
3.11 (a) Annual damage Weibull distribution for IGBT; (b) lifetime Weibull distribution for IGBT; (c) unreliability for IGBT; (d) annual damage Weibull distribution for diode; (e) lifetime Weibull distribution for diode; (f) unreliability for diode. 53
3.12 Unreliability of semiconductors over different switching frequencies (a) IGBT; (b) diode. 54

4.1 Proposed medium voltage dc (MVdc) topology selection methodology. . . 56
4.2 Converter topologies and RBDs of 2L-VSC and 3L-NPC. (a) 2L-VSC; (b) 3L-NPC; (c) RBDs. 57
4.3 Cascaded 3L-NPC topology and corresponding RBD. 59
4.4 MMC topology and corresponding RBD. 60
4.5 Availability of ±27 kV VSCs over redundancy for $T_M = 0.5$. 64
4.6 Availability of ±27 kV VSCs over redundancy for $T_M = 1$. 65
4.7 Reliability of ±27 kV VSCs for $T_M = 0.5$ years. 66
4.8 Failure rates of (a) 2L-VSC; (b) 3L-NPC; (c) C3L-NPC; (d) MMC with different redundancy level for ±27 kV with $T_M = 0.5$ years. 67
4.9 VSC power losses for ±27 kV with different maintenance intervals and redundancy. 68
4.10 The efficiency of VSCs over different loading conditions for ±27 kV with $T_M = 0.5$ years. 69
4.11 Normalised and discretised 11-segment wind power duration curve of Anholt wind farm. 70
4.12 Variation of ROI with MVdc voltage level (at the rated current of 500 A). 75
4.13 Variation of ROI with the change of rated current at different MVdc voltage levels (a) 100 A; (b) 200 A; (c) 300 A; (d) 400 A; (e) 600 A; (f) 700 A; (g) 800 A; (h) 900 A; (i) 1000 A. 76
4.14 Variation of voltage crossover points with the change of rated currents. . . 77

5.1 Radial-1 topology. 79
5.2 Radial-2 topology. 80
5.3 Radial-3 topology. 81
5.4 SP topology. 81
5.5 State transition diagram of a wind turbine ith subsystem. 84

5.6 Current flow in a radial feeder. 89
5.7 Objective function value with the number of clusters for 10 MW wind turbine. 92
5.8 EENS for different dc collection system options. 94
5.9 GRA of candidate dc collection system options for the 10 MW WT case. . 95
5.10 GRA of candidate dc collection system options for the 8 MW WT case. . 96
5.11 GRA of candidate dc collection system options for the 5 MW WT case. . 96
5.12 GRA of different topologies with all dc/dc converters working perfectly. . 97
5.13 Cost of 12 dc collection system schemes. 97
5.14 Evaluation of 12 dc collection system schemes. 98
5.15 Variation of GRA with the terminal voltage level of SP topology. 100

6.1 Typical wind turbine power output curve and its discrete state space. . . 104
6.2 Multi-state Markov model of the wind turbine. 105
6.3 Multi-state Markov model of the cable section. 106
6.4 Wind farm with four wind turbines w_1-w_4 and cables c_1-c_4. 107
6.5 Inter array cable configuration of the Anholt offshore wind farm. 110
6.6 Expected energy not served for the Anholt wind farm in function of the number of wind speed clusters. 113
6.7 Generation ratio availability for the Anholt wind farm. The generation ratio criterion (GRc) at which the impact of the collector system and wind turbine reliability starts is indicated using * and **, respectively. . . 113
6.8 Probability distribution of the power delivered at the point of common coupling (PCC) for the scenario (a) incl. wind turbine reliability, and (b) the scenario incl. wind turbine and cable system reliability. Each dot represents the probability of the wind farm delivering a specific power at the PCC. All probabilities $p \leq 1e$-5 are omitted. 114
6.9 Difference of the probability distributions between the scenario incl. wind turbine and cable system reliability and the scenario incl. wind turbine reliability. Each dot represents the difference in probability between both scenarios of the wind farm delivering a specific power at the PCC. All probability differences $|\Delta p| \leq 1e$-5 are omitted. 115
6.10 Difference of the probability distributions between modeling the component reliability as a multi-state system and binary system for the scenario incl. wind turbine and cable system reliability. Each dot represents the difference in probability between reliability models of the wind farm delivering a specific power at the PCC. All probability differences $|\Delta p| \leq 1e$-8 are omitted. 116

List of Tables

2.1 Summary of largest offshore wind turbines currently available. 10
2.2 OWF collection system options: advantages and disadvantages. 20
2.3 Technology readiness levels of key technologies for offshore wind farm MVdc collection systems. 26

3.1 Parameters of the dc wind turbine. 42
3.2 Key parameters of thermal model. 45
3.3 Accumulated damage per year due to power cycling and thermal cycling. 51

4.1 System parameters and base failure rates. 63
4.2 Required min. number of components and base failure rates. 64
4.3 Redundancy level of VSCs with different maintenance intervals. 65
4.4 Discretised wind power output clusters and their duration per annum. . 70
4.5 Cumulative annual energy losses of each VSC (in MWh). 71
4.6 Total cost of ownership of VSCs (in £). 72
4.7 Return on investment of VSCs ($\pm$27 kV). 73
4.8 Level of redundancy required with the change of DC voltage. 74

5.1 Cost of dc-wind turbine (dcWT)s with different capacities. 88
5.2 Coefficients for the dc cables 89
5.3 Wind turbine nameplate data. 91
5.4 OWF collection system options: advantages and disadvantages. 92
5.5 Failure and repair rates of dcWT different sub-assemblies. 93
5.6 dc/dc converter parameters. 93
5.7 EENS of SP topology with different dcWT voltage. 99

6.1 Illustration of wind turbine output clustering for eight clusters including their centre and transition rates. 111
6.2 Reliability of wind turbine sub-assemblies. 111
6.3 Reliability of the cable system. 112

Abbreviations and Symbols

Abbreviations

2L-VSC	Two-Level Voltage Source Converter
3L-NPC	Three-Level Neutral Point Clamped Converter
acWT	ac-wind turbine
C3L-NPC	Cascaded Three-Level Neutral Point Clamped Converter
CAPEX	Capital Expenditure
DFIG	Doubly-fed Induction Generator
DAB	Dual Active Bridge
dcWT	dc-wind turbine
EENS	Expected Energy Not Served
GRA	Generation Ratio Availability
GRc	Generation Ratio Criterion
GHG	Greenhouse Gas
GSC	Grid-side Converter
HVac	High Voltage Alternating Current
HVdc	High Voltage Direct Current
HTS	High Temperature Superconducting
IGBT	Insulated-Gate Bipolar Transistor
LV	Low Voltage
MV	Medium Voltage
MCS	Monte Carlo simulation
MMC	Modular Multi-level Converter
MSS	Multi-State Systems
MSC	Machine-Side Converter

MVdc	Medium Voltage dc
MVac	Medium Voltage ac
OWF	Offshore Wind Farm
PCC	Point of Common Coupling
PMSG	Permanent Magnet Synchronous Generator
PWM	Pulse Width Modulation
SM	Sub Modules
SAB	Single Active Bridge
RE	Renewable Energy
RBD	Reliability Block Diagram
TRL	Technology Readiness Level
UGF	Universal Generating Function
UGO	Universal Generating Operator

Symbols

p	Probability
v	Performance
$\mathcal{C}$	Cable Set
e	Element
$\mathcal{E}$	Element Set
f	Failure
$\mathcal{F}$	Failure Set
s	State
$\mathcal{S}$	State Set
$\mathcal{S}^{\text{red}}$	Reduced State Set
u	User
$\mathcal{U}$	User Set
$\mathcal{W}$	Wind Turbine Set
ϕ	Feeder
Φ	Feeder Set
ω	UGF
Ω	UGO
f^{prb}	State Probability Function
f^{str}	Structure Function

Chapter 1

Introduction

1.1 Background

The global trend towards power generation through renewable energy (RE) sources have been increasing over the last few decades due to significant advantages over coal- and fossil fuel- based power plants. The use of fossil fuels to meet the global energy demand has major drawbacks such as contributing to global warming and depletion of resources over time. According to [1], the use of coal for energy production in the global energy mix is set to decline by almost 7800 TWh between 2020 and 2040 under the sustainable development scenario.

In the context of Europe, by 2030 it is expected to produce at least 32% of total energy consumption from renewable energy and 40% cut in greenhouse gas emissions compared with 1990 [2]. In this regard, a portfolio of options is being explored to underline that it is possible to move to "net-zero" greenhouse gas (GHG) emissions by 2050, based on existing – though in some cases emerging – technological solutions. For this transition, empowering citizens and aligning action in key areas such as industrial policy, finance or research, while ensuring social fairness are essential. Further, the UK is the first major economy in the world to pass laws to end its contribution to global warming by 2050 [3, 4, 5]. Doing so would make the UK a net-zero emitter and the falling costs of key renewable technologies over fossil fuels will bolster this further.

As discussed above, concerns over global warming with GHG emissions have given rise to the promotion of RE solutions such as wind, solar PV, small hydro, biomass, geothermal, wave and tidal power. Additionally, to meet these ambitious policy goals, the significant contributions from onshore and offshore wind will be commendable [6]. For example, by end of 2019, the regional wind power production capacity was distributed as follows: 1.6

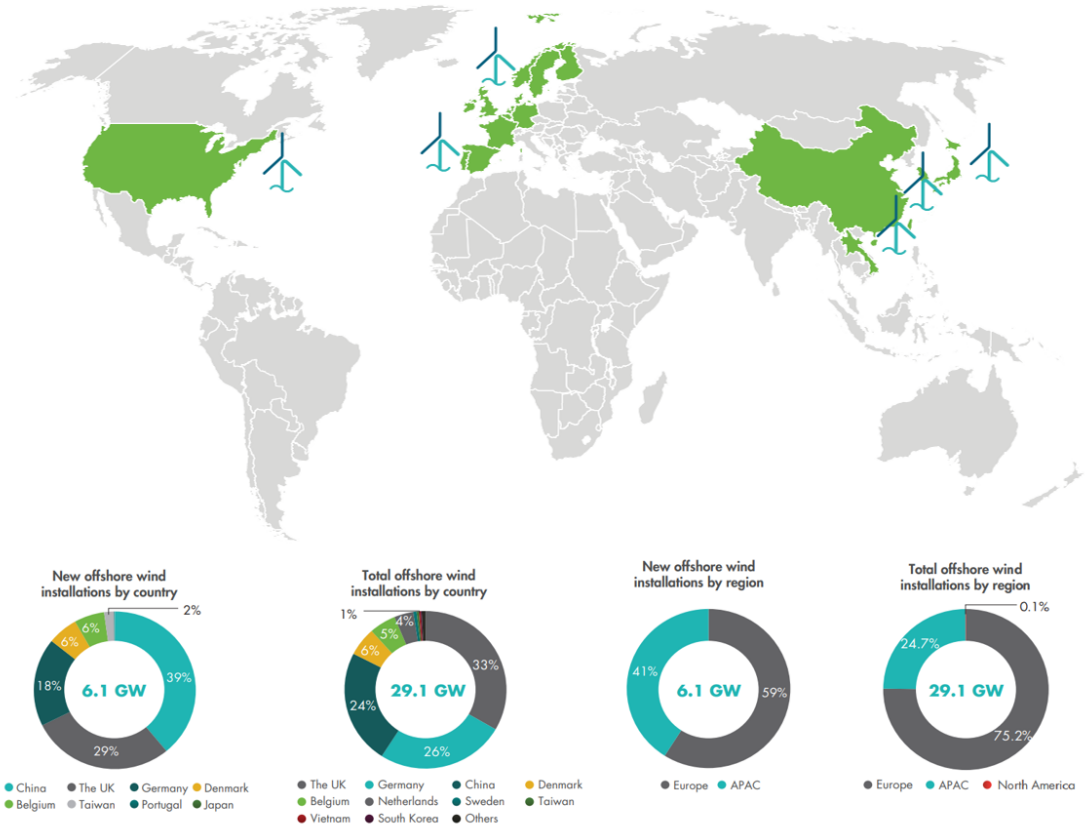

Fig. 1.1. Global offshore wind development by 2020.
Source: [6]

GW Europe; 284.1 GW Asia-Pacific; 105.4 GW North America; 42.7 GW Latin America; 6.7 GW Africa and Middle East regions [7]. The cumulative capacity of global total wind turbine (WT) installations was increased by 4.5% by the end of 2019 compared to 2018. These figures are forecasted to rise in the future with the advancement of wind power technology, incentives from governments and reduction in capital investment per MW.

Offshore wind technology provides added benefits such as higher energy yield and lesser public disturbance over its counterpart onshore wind technology. From being 1% of global wind installations by capacity in 2009, offshore wind has grown to over 10% in 2019. As of 2020, the total globally installed offshore wind capacity is 29.1 GW and more than 75% is concentrated in Europe [6]. At present, Europe is the leader in offshore wind farm (OWF) development. The European Commission estimates that total offshore wind installations between 240 and 450 GW will be needed by 2050, making offshore wind a crucial pillar in Europe's power mix. Following the sharp drop of the levelised cost of energy (LCOE) and the speeding-up of the global energy transition, the investment for offshore wind has become very positive. With a compound annual growth rate of 19.5%, more than 50 GW offshore is likely to be built in the next five years.

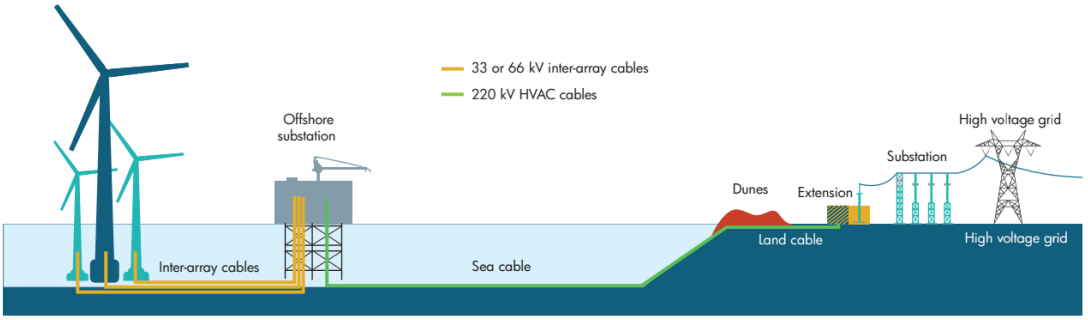

Fig. 1.2. Typical layout of an offshore wind farm.
Source: [6]

Ramping up offshore wind development is essential to accelerate the energy transition towards renewable energy sources. By end of 2020, the UK is the world leader in OWF development and export hub with a share of 33% by total installations globally. From its first 4 MW pilot project in Blyth in 2000, to 10.5 GW of installed capacity today, the progress of the UK's offshore wind is phenomenal [8]. Some major projects such as Walney Extension, London Array, Norfolk Vanguard and Norfolk Boreas are notable [9].

Among the transmission options available for bulk power transfer, both the high voltage alternating current (HVac) and high voltage direct current (HVdc) technologies are being used to export offshore wind energy to the onshore grid. However, with the increasing distances to the mainland grid, it is always beneficial to use HVdc technology over its counterpart HVac technology. The 400 MW BorWin1 project (located 125 km off the-shore) is one of the first large scale OWFs that used voltage source converter (VSC) HVdc technology. A typical layout of an OWF is shown in Fig. 1.2. Although at the transmission level both these technologies are used, at the collection system level only medium voltage ac (MVac) technology is being used to date.

1.2 Offshore Wind Farm Collection Systems

The selection of a pertinent network structure is one of the important preliminary studies performed at the early stage of an OWF development. Different offshore wind alternating current (ac) collection system topologies have been well analysed in the literature to obtain the optimised configuration with the consideration of system losses and associated life cycle costs [11, 12, 13]. In [14], it has been shown that closed-loop network configuration (i.e., ring configuration) is economically viable than the typical radial OWF collection system configuration. However, due to concerns such as (a) additional control complexity, and (b) the requirement to over-rate some cable sections (which incurs

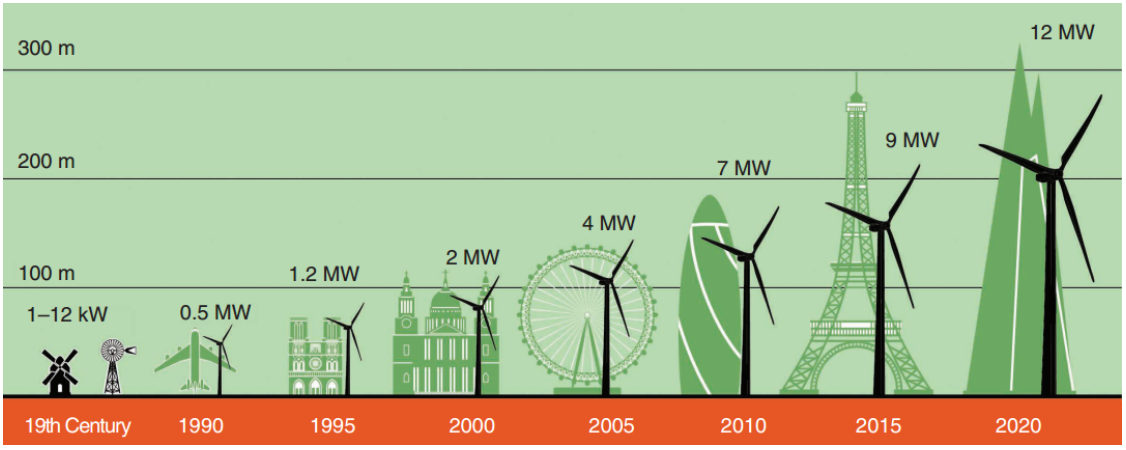

Fig. 1.3. Wind turbines throughout the decades.
Source: [10]

additional investment), the radial topology has only been deployed in commercially operating OWFs at present. One of the main advantages of radial topology is its control and operational flexibility. However, the main drawback of the radial connection is, upon failure of an upstream cable connection of the network, all the healthy WTs are required to be forced shutdown. With the uncertainties associated with severe weather conditions prevail in the offshore environment, component repair times could be much longer than anticipated.

On the other hand, with the increasing capacity of a single WT unit, more energy can be extracted with a fewer units as shown in Fig. 1.3. However, electrical losses also increase proportionately. In this regard, the use of direct current (dc) technology at the collection system level will help minimise network losses. Different dc collection system topologies have been proposed in the literature such as different variants of radial topology, dc-series and series-parallel structures [15, 16, 17]. Topologies such as series and series-parallel topologies do not require an intermediate collection system platform. This leads to lower capital investment over topologies that utilise intermediate collection platforms.

Unlike ac technology, dc technology does not require bulky power frequency transformers. This helps to increase the power density of intermediate collection platforms in dc collection system topologies. Further, the use of a pure dc system will eliminate the reactive power compensation issue which always encounters with long-distance ac transmission. In theory, MVdc grids could be the best technical solution for the integration of renewable energy resources in distribution networks, as they have the benefits of higher efficiency and increase power transfer capability, while offering lower size and weight [18].

1.3 The Requirement to Assess Reliability of Offshore Wind Farm Collection Systems

Although the OWFs yield higher energy, operational and maintenance costs are much higher than that of the onshore counterpart due to the poor accessibility with harsh marine weather conditions. In such environments, the reliability of all components is very much important to maintain higher availability levels. Thus, the investigation of reliabilities at the component level to the system level is important.

Various studies have been conducted on the reliability evaluation of ac collection systems in the open literature. In [19], a multi-objective optimisation model based on the redundancy of the power collector system has been used to evaluate several ac collection system options. However, the main objective of this study was to identify the optimal redundant structure and a detailed availability analysis considering the stochastic behaviour of components has not been considered. A Genetic algorithm-based optimisation technique is used in [20] to evaluate the investment cost and reliability of different ac collection system topologies. It has demonstrated that the number of collection system platforms and their geographical locations influence the overall system reliability. The results show that the ring-type collection system with a single collection system platform is more reliable than a radial configuration with two intermediate collection system platforms.

In [21], an efficient methodology based on the genetic algorithm and minimum spanning tree has been used to identify the optimal OWF grid layout to minimise the total cost which is a sum of construction, power losses, maintenance, and costs of reliability. However, all the above studies have only been focused on identifying the optimal ac collection system configuration and very few works have been conducted on reliability assessment of dc collection system configurations and their associated components.

1.4 Research Objectives

This thesis focuses on analysing and evaluating the reliability requirements of emerging MVdc technology applied to large-scale offshore wind farms from the component level to the collection system level. The main research objectives of this work include:

- To investigate the lifetime and annual damage of power semiconductors of permanent magnet synchronous generators (PMSG) based dcWT using mission profile and physics-of-failure based analysis.

- To develop a methodology to identify the optimal converter topology at different MVdc voltage levels and power levels based on reliability and other functional factors.
- To develop an analytical reliability model including associated economic factors and to identify the suitable MVdc collection system topology.
- To investigate the impact of the inclusion of inter-array cable network reliability in the availability assessment of large-scale offshore wind farms irrespective of their lower failure rates.
- To develop an analytical reliability model considering the network dependency and component sub-systems to assess the availability of offshore wind farms.

1.5 Thesis Structure

Chapter 2 – *Literature Review*

In this chapter, the state-of-the-art offshore wind farm technology is overviewed. The emerging challenges with the increasing capacity of single WT are discussed. Different candidate dc collection systems are summarised and critically reviewed. The existing research on analysing the reliability of power electronic converters and their applicability in MVdc converter selection is presented. In the offshore wind farm availability assessment, the existing research gaps in combining the multiple system states of individual component sub-systems and incorporating network dependency into a single stochastic process are described.

Chapter 3 – *Lifetime Estimation of dc-Wind Turbines*

In this chapter, the failure rate and annual consumed damage of power semiconductors of a dual active bridge based dcWT are investigated. Annual damages and power cycles of semiconductors are calculated separately under long-term and short-term thermal cycles. To ensure an effective lifetime evaluation of the entire converter system, a Monte Carlo method is used to generate the lifetime distributions and entire unreliability functions for power semiconductors.

Chapter 4 – *Reliability and Cost-Oriented Analysis, Comparison and Selection of Multi-Level MVdc Converters*

In this chapter, a selection guideline based on reliability and optimum redundancy levels of VSCs combined with other functional factors such as operational efficiency and return-on-investment is proposed to select the suitable converter topology at different MVdc levels and power levels of offshore dc collection systems.

Chapter 5 – *Reliability and Economic Assessment of Offshore Wind Power DC Collection Systems*

In this chapter, different candidate dc collection systems have been evaluated in terms of reliability together with associated economic factors. The analytical reliability evaluation technique called universal generating function (UGF) has been used to represent different collection system options mathematically. Then, the analyses have been performed with different dcWT capacities for four different collection system options to identify the most reliable and economic option.

Chapter 6 – *Availability Assessment of Large-Scale Offshore Wind Farms including their Collector Systems*

In this chapter, a holistic approach combining multi-state Markov processes and the universal generating function for the availability assessment of radial large-scale offshore wind farms is proposed. The proposed model combines multi-state wind turbine output, wind turbine reliability, and inter-array cable reliability models to assess the wind farm output at the point of common coupling. A strategy is developed to split the network into its feeders while still accounting for the wind turbine output dependence, significantly reducing the computational burden.

Chapter 7 – *Conclusions*

This chapter summarises the major findings and contributions of this thesis. The future scope of work that requires elevating the dc collection system concept to the next technology readiness level is discussed.

Chapter 2

Literature Review

2.1 Introduction

In this thesis, the reliability of emerging dc collection system concept is investigated from the power electronic component level to the offshore wind farm collection system level. Different probabilistic methods are introduced, which are pertinent to solve specific problems identified in this thesis. Previous work on this technology choice has focused on how different technologies influence capital costs and efficiency; however, many arguments are based on their reliability and the impact of availability and operational and maintenance costs.

In this chapter, first, an overview of the state-of-the-art offshore wind farm technology is discussed. Then, different candidate dc-wind turbine concepts and dc collection system configurations have been discussed with their advantages and disadvantages. Next, the technology readiness level of key components have been summarised. This is followed by reviewing different reliability evaluation methods pertinent for solving different problems discussed in this thesis. Finally, the lifetime estimation of wind turbine power converter semiconductors, reliability assessment of power electronic converters, and availability assessment of OWF collection systems are described and discussed.

2.2 State-of-the-art Offshore Wind Turbine Technology

Among different WT technologies available, horizontal axis with geared high-speed doubly-fed induction generators (DFIG), medium-speed geared PMSG and low-speed direct-drive PMSG are the three main WT configurations utilised by offshore wind industry at

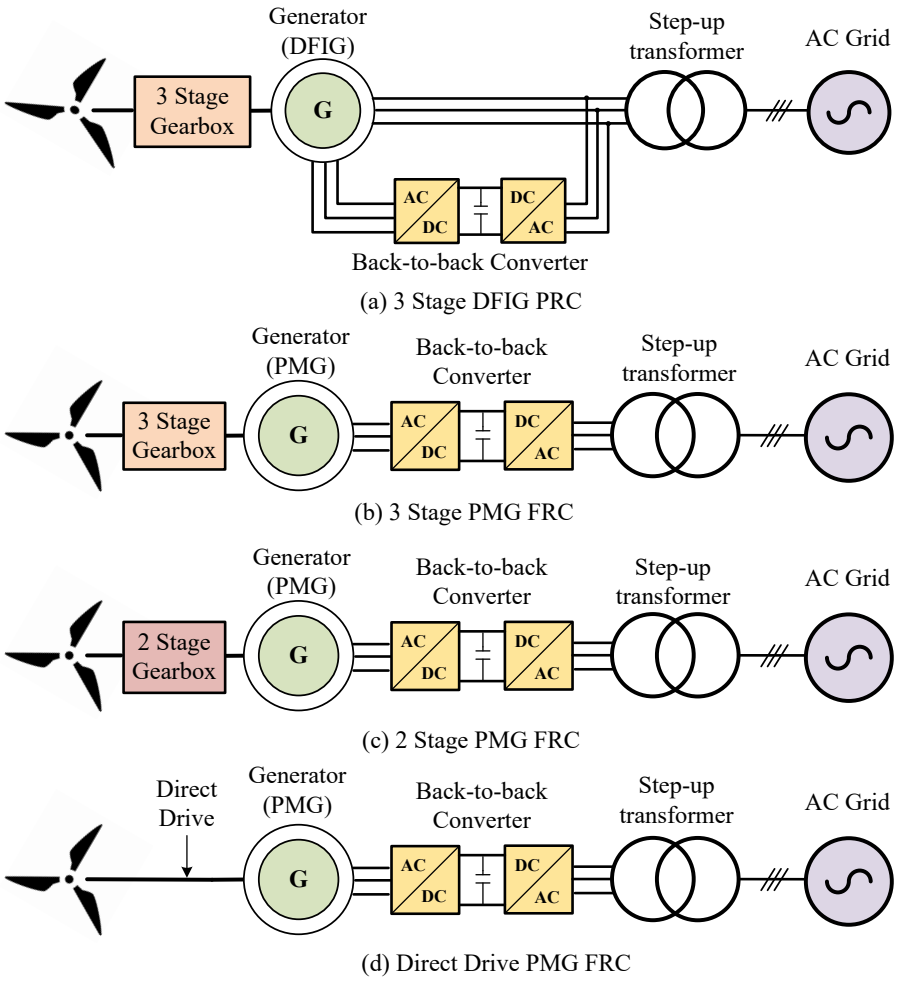

Fig. 2.1. Different drive train configurations with different gearbox, generator and converter types.

present [22]. Fig. 2.1 illustrates different drive train configurations with different gearbox, generator and converter types of these WT models. They can be mainly identified as:

(a) *The DFIG Configuration* (Type-3)
This needs a gearbox, generator, and a partially-rated converter (PRC) (around 30%). The gearbox couples the blades with the generator, increasing the rotational speed from the rotor hub to the induction machine. The stator is directly connected to the grid, whereas the rotor is connected to the power converter. As a result, the converter only covers the power produced by the rotor of the DFIG [23].

(b) *The PMSG Full-power Converter Configuration* (Type-4)
This PMSG fully-rated converter (FRC) WT is excited by an external dc source or by permanent magnets. In this case, the whole generator is connected to the grid through a power converter. Hence, all the generated power from the WT can

Table 2.1. Summary of largest offshore wind turbines currently available.

Rated Power (MW)	**Manufacturer**	**Model**	**Drive Train Type**	**Diameter (m)**
8.0	Siemens Gamesa	SG 8.0-167 DD	DD	167
8.3		V164-8.3 MW	G	164
8.8		V164-8.8 MW	G	164
9.0	MHI Vestas Offshore	V164-9.0 MW	G	164
9.5		V164-9.5 MW	G	164
10.0		V164-10.0MW	G	164
		YZ150/10.0	DD	150
10.0	Swiss Electric	YZ170/10.0	DD	170
		YZ190/10.0	DD	190
10.0	Siemens Gamesa	SG 10.0-193 DD	DD	193
12.0		GE HALIADE-X	DD	220
13.0	General Electric	GE HALIADE-X 13 MW	DD	220
14.0		GE HALIADE-X 14 MW	DD	220
15.0	Vestas Offshore	V236-15.0 MW	G	236

G - Gearbox, DD - Direct Drive

be regulated accordingly. They have low maintenance costs and negligible rotor losses [24]. Moreover, some of the PMSG full-power converter models do not have a gearbox, as depicted in Fig. 2.1(d). This configuration uses a direct drive multipole generator.

As shown in Fig. 2.1, the WTs which utilise gearbox to transmit extracted energy from wind has either 2- or 3- conversion stages. For instance, Fig. 2.1(a) shows a 3 stage DFIG with a PRC. However, majority of offshore WTs are constructed with variable speed PMSG with FRC due to benefits such as compact in size, no requirement of external power supply for magnetic field excitation, robust construction, and less maintenance compared to classical asynchronous wind generators. Historically, failures of gearboxes have been reducing the reliability of offshore WTs, and there has been a trend in the industry towards omitting the gearbox by introducing direct drive technologies based on copper field windings or permanent magnets [25].

Table. 2.1 summarise largest offshore WTs currently available in the market. Notably, *Vestas* announced a 15 MW variable speed full-scale offshore WT (V236-15.0 MW) in February 2021. At present, this is the largest single capacity WT expected to be installed in 2022, while the serial production is scheduled for 2024 [26]. Further, the *GE* 14 MW Haliade-X; an upscaled version of the 13 MW unit which will be installed at the third phase of the Dogger Bank offshore wind project (130 km off the North East coast

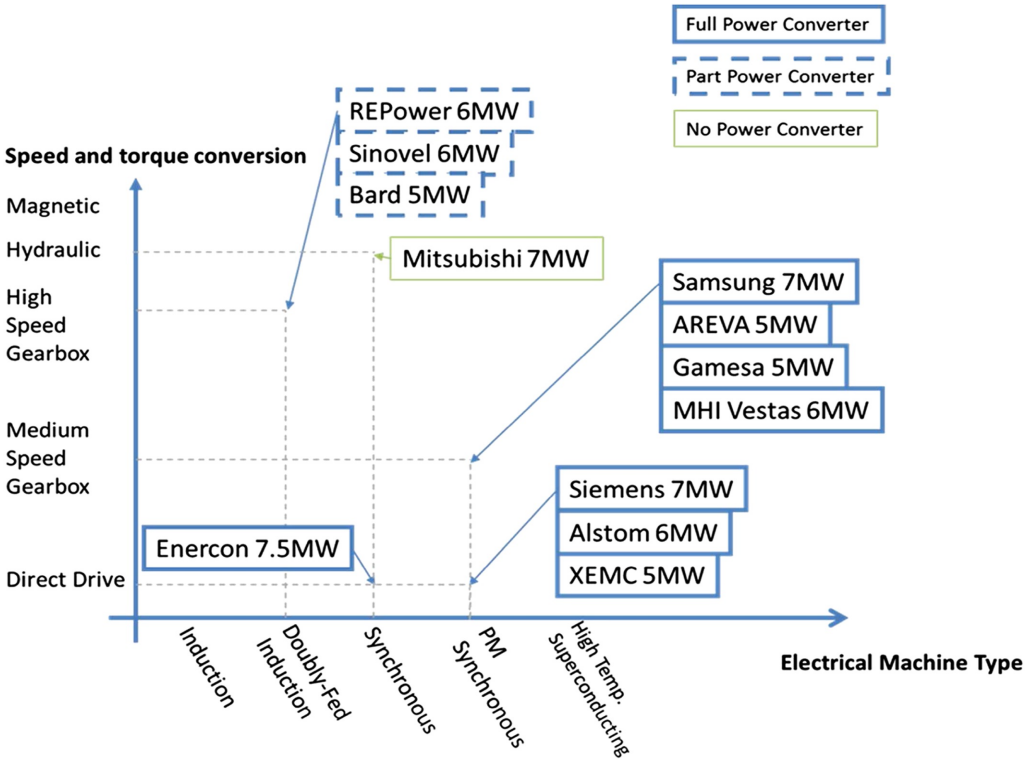

Fig. 2.2. Drivetrain choice for some large wind turbines, specified by speed and torque conversion, generator type and rating of power converter.
Source: [28]

of England) is considered to be the largest offshore WT which has secured a supplier contract at present [27].

Fig. 2.2 illustrates a variety of drive train technologies for some large offshore WTs, specified by (a) speed and torque conversion, (b) generator type, and (c) power converter rating. Notably, the WT technology which is based on full power converter, i.e. Type-4 uses direct drive or medium speed gearbox for speed and torque conversion.

2.2.1 Control of a Full-scale Wind Turbine

In a conventional variable speed full-scale offshore WT, the generator output is connected through a back-to-back (ac/dc/ac) converter, with a constant frequency and voltage. At the collection system level, the WT output voltage increases up to 33 kVac or 66 kVac using a step-up transformer. The control schematic of a typical grid connected PMSG based full-scale acWT is shown in Fig. 2.3.

There are three different control objectives of a full-scale wind turbine:

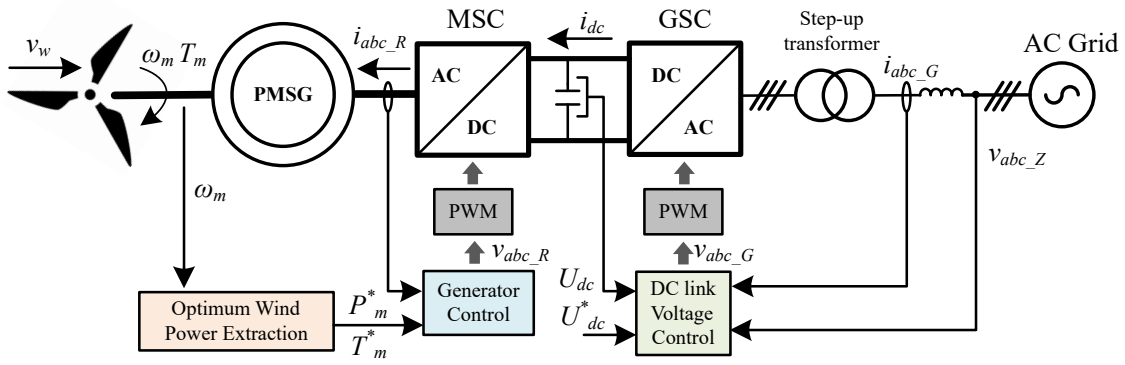

Fig. 2.3. Control scheme of a PMSG based full-scale acWT.

(a) **Optimum Wind Power Extraction**

It provides the necessary power (P^*_m) or torque reference (T^*_m) based on the operational points of maximum efficiency. The optimal reference value depends on the rotor speed, wind speed, and pitch angle.

(b) **DC link Voltage Vontrol**

The grid-side converter (GSC) is responsible for maintaining a constant dc link voltage and it is able to provide reactive power. Typically, the control objective is achieved by the vector control which is based on d-q components. This consists of an outer loop that regulates the dc voltage through a proportional integral (PI) controller and an inner loop that controls the current.

(c) **Generator Control**

The machine-side converter (MSC) controls the power extracted from the wind turbine or the mechanical torque. However, in [29] it has shown that it is possible to swap control objectives of GSC and MSC with enhanced fault ride-through and voltage support capabilities.

2.2.2 Emerging Wind Turbine Technologies

Cutting-edge technologies in wind energy generation have the potential to significantly impact the industry by increasing power output per wind turbine and overall capacity factor of wind turbines. This enables reducing the capital expenditure (CAPEX) and levelised cost of electricity. In this regard, continuous research and development is required to increase the performance and reliability of next-generation wind technologies to enhance the economies of scale. Several leading WT technologies currently under different research phases have been discussed in this section.

2.2.2.1 Super Conducting Wind Generators

Since 2005, permanent magnet generators have gained popularity, especially in offshore turbines, as they allow for high power density and small size with the highest efficiency at all speeds. This offers a high annual production of energy with a low lifetime cost [30]. Although, the use of permanent magnet provides significant benefits for large scale offshore WTs, the availability of this rare earth element confine to specific geographic locations. For instance, China is the world's largest producer and exporter of rare earth permanent magnets with a share of 90.5%. In recent years, China has taken rare earth, the upstream of rare earth permanent magnet materials industry, as a resource of strategic importance and restricted the total mining and smelting volume [31]. However, Canada and Australia emerging as alternative locations for the extraction and processing of rare earths.

The ability of superconducting materials to carry high current densities with very small losses could facilitate a new class of generators, i.e., High Temperature Superconducting (HTS) generators. These WTs are able to operate with an air gap flux density considerably higher than the conventional generators, which are smaller in size and weight [32]. Compared to permanent magnet, up to 50% of the generator mass can be saved with HTS generators, which also means that the cost of construction and installation can be significantly minimized. The rotor of the HTS generator is subject to low thermal ageing of the insulation, thus lower risk of insulation breakdown.

In addition, HTS generators also have high overload capability without thermal excursion. The main challenge of the super conducting generator is the cost of the cryocooler which is used to cool down the rotor. On top of the additional cost, the reliability of the cooling technology has not been proven yet for offshore operations. However, EU-funded EcoSwing project successfully aimed at demonstrating world's first superconducting low-cost and lightweight onshore 3.6 MW commercial WT located at a coastal site in Western Denmark, Thyborøn, near-shore to the North Sea [33, 34]. This demonstrates the technology readiness level (TRL) of the super conducting wind generator concept of TRL–6,7 (Prototype system tested in intended environment). In this regard, HTS generator is a promising candidate for future large-scale offshore wind farms.

2.2.2.2 Multi-rotor Wind Turbines

Multi-rotor technology has a long history which goes back to the start of 19th century. This concept persists in a variety of modern innovative systems. This had generally fallen out of consideration in mainstream WT design from a perception that it is complex and

Fig. 2.4. Vestas multi-rotor wind turbine.
Source: [35]

unnecessary as very large single WT units are technically feasible. However, the research and innovation project INNWIND, demonstrates its feasibility to replace a large single rotor with a multiple-rotor system (MRS) which can improve efficiency and reduce overall loads on a WT [36].

This innovative solution could allow a large power system (20 MW or more) to be installed at a single site by means of a high number of standardised rotors [37]. With individual control of rotors, it is possible to respond to a turbulent wind field across the device, allowing for more efficient generation and with the potential to alleviate loads. The prototype used in INNWIND project; Vestas 4R-V29 which consists of four V29-225 kW rotors is shown in Fig. 2.4. It was demonstrated that MRS power production was estimated to be 8% higher than a single rotor system of the same overall swept area.

One of the possible advantages of the MRS can be to mitigate the structural and material problems associated with the scaling up of larger WT. The production process of smaller rotors could be industrialised and could have lower costs while present production methods of large turbines require customisation [38]. Moreover, in the case of malfunctioning of one rotor, this eliminates any interruption of energy production from the working rotors of the array.

2.2.3 DC Wind Turbine Technology

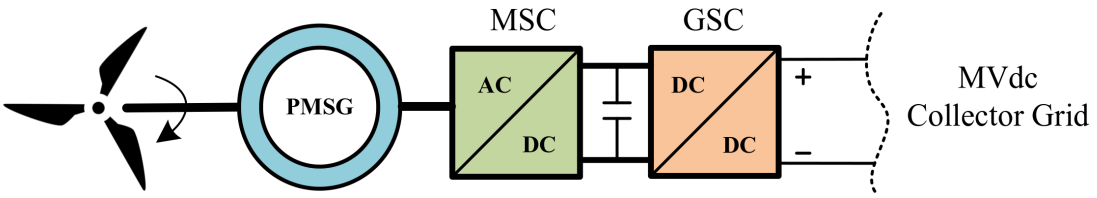

Fig. 2.5. A typical block diagram of a dc-wind turbine

With the significant advancements in offshore WT technology, the rated capacity of a single unit has been increased over the last few years. This enables extracting more energy with fewer units or expand the total wind farm output concentrated to a unit marine area. However, with the increasing size of ac-wind turbine (acWT), the volume and weight of the 50/60 Hz power frequency transformer becomes larger. This results in;

1. requirements to strengthen the structure and foundation of the WT, and
2. difficulties in equipment handling under harsh offshore environment.

Essentially, the network losses also increase with more currents flow through the collection system; which can be significantly reduced with the use of MVdc network architectures [17]. The study in [15] shows that MVdc collection systems present (a) capital costs comparable with conventional MVac systems, and (b) lower energy losses, concluding that dc collector grids could be of interest for future OWF installations. This study was conducted by referring to the 160 MW Horns Rev offshore wind farm located in Denmark. In this regard, the use of dc technology at the collection system level is more economical. These advantages over the state-of-the-art MVac technology will enable establishment of MVdc offshore wind collection systems in the future. A simplified configuration of a dcWT is shown in Fig. 2.5.

In [18], a research work has been carried out to identify a suitable dcWT topology that has the lowest technological risk based on multi-dimensional techno-economic factors. In this work, a 10 kW prototype has been developed to demonstrate the TRL of the dcWT concept from TRL–2 (Basic research - Principles postulated and observed but no experimental proof) to TRL–4 (Small scale prototype built in a laboratory environment). A detailed discussion of different topologies is presented in Section 2.2.3.1.

2.2.3.1 Candidate dc-Wind Turbine Topologies

When selecting a suitable dcWT topology for all-dc OWF, the associated technological risk is a key factor to consider. Assuming that state-of-the-art WT generators are

employed, a number of dc wind turbine concepts have been classified by the number of power electronic conversion stages [17, 18].

When selecting a suitable dcWT topology, minimum number of components, simplicity, and galvanic isolation are the important factors to consider. As shown in Fig. 2.6, the simplest design is the topology-(a). However, the maximum output voltage is restricted

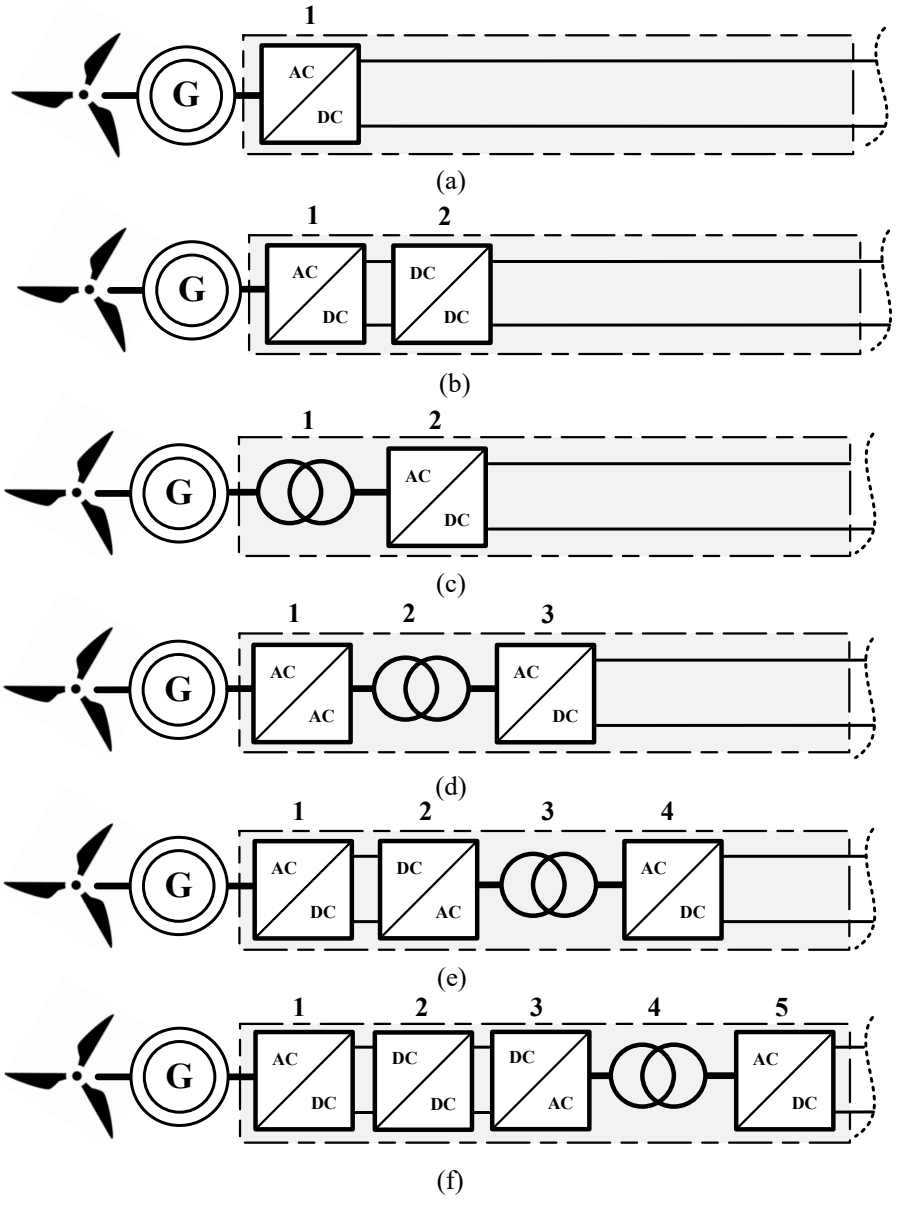

Fig. 2.6. Different dcWT configurations: (a) active rectified based dcWT; (b) non-isolated dc/dc converter based dcWT; (c) ac transformer and passive rectifier based dcWT; (d) matrix converter, medium frequency transformer and passive rectifier based dcWT; (e) active rectifier and galvanic isolated dc/dc converter based dcWT; (f) boost converter between the active rectifier and galvanic isolated dc/dc converter based dcWT.

by generator's nominal voltage level and it has no galvanic separation. This voltage boost issue in concept-(a) can be eliminated by adding a non-isolated dc/dc converter as shown in Fig. 2.6(b). The topology in Fig. 2.6(c) uses a low-frequency transformer with a passive rectifier as proposed in [39]. However, fixed speed operation and transformer saturation are the main disadvantages.

Concept-(d) deploys a matrix converter (MC) at stage-1 which is proposed in [40] with galvanic isolation. However, the MC requires advanced control strategies to coordinate with variability of wind power which could be an interesting research topic. Concept-(e) provides galvanic isolation and uses state-of-the-art acWT and active rectifier which is similar to type-4 ac wind generator. In this topology, only a high-power dc/dc converter is required to add at the front-end to build a dcWT. The topology-(f) uses a boost converter between the active rectifier and the isolated dc/dc converter. It assumes that the boost converter actively controls the LV side dc link, while the dc/dc converter operates in an open loop. Among the topologies discussed, concept-(e) is the most suitable topology due to the lowest technology risk.

2.2.4 Selection of a Suitable DC/DC Converter Topology for dc-Wind Turbine

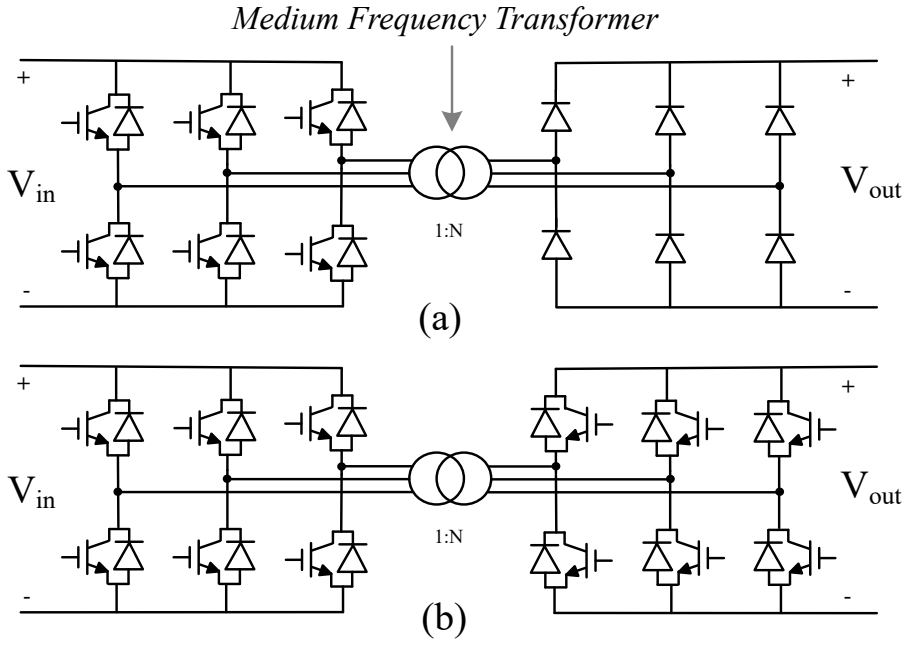

Fig. 2.7. Different dc/dc converter configurations; (a) single active bridge, (b) dual active bridge.

As discussed above, the dcWT concept-(e) which demonstrates a lower technological risk comprises of a dc/dc converter. This dc/dc converter shown in Fig. 2.6(e) can be considered as a combination of power conversion stages 2,3 and 4 which can be a Single Active Bridge (SAB) or a Dual Active Bridge (DAB) as shown in Fig. 2.7. The terms V_{in}, V_{out} and N denote the dc input voltage, output voltage, and transformer turns ratio, respectively.

The power transfer capability of 3-phase SAB and DAB can be represented by [41]:

$$P_{SAB(3\phi)} = \frac{V'_{\text{out}}}{9 \cdot f_s \cdot L_\sigma \cdot V_{in}} \cdot \left(V_{\text{in}}^2 - V_{\text{out}}'^2\right) \tag{2.1}$$

$$P_{DAB(3\phi)} = \frac{V_{in}^2}{2\pi f_s L_\sigma} \cdot d \cdot \phi \left(\frac{2}{3} - \frac{\phi}{2\pi}\right); \quad 0 \leq \phi < \frac{\pi}{3} \tag{2.2}$$

where:

V'_{out} - secondary side output voltage referred to the primary
L_σ - stray inductance of the transformer.
ϕ - the phase shift
d - dc conversion ratio i.e., the primary-referred dc voltage gain
f_s - switching frequency

In wind power applications, the active power flow is always unidirectional i.e. from WT side to the grid side. Therefore, SAB will primarily serve our requirement. However, the major limitation of SAB is the phase-shift between primary and secondary occurs due to the leakage inductance of the medium frequency transformer as shown in (2.1). To transfer a large amount of power, the transformer leakage inductance should be made very low [42]. This problem can be eliminated with the use of DAB.

In (2.2), it can be noted that both the f_s and ϕ can be used to control the output power. Generally, DAB is used when bi-directional power transfer is required such as in dc microgrids. However, DAB shall support the OWF black-start by enabling reverse power flow to charge the dc-link of the dcWT. If SAB is used, it will require a stand-by diesel generator ready at all the times. However, with harsh marine weather conditions, re-fuelling of diesel generators could be problematic. Thus, the use of DAB as the dc/dc converter in topology-(e) is advantageous.

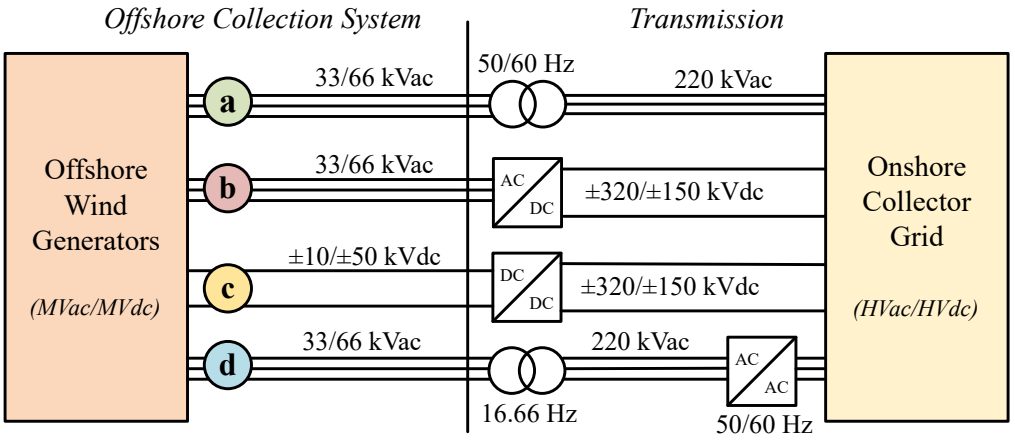

Fig. 2.8. Different OWPP collection system options: (a) MVac collection with HVac transmission; (b) MVac collection with HVdc transmission; (c) MVdc collection with HVdc transmission; (d) low frequency MVac collection and HVac transmission.

2.3 Offshore Wind Power Collection Systems

The selection of a suitable network structure is one of the important preliminary studies performed at the early stage of an OWF development. In order to yield maximum economic return from an OWF, identifying a suitable collection system topology is essential. Irrespective of the technology used, the main factors to be considered are CAPEX, operational and maintenance costs, system losses, and reliability.

At present, all the existing OWFs feature an internal ac network with either ac or dc transmission to onshore power grids. Different offshore wind ac collection system topologies have been well analysed in the literature to obtain the optimised configuration with the consideration of system losses and associated life cycle costs [11, 43]. In [14], it has been shown that closed-loop network configuration (i.e., ring configuration) is economically viable than the typical radial OWF collection system configuration.

However, due to concerns such as (a) additional control complexity, and (b) the requirement to over-rate some cable sections which incurs additional investment, the radial topology has only been deployed in commercially operating OWFs at present. One of the main advantages of radial topology is its control and operation flexibility. Conversely, the main drawback of this radial connection is, upon failure of an upstream cable connection of the network, all the healthy WTs are required to forced to shut-down. With the uncertainties associated with severe weather conditions prevail in the offshore environment, component repair times could be much longer than anticipated.

Different OWF collection system options with transmission technologies are shown in Fig. 2.8. The advantage of using the state-of-the-art ac technology from the onshore power grid is obvious in terms of know-how, experience, and, to a certain extent, cost [44]. However, as the OWF distance to onshore grid increases (where wind conditions are superior) the ac cable transmission may become problematic due to high capacitive cable charging. Thanks to the advancements in VSC technology, particularly with the modular multi-level converter (MMC), the HVdc technology is an alternative for long-distance offshore power integration [45].

Table 2.2 summarises different OWF collection system options with their advantages and disadvantages. Due to additional benefits such as lower losses, zero reactive power compensation, elimination of 50/60 Hz bulky transformers, lightweight and reduction in the size of power electronic converters MVdc technology will be a promising option for future OWF collection systems [16, 17].

Table 2.2. OWF collection system options: advantages and disadvantages.

Options	**Advantages**	**Disadvantages**
MVac collection with HVac transmission	a) Maturity of the ac technology	a) Higher losses with increase distance to shore
	b) Comparatively low capital investment	b) Large offshore platform
	c) Market availability	c) High capacitive cable charging
MVac collection with HVdc transmission	a) Suitable for longer distance power transmission	a) High capital investment
	b) Higher transmission efficiency	
MVdc collection with HVdc transmission	a) Less power conversion stages (SP Topology)	a) Uncertainty in reliability and typical availability of dc wind turbines
	b) Lower losses compared to ac solution	b) MVdc protection technology not fully developed
	c) High power density with increased size and capacity of single WT	c) Higher capital investment

Low frequency MVac collection and HVac transmission	a) Increase of power capacity and transmission distance for a given submarine cable compared to ac solution	a) Higher risk associated with low-frequency ac (LFac) technology know-how
	b) Use of normal ac breakers for protection with necessary modifications	b) Larger size of the LFac transformer
		c) No specific standard available for LFac technology

2.3.1 DC Collection System Options

As discussed above, with the increasing capacity of a single WT unit, more energy can be extracted with a fewer units. However, electrical losses also increase proportionately. Hence, the use of dc technology at the collection system level will help minimise network losses. In [42, 46], it has shown that the use of MVdc over existing MVac technology is economically beneficial. In an dc collection system, the power from the dcWT would essentially go directly through MVdc connections to the onshore system with a much smaller or even completely without a offshore substation platform.

Different dc collection system topologies have been proposed in the literature such as different variants of radial topology, dc-series, and series-parallel structures [15, 16, 17, 47, 48]. The radial collection system comprises of several MVdc clusters (typical voltage range between $\pm$10 kV to $\pm$50 kV) which will be collected by one or several offshore collection system platforms (depending on the distance to the shore) and export to the onshore grid via HVdc transmission.

(a) Radial Topology

The main characteristic of the radial topology is that the output voltage of each WT is kept constant, while the current flowing through the inter-array cables depends on the number of turbines connected to it. There are several radial collection system topologies based on the number of dc/dc transformation steps and number of offshore platforms.

(i) Configuration-1

This topology (Fig. 2.9) is configured to connect all the MVdc cables directly to the offshore HVdc converter platform. One step-up stage is used where the output voltage of each wind turbine is stepped-up by a dc/dc power converter.

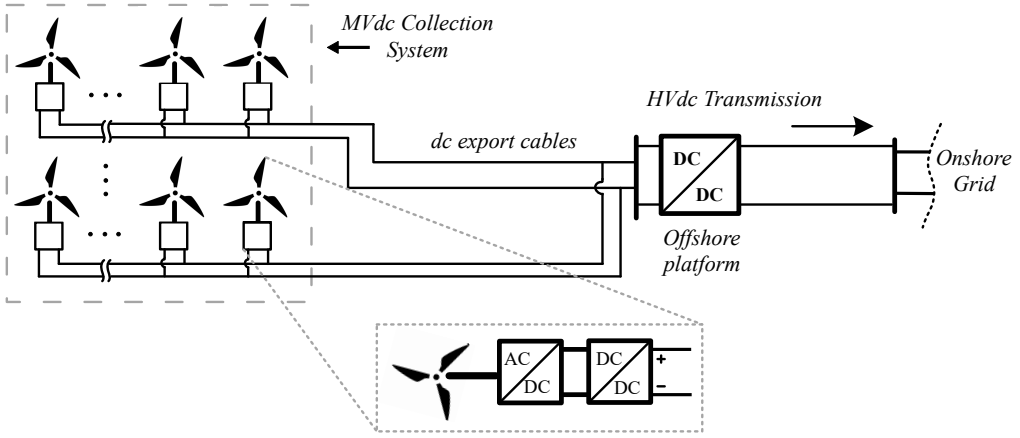

Fig. 2.9. DC radial configuration-1.

(ii) Configuration-2

In this scheme (Fig. 2.10) an offshore collector platform is added to gather all the inter-array cables. Thereby, the WTs are connected to the collector platform by means of inter-array cables, while the export cable connects the collector platform with the HVdc offshore platform. The step-up stage is similar to the Configuration-1.

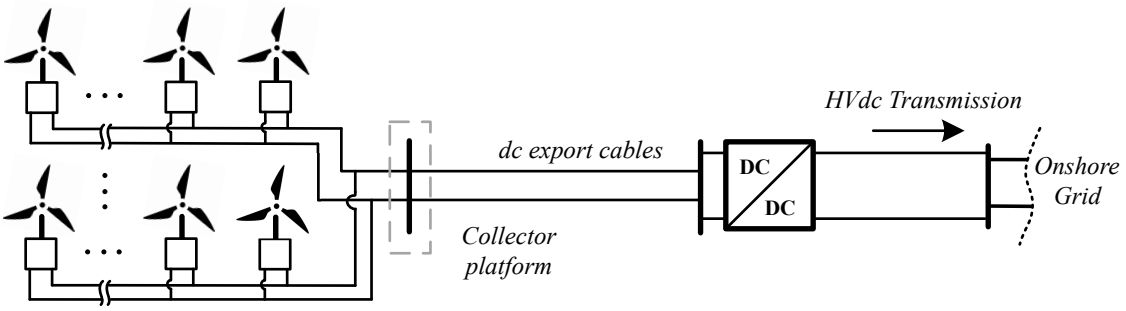

Fig. 2.10. DC radial configuration-2.

(iii) Configuration-3

The higher export cable losses due to the use of lower MVdc voltage levels can be minimised with this option. It is based on installing a dc/dc power converter at the intermediate offshore platform (Fig. 2.11). The result is having two step-up stages (both at the wind turbine and the collector platform level).

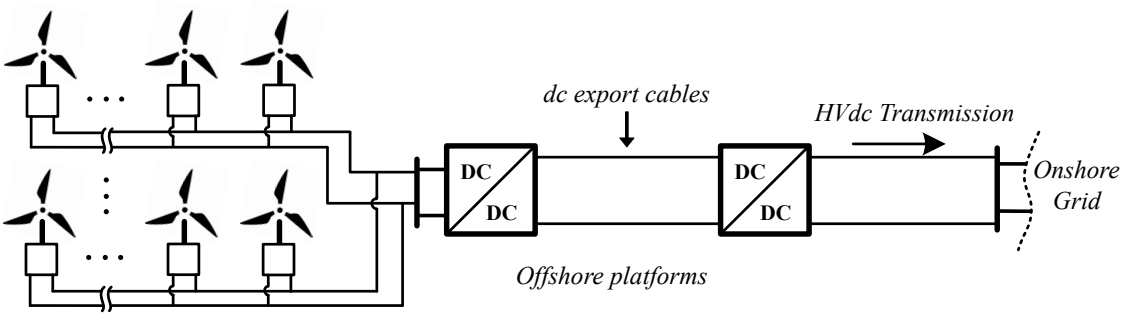

Fig. 2.11. DC radial configuration-3.

(iv) Configuration-4

In this scheme, a dc/dc power converter is installed at each feeder as shown in Fig. 2.12. This configuration is more suitable for offshore locations where the distance between feeders are relatively longer than the above three configurations. The use of more power electronic components is one of the disadvantages which leads to higher collection system losses.

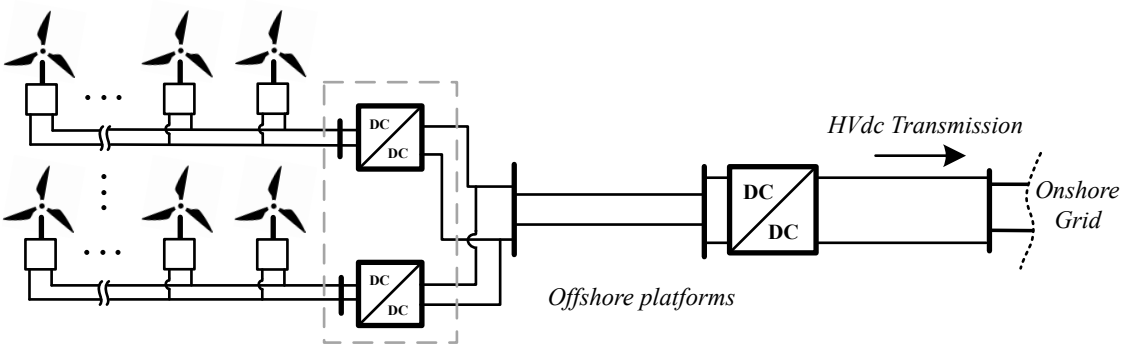

Fig. 2.12. DC radial configuration-4.

(b) Series Topology

As the name implies, in series topology, the dcWTs are connected in series. As a result, the output voltage is increased to an HVdc transmission level while the current of each wind turbine in a string remains constant. The aim is to eliminate the offshore converter platform. As shown in Fig. 2.13, the series-parallel topology is configured as a number of wind turbines electrically connected in "series" but the feeders are connected in "shunt" between them. The main drawbacks are the requirements in regulating the voltage instead of the current and the over-rating of some electrical components of the wind farm.

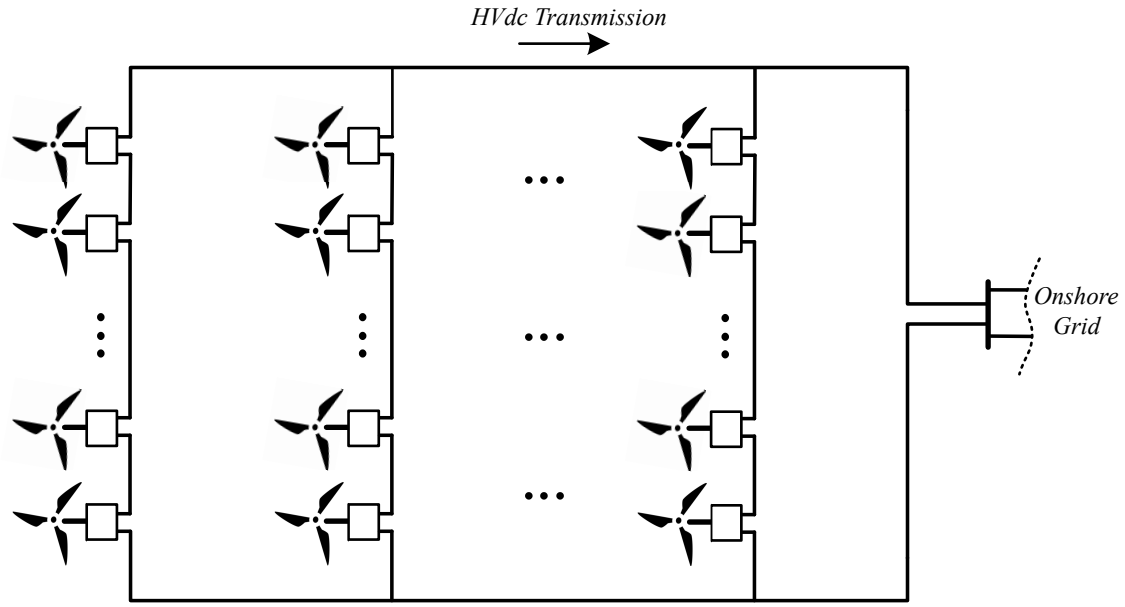

Fig. 2.13. DC series-parallel configuration.

2.3.2 Economies of scale of DC Collection System Concept

To measure the economic viability of offshore wind power dc collection systems over ac collection systems, several comparative studies have been performed in the literature. In [15], a technical and economic assessment of four candidate dc offshore collection systems was conducted. The key objective was to determine their cost effectiveness compared to conventional ac OWF. This study proposed a novel methodology to account the uncertainty of dc technology considering various parameters, which may affect technical and economic feasibility of dc OWFs, for example, dc equipment efficiencies, dc component costs, OWF rated power, export cable lengths, etc. The results showed that dc collection systems present capital costs comparable with conventional ac OWFs, as well as lower energy losses.

In [16], a comparative study between radial ac and dc collection systems was conducted based on their losses and investment costs. This study considered most of the essential components such as collection cables, power electronic converters, switch gears and offshore platforms. The costs of individual components were calculated based on different analytical cost models. The results showed that the losses in dc collection systems are higher than ac collection systems. It was identified that a higher percentage of losses of dc collection systems mainly refer to dc/dc converters. However, this study considered a relatively shorter distance of 5 km between the centralised converter platform and the OWF collection system with 5 MW single WT capacity. The dc collection system concept

could be more favourable over the state-of-the-art ac technology with larger capacities of single WT units and greater distance to the shore.

In [49], the dc series configuration was compared in terms of losses, cost, and reliability over the state-of-the-art ac radial configuration which uses HVdc transmission. The results showed that the dc series system becomes comparable with the ac radial design for higher dcWT capacities. Furthermore, this analysis showed the requirement to reduce the electrical losses in dcWT power conversion system.

The cost and losses of the several OWFs based on centralised collection system platform were compared for both the ac and dc collection system configurations in [50]. It was shown that dc OWF topologies offer a reduction in losses, because of the reduced number of conversion steps, and costs because of the reduced cable cost. However, the lack of commercially available high-power converters would influence the overall cost reduction up to some extent. Lower power electronic component prices will enable the advantages of the dc collection systems in the future.

A detailed economic model considering the life cycle costs of components was presented in [42]. To calculate the total investment, the interest rate of the debt capital, the economic lifetime, the discount factor, and the equity-asset-ratio factors were considered. It was shown that the centralised dc collection system concept (Fig. 2.9) offers about 43% and 40% reduction in lifetime cost for compared to a 500 MW and 1000 MW radial ac-OWF, respectively. Although the series-parallel concept leads to a lower CAPEX compared to that of the ac solution of the same capacity, it is still inferior to the centralised dc collection system concept.

2.3.3 Technology Readiness Level of the DC Collection System Concept

In MVdc collection systems, the power from the dcWT would essentially go directly through MVdc network to the onshore system with or without the offshore substation platform. A review of the state-of-the-art and ongoing research and development, and an assessment and detailing of the required technology maturity levels are summarised in Table 2.3 [51].

The MVdc cable systems are seen as a mature technology for OWF-MVdc collection systems. MVdc cables have already been delivered to the market and there are several projects in operation where the MVdc cables are implemented in different dc voltage levels. MVdc protection technologies are also available, which still in an early development

Table 2.3. Technology readiness levels of key technologies for offshore wind farm MVdc collection systems.

Technology		**TRL**	**Maturity Status**	**Remarks**
dc-Wind Turbine	dcWT Integration	3	Immature	Limited progress. Much dependent to market pull.
	WT generator	9	Mature	Technology is ready, 15 MW acWT commercially available in a few years [26]
	WT converter (dc/dc)	3-4	Immature	Technology is possible, only demonstrated with a 10 kW laboratory prototype [18].
	dc switchgear	7-8	Early stage	Technology is possible for other applications, without much interest in WT.
dc/dc converter		2-3	Immature	Technology is possible, but has not been demonstrated at hundreds of MW levels.
MVdc protection	dc circuit breaker	7-8	Semi-mature	Technology is available, but in limited applications, more for HVdc and still costly.
MVdc cable		9	Mature	Technology is ready.

stage but considers for commercial use soon. For dc circuit breakers, there are different solutions available. Both mechanical and hybrid circuit breaker in MV-level has been demonstrated in projects and MVdc switchgear has also been reported to be used.

Nonetheless, dc/dc converters and dcWTs are considered to be the most critical components for MVdc collection systems. So far, dc/dc converters have not been used commercially for HVdc and MVdc transmission systems. Further, the dc wind turbines have not attracted much market attention with only a few manufacturers actively involved in the development, however this remains at an early stage.

Based on the above review, following aspects are required to consider for the further development of OWF dc collection system concept.

(a) **Develop and create market pull for enabling technologies** - The key drive to enable MVdc array technologies for offshore wind is to create a strong business case with a thorough risk investigation and mitigation strategy. dcWTs are a critical

component of all dc array topologies and there has been limited progress in this area. A demonstration project will therefore be critical to addressing operational concerns, reducing key risks and providing increased confidence in reliability, availability and operational considerations, which will provide additional confidence to the market.

(b) **Further development of topologies and configurations** - Several analyses showed that the main advantage of the OWF dc collection system technology compared to conventional ac technology, is the reduced size or possibly even elimination of the offshore platform. Also, in [51] it was determined that with larger WT power ratings, the total losses and costs are reduced. Therefore, a detailed assessment including their technical competencies and reliabilities from component-level to the system-level are further required to evaluate.

2.4 State-of-the-art Reliability Evaluation Techniques

Reliability assessment in the conventional electrical system is defined as "the probability that it performs its functions properly, without any failure within a stipulated period of time, when it is subjected to normal operating conditions" [52]. This is divided into two basic aspects of the system: adequacy and security. The first is the capacity of the system/component to satisfy customers' demand and operational constraints in a range of technical values, related only to static conditions of the electrical system. The latter is the capacity of the system to respond to transient phenomena or dynamic disturbances that arise in the system. In this thesis, the adequacy requirements of the dc collection system concept are investigated from the component level to the system level. Some of these methods originate from general reliability analysis or mathematics, while some methods have been specially developed for reliability analysis of semiconductor devices, such as mission profile and physics of failure based models.

Power system reliability evaluation methods can be divided into two categories: (1) analytical methods, and (2) simulation methods. In addition, the reliability evaluation may be a qualitative study, in which the main factors that impact system reliability can be determined and prioritised, or a quantitative study, where the reliability is assessed through different parameters and indices defined and calculated for the system or load point [53].

Analytical techniques represent the system by a mathematical model and evaluate the reliability indices from this model using direct numerical solutions. They generally provide expectation indices in a relatively short computing time. Some of the most common analytical methods are:

(a) **Fault Tree Analysis (FTA)** - This analytical method is mainly used to understand how systems can fail, to identify the best ways to reduce risk and to determine (or get a feeling for) event rates of a safety accident or a particular system level (functional) failure. This is a top-down, deductive failure analysis in which an undesired state of a system is analysed using Boolean logic to combine a series of lower-level events.

(b) **Reliability Block Diagram** - This is a graphical and mathematical model of the elements of a system permitting the calculation of system reliability given the reliability of the elements. An RBD is drawn as a series of blocks connected in parallel and/or series configuration. Parallel blocks indicate redundant subsystems or components that contribute to a lower failure rate. Each block represents a component of the system with a failure rate. To evaluate an RBD, statistical independence of blocks or components are generally assumed. However, when statistical independence is not satisfied, specific methods such as dynamic RBD can be used [54].

(c) **Markov Chain** - A Markov chain is a stochastic model describing a sequence of possible events in which the probability of each event depends only on the state attained in the previous event (a memory-less process). A countably infinite sequence, in which the chain moves state at discrete time steps, gives a discrete-time Markov chain and a continuous-time process is called a continuous-time Markov chain.

(d) **Minimal Cut Set method** - Minimal Cut Set method is used to obtain an estimate of reliability for complex RBDs or fault trees that can not be simplified by a combination of the simple constructs (parallel, series, *k-out-of-n*). Cut sets are the unique combinations of component failures that can cause complete system failure.

(e) **Failure Mode and Effect Analysis (FMEA)** - This is a systematic and proactive method for evaluating a process to identify where and how it might fail and to assess the relative impact of different failures, in order to identify the parts of the process that are most in need of change. FMEA includes review of steps in the process, failure modes (What could go wrong?), failure causes (why would the failure happen?), and failure effects (what would be the consequences of each failure?).

Analytical approaches are based on assumptions concerning the statistical distributions of failure rate and repair times. On the contrary, assumptions are frequently required in order to simplify the problem and produce an analytical model of the system. This is particularly the case when complex systems and complex operating procedures have to be modelled. The resulting analysis can therefore lose some or much of its significance.

Simulation methods estimate the reliability indices by simulating the actual process and random behaviour of the system. Monte Carlo simulation (MCS) is the widely used

simulation method which has two different categories [52]: (1) non-sequential, and (2) sequential. In a non-sequential MCS, the samples are taken without considering the time dependency of the states or sequence of the events in the system. Therefore, using this method, a non-chronological state of the system is determined. On the other hand, a sequential MCS can address the sequential operating conditions of the system, and may be used to include time-correlated events and states such as output generation of renewable-based generating units, demand profile, and customer decisions, which is more applicable for power system reliability studies.

Although there are several methods available, the actual point-of-view of system reliability depends on the particular study. For example, an OWF owner might be concerned about the financial risk related to the offshore grid, while he is less sensitive in the security of supply for the end-user. On the other hand, a system operator might be mainly concerned with the security of supply [55].

2.5 Reliability Requirements of Offshore Wind DC Collection System Concept

Offshore locations present challenges for maintenance and repair operations. The time to repair can be very high and mostly during the winter period and may also be inaccessible. In this regard, the reliability calculations provide insight for operational strategies and topology selection and is a valuable procedure for the following reasons.

(a) It enables comparative performance of different candidate options under common grounds i.e., compare alternative options.

(b) It helps to identify redundancy levels that require to maintain to comply with standards, grid codes, etc.

(c) It establishes the chronological changes in system performance and therefore helps to identify weak areas and the need for reinforcements.

(d) It establishes existing indices which serve as a guide for acceptable values in future reliability assessments (ex. to decide future preventive maintenance requirements).

Hence, reliability assessment in the context of OWF dc collection system can be considered as a measure of the system's ability to meet the requirements of consumers or regulators, which can be used as a means of predicting its future performance.

2.5.1 Reliability Estimation of Components

Reliability analysis is an important tool for assisting the design phase of a power electronic converter to fulfil its life-cycle specifications. This helps identification of optimal preventive maintenance strategies and required improvements in the design such as optimum redundancy levels [56]. Further, the lifetime of an MVdc converter depends on the topology and individual failure rates of different subsystems [57].

The typical life-cycle of a power electronic component is characterised by the well-known "bathtub" curve. As shown in Fig. 2.14 the life of a population of semiconductor devices (a group of devices of the same type) can be divided into three distinct periods:

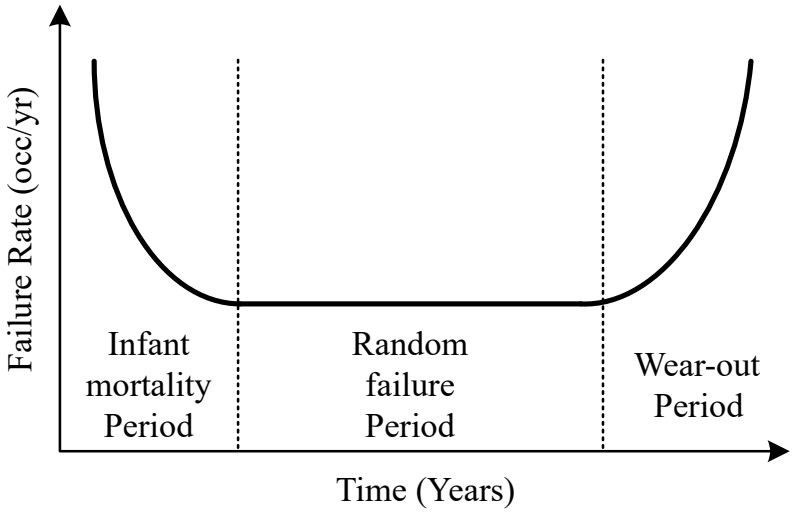

Fig. 2.14. Reliability bathtub curve.

- *Early Life* - The first period is characterised by a decreasing failure rate. It is what occurs during the "early life" of a population of units. The weaker units fail leaving a population that is more rigorous.

- *Useful Life* - The next period is the flat bottom portion of the graph. It is called the "useful life" period. Failures occur more in a random sequence during this period. It is difficult to predict which failure mode will occur, but the rate of failures is predictable. The length of this period is also referred to as the "system life" of a product or component. This is the period of time that the lowest failure rate occurs.

- *Wear-out* - The third period begins at the point where the slope begins to increase and extends to the rightmost end of the graph. This is what happens when units become old and begin to fail at an increasing rate. It is called the "wear-out" period.

To estimate the reliability of a component there are several different handbook methods available. The most commonly used method relies on MIL-HDBK-217. However, the data provided in this handbook has been considered as out-of-date for new technologies as it was last updated in 1991. The IEC-61709:2017 provides guidance on the use of failure rate data for mission profile-based failure rate prediction reliability prediction of electric components. The most recent update of MIL-HDBK-217 is the FIDES guide which considers the component physics of failures. Hitherto, the FIDES guide is the most recent update on the failure rate estimation of electronic components.

Once the component failure rates are obtained, the converter level reliability can be obtained using methods such as reliability block diagram (RBD), FTA, and the Markov Chain. The Markov Chain technique can only be used if the system component failures only hold Markov properties.

2.5.2 Mission Profile based Reliability Assessment of Semiconductor Devices and Power Converters

The lifetime of a power electronic converter is influenced by its mission profile and ambient temperature [58]. Therefore, depending on the application (MV distribution systems, shipboard and traction applications, large scale solar PV generation system etc.) the reliability of the converter is changed.

The thermal dynamics of power semiconductors and power capacitors are closely related to the reliability and affect the cost and lifetime of power electronic converters. A survey conducted in [59] identified that approximately 37% of the total unexpected failures of a 3.5 MW photovoltaic plant are caused by the inverter. Moreover, the cost of inverter failures even reaches 59%, which classifies the power converter as the bottleneck seen from the point of view of the system-level reliability [60]. A component-level reliability survey carried out in [61] concluded that the power devices and capacitors were the most fragile components of the power electronic system. The power devices such as insulated-gate bipolar transistor (IGBT) are subjected to a variety of temperature profiles, which cause cyclic thermomechanical stresses in all the layouts and joints of the modules and finally lead to device failure. For instance, due to the considerable differences in thermal expansion coefficients among the layers in IGBT, the bond wires, chip solder joints, and substrate solder joints suffer most from the thermal stress. As discussed in [62], the lifetime model of the solder joint in IGBT is based on the time-dependent creep, and therefore the cycle period affects the solder joint lifetime.

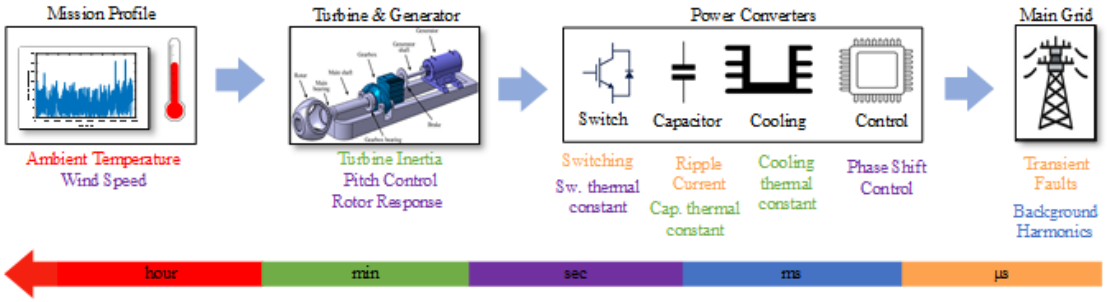

Fig. 2.15. Timescale of mechanical and electrical components in a dc-wind turbine system.

As this model assumes that the immediate plastic deformation leads to fatigue instead of time-dependent creep, the lifetime model for the bond wire is independent of the cycle period. Further, there are two kinds of thermal cycles in the power semiconductors [63]: (a) the loading variation based thermal cycles, which are caused by different loading currents and ambient temperatures with cycle period from seconds to years, and (b) the fundamental-frequency-based thermal cycles ranging from milliseconds to seconds, which are induced by the complementary conduction between the IGBT and the freewheeling diode within a fundamental period of the ac current.

However, the component loading of a system is governed by many factors, which presents various time constants from microseconds to hours. Determining the system availability in such system is a challenge and need detailed analysis. In [60], a detailed method was presented to evaluate component-level reliability of a DFIG based acWT according to the long-term electro thermal profile. The reliabilities of component- to converter- level were obtained using the Weibull function based on time-to-failure distributions.

The main disturbances for the thermal behaviour of the key components of a wind power converter system are summarised according to their dominant response time in Fig. 2.15. Notably, these thermal disturbances have a wide range of time constants from microseconds (device switching and capacitor ripple current) to hours (ambient temperature changing). The existing models to observe power electronic thermal performance are either use very detailed models but limited to short time span and small time-steps [64], or only use steady-state conditions under the assumption of lesser accuracy of many of the important thermal dynamics [58].

2.5.3 Component-Level Lifetime Assessment of dc-Wind Turbines

Different approaches have been proposed in the literature to assess the lifetime of WTs. In [60], the motivation of the proposed method was to predict the reliability of the DFIG

power converter at the end of service life. This will help to identify the bottleneck components and to better size the key components for the next generation product. To facilitate the converter-level reliability calculation linked by the RBD method, the proposed method encompasses: (a) efficient and simplified models with low sample rate mission profile, and (b) component level lifetime distribution considering the parameter variations in the lifetime model. The Weibull function based time-to failure distribution has been used to link from component-level to converter-level reliability. The analysis of a 2 MW DFIG wind turbine system showed that the dc-link capacitor bank dominates the converter-level reliability.

A lifetime comparison of MSC of two types of PMSG models, i.e., low-speed (LS; direct-drive) and medium-speed (MS; one-stage) models were conducted in [65]. Similar to the previous approach, a translation from the mission profile of the turbine to the current and voltage loading of each power semiconductor was achieved based on synchronous generator modelling. Then, a simplified approach to calculate the losses profile and the thermal profile was used to determine the most stressed power semiconductors in the converter. It was concluded that, although the LS PMSG is able to eliminate the gearbox, the lifespan of its MSC is lower than the one-stage MS generator.

The impact of the pulse width modulation (PWM) modulation strategy applied to three-level neutral point clamped converter (3L-NPC) back-to-back converter for a 10 MW PMSG wind turbine was investigated in [66]. The results showed that the 60° discontinuous PWM strategies allow better thermal performance and increase the estimated lifetime of the converter. Furthermore, it was identified that the increment of the wind roughness class causes a larger dispersion of the mean values and the variation of the junction temperatures, which also affects the lifetime of the converter.

To investigate the influence of reliability caused by the amount of semiconductor components and the current for each component, several multiple-converter structures and their RBDs were used for the MSC for a wind turbine equipped with a 2 MW direct-drive PMSG in [67]. The results concluded that the component current dominates in the system-level reliability analysis of the MSC and the standby structure can also improve the reliability under the same current level.

2.5.4 Medium Voltage dc Converters and Reliability Requirements

MVdc technology is becoming an attractive solution thanks to its high power transfer capability, excellent controllability and operational flexibility. Potential applications of VSC based MVdc range from the integration of RE sources [68], traction and shipboard

power systems [69, 70], smart distribution systems [71] and future offshore dc collection grids [17]. In particular, the use of VSC technologies at MVdc voltage level is beneficial in terms of their applicability in weak rural and complex urban distribution networks.

Among the VSC technologies for low voltage (LV) applications, the two-level VSC (2L-VSC) has been considered as one of the simplest and cost-effective solutions [72]. Another candidate topology is the 3L-NPC, which offers higher efficiency and better harmonic performance compared to the 2L-VSC [73]. Due to lower switching frequencies required to maintain the harmonic levels defined in standards such as IEEE 519 [74], 3L-NPC is relatively more efficient than 2L-VSC. However, for HVdc applications, the MMC has been the most favoured choice due to its exceptional waveform quality, compact and modular design [75].

To this end, the assessment of VSC topologies at different dc voltage levels has been a key research area that received interest recently [72, 76]. This is also evidenced in the several demonstration projects that have been or being implemented around the globe. The first ac to dc conversion MVdc link demonstration project in the UK, the "ANGLE-DC" project, aims to demonstrate the application of MVdc by converting an existing 33 kV ac double-circuit to a rigid bipolar dc circuit at $\pm$27 kV [77]. Due to the technological maturity of the 3L-NPC and lower cost compared to MMC, a special designed cascaded three-level neutral point clamped converter (C3L-NPC) has been deployed in the "ANGLE-DC" project. However, the first multi-terminal MVdc project in China used MMCs to demonstrate and supply reliable and quality power to the distribution networks [78]. The voltage of this multi-terminal MVdc project is $\pm$10 kV. Other MVdc demonstration projects include the underground MVdc grid within the campus infrastructure in Aachen, Germany [79] and the MVdc system in an industrial area of Shenzhen, China [80].

Although the above projects demonstrate different MVdc technologies, the selection of VSCs for these applications were largely project dependent and varies case by case. A general MVdc converter design and optimal selection principle considering reliability, efficiency and economics are not yet considered in the open literature.

Very few researches were focused on the selection of VSC on medium voltage (MV) applications with dc solutions. In [81], the feasibility of utilising MMC and 3L-NPC for battery energy storage applications at 10 kV dc was evaluated based on efficiency and capital investment. However, the long term investment benefits or redundant designs were not been investigated. Redundant designs are required for the secure and economic operation of converters [82]. At LV levels, topology reliability is not much of a concern due to lower repair times and financial loss is comparatively minimal. Thus, the n+1

redundant design approach is used [72]. However, at HVdc levels, the unavailability of converters may cause high revenue losses and redundancy is an important aspect. The benefits of using active redundant sub modules (SM)s for improving the reliability of MMCs have been discussed in [83]. However, the optimal redundancy level has not been considered in any of these studies.

2.5.5 The Reliability of DC Collection System Configurations

As discussed above, network reliability is one of the prime factors that is essential to consider in identifying a suitable network topology. In the context of selection of a viable dc collection system option, this is equally important.

In [84], different candidate dc wind farm topologies were evaluated based on system losses, reliability, and costs. This analysis intended to identify dc series and series-parallel wind farms as lucrative options. The RBD based analytical method was used in this analysis to compare the load point reliability parameters such as expected energy not served (EENS), annual interruption frequency, annual interruption duration. However, a detailed availability analysis considering the stochastic behaviours of wind speed was not taken into account.

In [85], the same RBD technique was used to evaluate dc wind farm reliabilities at the load point. It was concluded that series-parallel connection has higher reliability. It was also identified that the redundancies in transmission and collection system could be a worthy investment due to the possibility of significant additional income generation at the expense of capital cost. In general, fault handling is a major challenge in dc systems and is also an important issue for dc-series collection systems. In this configuration, the dcWT internal faults could be handled with a bypass diode, but, for collection system faults one possible option is to de-energise the stack of dcWTs that are connected in series.

The string failure issue (the requirement to forced shutdown of the whole string) of the dc series-parallel topology due to failure of one or more series connected dcWTs can be eliminated by using the matrix topology [86]. The proposed topology benefits from the extra connection paths between the branches that allow the reconfiguration of the collector system following failure conditions. Proper topology change mitigates the overvoltage of units upon failure occurrences and enhances the efficiency of the wind farm. Although the matrix topology enhances the reliability of series-parallel configuration, additional control complexity and higher CAPEX are some disadvantages.

Although the few published works find in the open literature considers reliability as a deciding factor to identify a suitable dc collection system, the variability of the wind speed or multiple component failures has not been considered. In this regard, a detailed evaluation of the reliability of candidate dc collection system topologies considering associate economic factors is yet to exploit.

2.6 Overall Offshore Wind Farm Reliability Assessment including the Medium Voltage Cable Network

An OWF is composed of a large number of components, e.g., wind turbines, inter-array cables, busbars, converters, transformers, etc. All these components are comprised of several subsystems, e.g., a typical type-four wind turbine consists of a generator, drive-train and power converter subsystem. Generally, these subsystems are subject to competing risks, i.e., have different failure characteristics and corresponding repair rates, each with a distinct impact on the components' availability.

Further, the OWF collection system is made up of a considerable number of inter-array cables. The effectiveness of the OWF to export energy to the grid depends on the availability of that network. Therefore, it is imperative to include the reliability of the collection system in the overall availability assessment. However, this increases the number of components significantly, introducing the dimension curse. This combined with wind turbine output dependence makes the inclusion of the collection system in OWF availability assessment computationally intractable.

In probabilistic reliability assessment of OWFs, the variability of wind speed and stochastic failure nature of all the associated components must be taken into account. In this regard, the availability assessment of large-scale offshore wind farms required to consider the (a) reliability of individual collector system cables, (b) reliability of individual wind turbines, and (c) output of wind turbines dependent on a single stochastic source: the wind, geographically distributed over the network. However, the existing literature considered only two aspects of the above. The work can be classified which accounts:

1. independent sources, geographically distributed over a network, i.e., including features (a) and (b), and

2. dependent sources without considering the network, i.e., including features (b) and (c).

In general, conventional generators are driven by independent inputs. For instance, in hydropower plants, a synchronous generator requires adequate water resource to generate electricity. In contrast, WTs can also be considered to operate in a similar manner but with some probabilistic distribution of wind [87]. Electric power cables are the backbone of an OWF collection system. A single point of failure can lead to a strongly undesired contingency. Therefore, it is necessary to include the stochastic failure nature of the sub-sea cables in the reliability problem. In [88], [89] the offshore sub-sea cable failure has been considered for cable network optimisation. The main objective of these studies was to minimise the overall cable investment cost. The reliability problem has been solved using a two-stage scenario tree technique and each system state assumed to have at most one component unavailable. However, when network dependency is considered this assumption is no longer valid.

In [90], RBD and minimal path technique based method has been used to evaluate the reliability of a hypothetical OWF network. Further, the network reduction technique has been considered in [91] to evaluate different OWF topologies. However, collector system cables have been considered as independent components and the network dependency or multiple failure events have not been considered. The independent assumption of cable failures without properly defining their dependencies can cause calculation errors. Further, to represent the detailed availability levels of an OWF using a reliability index, for example, with generation ratio availability (GRA), multiple failures of components are required to consider.

To evaluate the reliability of an OWF (and subsequently calculate their availability levels) (a) the chronological simulation method [92, 93] or (b) the analytical methods based on RBDs [94] and Markov chain models [95] can be used. Among the chronological simulation methods, MCS technique has been used in [93], for economics- and reliability-evaluation of OWFs considering the cable with 1000 iterations. A sequential MCS technique has been proposed in [96] for reliability assessment of OWF using a new synthetic wind-speed generator. In [97], the same technique has been used for evaluation of reliabilities of different offshore HVdc grid configuration options. This chronological method under Markovian assumption (Markov chain MCS) has been used in [92] to evaluate the reliability of OWFs considering severe weather conditions. The Markov property means that evolution of the Markov process in the future depends only on the present state and does not depend on past history. The Markov process does not remember the past if the present state is given. Hence, the Markov process is called the process with memoryless property. However, with the increase of the number of system components, the

cardinality of the overall state space becomes too large and the use of such chronological simulation methods to assess the availability levels of OWF collection systems are computationally inefficient.

2.6.1 Multi-State System Modelling of Offshore Wind Plants

Incorporating variability of wind speed combining the WT failures in the reliability assessment has been well addressed in the literature. The importance of the use of multi-state wind speed models for wind farm reliability assessment was first proposed in [98]. To obtain a finite number of multi-state WT outputs from measured time-series data, different clustering techniques based on minimum Euclidean distance can be used [98]. In [87, 99], further improvements have been made incorporating the wind speed variability together with WT failure rates when evaluating the reliability of an OWF. However, the inter-array cable network reliability has not been considered in any of these previous studies.

The influence of environmental effects on the reliability of OWFs has been evaluated using the common-cause failure method in [100]. The failure causes due to continuous operation of an OWF under higher wind speed conditions have been considered. However, this analysis only considered the first-order component failures and neither network dependency nor the wind speed stochasticity has not been taken into account.

In [101], a multi-state systems (MSS)-WT model has been developed based on the COPT to calculate frequency-based reliability indexes. However, network reliability is not included in this COPT approach. Alternatively, in [98, 99] an analytical method based on binary birth-death Markov process has been used for reliability assessment of wind farms including the multi-state wind farm output. In addition to the Markov model, Auto Regressive Moving Average (ARMA) model is another useful tool which can be used for reliability modelling of wind farms chronologically [102]. However, heavy computation overhead and dependency on a large amount of wind speed data for training ARMA parameters are some of the inherent drawbacks. In all of these works, the WT has been modelled with binary birth-death Markov process and inter-array cable network reliability has not been considered. However, when using average failure and repair rates in binary birth-death Markov reliability modelling, information on individual failure and repair rates of component sub-assemblies are required.

2.7 Summary

The state-of-the-art offshore wind farm technology is discussed in this chapter. It can be seen that with the increasing capacity of single WT size improving the power density and electrical losses minimisation is essential. However, due to technological maturity, only ac technology is being used at the OWF collection system level. On the contrary, several techno-economic analyses showed that the use of dc technology is beneficial for large scale OWFs.

In assessing the overall technology readiness level of a new concept, reliability is one of the key factors to consider. First, it requires evaluating the reliability of the power generating source of the offshore wind collection system i.e., dcWT. Then, the reliability of other key components of the all-dc OWF collection system needs to be studied. Finally, identification and selection of a pertinent dc collection system topology which is reliable and economical are important.

Particularly, more attention is necessary to be paid to component level to the system level reliability assessment of this OWF-MVdc technology which is an under-researched topic.

The research work in this thesis investigated the above problems and proposed relevant solutions.

Chapter 3

Lifetime Estimation of dc-Wind Turbines

3.1 Introduction

One of the key building blocks of a dc collection system is a dcWT. In section 2.2.4, different configurations of dcWT topologies have been discussed based on [17, 18]. Mainly they are classified according to the number of conversion stages assuming the state-of-the-art wind generators are employed. Minimum number of components, simplicity and galvanic isolation together with low technological risk are the important factors to be considered when selecting a suitable dcWT topology.

When proposing a new technology, capability and adaptability of utilising the existing technology will reduce the associated technological risk. With regard to the acWT technology, majority of the offshore WTs are constructed with variable speed PMSG due to benefits such as compact in size, no requirement of external power supply for magnetic field excitation, robust construction and less maintenance compared to classical asynchronous wind generators. Among the different dcWT topologies discussed in section 2.2.4, concept-(e) is considered to be less technological risk than the other proposed configurations.

An OWF is supposed to operate between 20-25 years [103]. Although random failures are unavoidable, the average lifetime of components should be at least within the operating period. Therefore, when introducing a new technology it is of utmost important to observe their healthy operating period. In general, the lifespan of a wind power system is highly influenced by the reliable operation of its power converters. Therefore, it

is imperative to analyse the component level reliabilities of main building blocks (IGBTs and diodes) of the dcWT. A mission-profile based reliability assessment technique considering long-term and short-term thermal cycles is proposed to evaluate the annual damage of this dcWT configuration. The annual accumulated damage for power semiconductors, which is regarded as B_{10} lifetime (a measurement of the time by which ten percent of a population of semiconductors have failed), the overall failure tendency profile for one power component still needs to be generated using a Monte Carlo method. In this chapter, the lifetime of a DAB based dcWT is investigated based on a specific mission-profile.

3.2 Methodology

3.2.1 Long- and Short- term Thermal Cycles under a Mission Profile

Generally, the lifetime estimation of a WT power converter is mainly evaluated according to the long-term thermal cycles [60]. However, as shown in Fig. 3.1, the wind-speed is considered to remain at a number of steady-state values at different sampling points, and the long-term thermal cycles are calculated during each sampling interval. Although the sampling time is fairly shorter, it has been shown that high-frequency junction temperature fluctuations exist in the chip of the power module in the converter [104]. This high-frequency junction temperature fluctuation is introduced by the alternating current through the power converter, which leads to the conduction of power devices. Therefore, calculating only the long-term thermal cycles will not yield the accurate results since it is unknown which of the two thermal cycles dominates in the converter reliability.

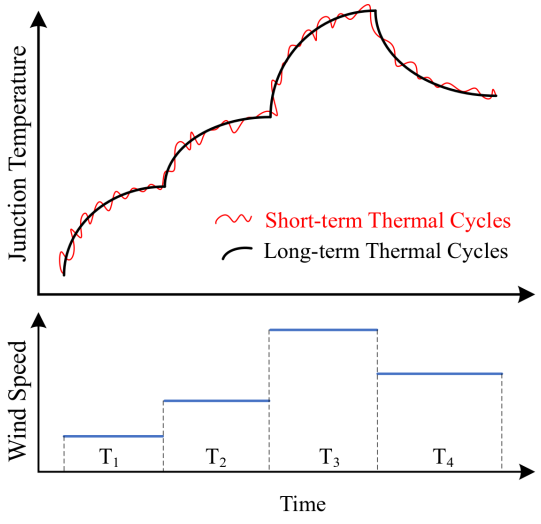

Fig. 3.1. The long- and short- term thermal cycles under a mission profile.

3.2.2 Reliability evaluation of semiconductors of a dcWT with long-term thermal cycles

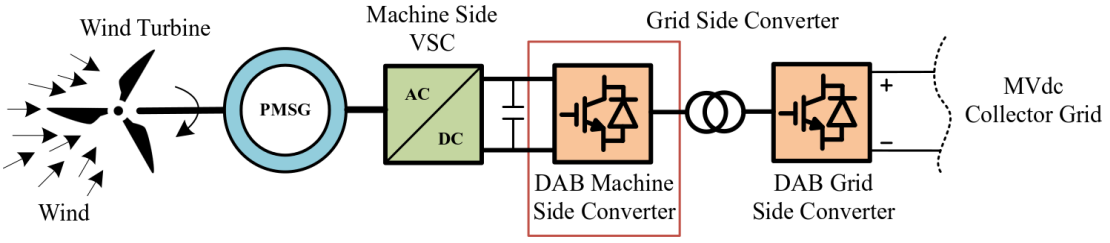

Fig. 3.2. Dual active bridge based dc wind turbine system.

The configuration of a DAB based dcWT power generation system is shown in Fig. 3.2. It can be seen that a dual active bridge power converter consists of a MSC and a GSC coupled through a medium frequency ac-link. The MSC and GSC converters can be configured as single- or three- phase full bridges. However, the use of three-phase configuration is beneficial in terms of transferring more energy with just additional two extra switches.

Additionally, the medium frequency ac transformer serves two purposes, (1) provides the galvanic isolation between the MVdc grid and the wind turbine, and (2) step-up the ac voltage to match with the required modulation index of the GSC. As discussed in [67], the component current dominates in the MSC. Thus, this work mainly focuses on the reliability analysis of the DAB-MSC. A similar approach can be expanded to the GSC following the same methodology. In here, a 10 MW dcWT with parameters provided in Table 3.1 was considered as a case study. In this analysis Vestas V164-9.5 power curve parameters had been referred to obtain the dcWT power output. Further, ABB 5SNA-1000G650300 IGBT module had been used for DAB power electronic switches.

Table 3.1. Parameters of the dc wind turbine.

Parameter	Value
Rated Power	10 MW
Cut-in wind speed	3.5 m/s
Rated wind speed	14 m/s
Cut-off wind speed	25 m/s
DAB switching frequency	10 kHz
DAB primary voltage	6 kV
DAB secondary voltage	24 kV
DAB IGBT rated parameters	1 kA/ 6.5 kV
IGBT de-rating factor	56%

3.2.3 Control of a DAB based dcWT

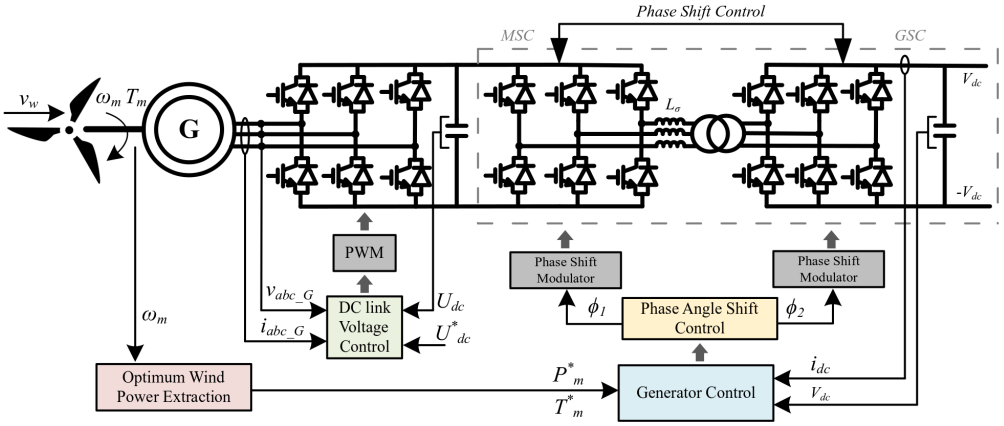

Fig. 3.3. Control of a DAB based dc wind turbine.

The control and operation of a conventional variable speed full-scale offshore wind turbine in which the generator output is connected through a back-to-back (ac/dc/ac) converter was discussed in 2.2.1. On the contrary, the dcWT output voltage could increase between 10kVdc and 50kVdc using a dc/dc converter. The control schematic of a typical grid connected PMSG based full-scale dcWT is shown in Fig. 3.3. The control objectives of a PMSG based full-scale dcWT are:

(a) **Optimum wind power extraction**
Similar to PMSG based full-scale acWT it provides the necessary power (P*m) or torque reference (T*m) to extract the maximum wind energy. The optimal reference value depends on the rotor speed, wind speed, and pitch angle.

(b) **DC link voltage control**
The machine side VSC is responsible for maintaining a constant dc link voltage. The control objective is achieved by the vector control with an outer loop that regulates the dc voltage through a PI controller and an inner loop that controls the current.

(c) **Generator control**
The dc/dc converter controls the power output of the wind turbine which is based on phase-shift control mode. As discussed in [42], the maximum power is achieved at a phase angle of 90°. Although both hard- and soft- switching modes can be used, with high dc transformation ratios the GSC is required to operate under hard switching conditions with partial loads.

Since in an offshore wind farm partial load conditions occur quite often, the main focus of this work is to observe the lifetime of MSC of dcWT under hard switching mode.

3.2.4 B_{10} Lifetime Estimation under Long-term Thermal Cycles

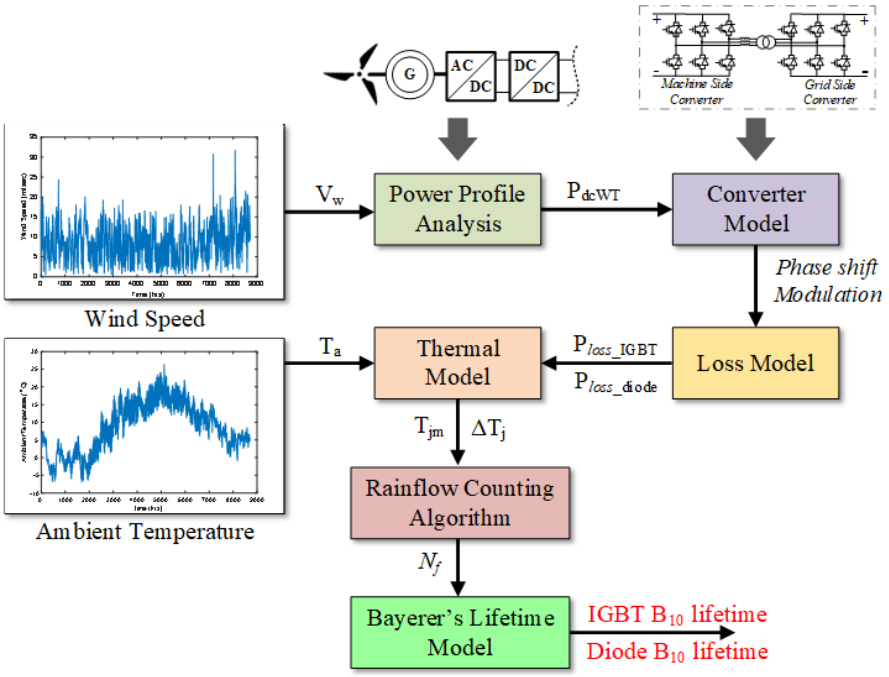

Fig. 3.4. Flowchart to calculate B_{10} lifetime of IGBT and diode under real-time wind speed and ambient temperature under long-term thermal cycles.

To determine the total availability in a wind turbine system a detailed analysis is required. When calculating B_{10} lifetime of power electronic components for a certain mission profile (such as wind speed distribution and wind class) with average 10 minutes sample rate, (a) a simplified circuit model, (b) a loss model, and (c) a thermal model of the active power switches are required. According to the long-term electrothermal profile, the percentile lifetime of a single component can be predicted. An overall flowchart for the estimation of power semiconductor B_{10} lifetime of the DAB-MSC is illustrated in Fig. 3.4.

The procedure starts with the calculation of the dcWT power output profile P_{dcWT} using the time series wind speed data V_w. In this analysis also the wind speed data had been obtained from Anholt wind farm [105]. With the help of the dcWT-DAB model and the loss model of the power electronic components, the loss dissipation of the IGBT P_{loss_IGBT} and the diode P_{loss_diode} were calculated according to the loading profile of the power converter. Based on the thermal model of the power module, the thermal profile of the power semiconductors can be calculated in terms of the mean junction temperature T_{jm} and the junction temperature fluctuation ΔT_j.

Next, the power cycles of the power semiconductor N_f can be obtained using the rainflow counting algorithm. (The rainflow counting algorithm is used in the analysis of fatigue data in order to reduce a spectrum of varying stress into an equivalent set of simple stress

reversals. In other words, to predict the life of a component subjected to a variable load history, this method can be applied to determine the number of fatigue cycles present in that load-time history.) Finally, the Bayerer's lifetime model which is an improved version of Coffin–Manson model that generally uses for fatigue analysis was used to estimate the the B_{10} lifetime of the key building blocks of dcWT-DAB. The Bayerer's lifetime model can be represented by:

$$N_{f_{(\mathrm{diode}/IGBT)}} = A \cdot dT_{j_{(\mathrm{diode}/IGBT)}}^{\beta_1} \cdot e^{\left(\frac{\beta_2}{T_{jm_{(\mathrm{diode}/IGBT)}}+273}\right)} \cdot t_{on}^{\beta_1} \tag{3.1}$$

wherein, N_f, T_{jm} and dT_j represent the number of power cycles to failure, the mean junction temperature, and the junction temperature fluctuation, respectively; subscript "diode" and "IGBT" denote the value for diode and IGBT, respectively; t_{on} is the on-state time, and $A, \beta_1, \beta_2, \beta_3$ are fitted coefficients which have been obtained by referring to the parameters available in [106].

(a) *Calculation of Semiconductor Losses and Thermal Model*

To evaluate the semiconductor losses, the PLECS software tool was used which is based on multi-dimensional lookup tables on manufacturer information at various semiconductor junction temperatures. For the losses analysis conducted, the ambient temperature at Anholt wind farm for the concerned period was used [105]. Combined with the real-time ambient temperature, the junction temperature of each component was estimated from the thermal models. In here, the thermal impedances of power semiconductors and air-cooling system were considered, with an industrial Foster thermal structure. The key thermal specifications are shown in Table 3.2.

Table 3.2. Key parameters of thermal model.

Parameter	**IGBT**	**Diode**	**Air Cooling System**
Thermal Resistance (x10^{-3} K/W)	1^{st} layer 9.00 2^{nd} layer 2.35	1^{st} layer 1.95 2^{nd} layer 6.11	1^{st} layer 6.60
	3^{rd} layer 4.84 4^{th} layer 1.68	3^{rd} layer 5.90 4^{th} layer 2.06	2^{nd} layer 19.5
Thermal time constant (s)	1^{st} layer 3.609 2^{nd} layer 0.364	1^{st} layer 2.283 2^{nd} layer 0.16	1^{st} layer 17.93
	3^{rd} layer 0.0510 4^{th} layer 0.0037	3^{rd} layer 0.032 4^{th} layer 0.0027	2^{nd} layer 5.27

3.2.5 B_{10} Lifetime Estimation under Short-term Thermal Cycles

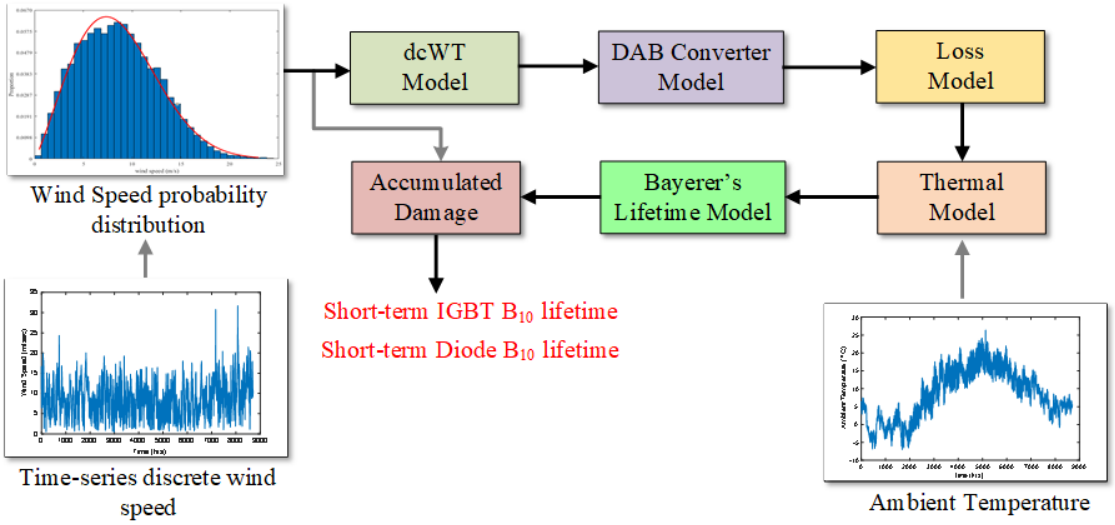

Fig. 3.5. Flowchart to calculate B_{10} lifetime of IGBT and diode under real-time wind speed and ambient temperature under short-term thermal cycles.

As indicated in Fig. 3.1, short-term thermal cycles in thermal profile are mainly related to the fundamental switching frequency of DAB. Although a relative short period is selected to sample the real-time wind speed and ambient temperature, the frequency of fluctuations caused by short-term thermal cycles cannot be reflected by the long-term thermal cycle based calculation. However, the reliability evaluation under short-term thermal cycle shares the same group of key parameters that of the long-term thermal cycle based evaluation. The flowchart of lifetime calculation for the power semiconductors under the short-term thermals cycle is shown in Fig. 3.5.

The short-term thermal cycle based semiconductor lifetime was obtained using the one-year wind speed Weibull distribution via a similar process without the Rainflow counting algorithm. This is because, in this case, the lifetime power cycles can be obtained directly under different wind speeds [65]. The cycle frequency is related to the fundamental switching frequency of DAB which is several kHz. It is worth to note that, in the thermal model, besides the temperature rise due to the loss dissipation of components, the ambient temperature should also be considered and added to obtain the chip junction temperature.

In the calculation process presented in Fig. 3.5, the input Weibull wind speed distribution is a statistical result generated from the annual real-time wind speed. In this distribution, the lowest speed was the same as turbine cut-in speed of 3.5 m/s and the highest speed was the same as the turbine cut-off speed of 25 m/s, from the lowest to the highest speed, a resolution of 0.68 m/s (bin width in histogram) was selected to obtain discrete speed

statistical results. By dividing the total wind speed sampling amounts with each speed statistical results, the proportion factor for each speed value can be obtained. Afterwards, based on a Bayerer's model, total B_{10} lifetimes of IGBT and diode under different wind speeds are calculated and the annual accumulation damage can be estimated according to the wind speed distribution.

3.2.6 Assumptions made when estimating the lifetime

The power electronic reliability involves multidisciplinary knowledge, which covers (a) analytical physics to understand the failure mechanisms of power electronic products, and (b) the design for reliability and robustness validation process to build up reliability and sufficient robustness during the development process of the power electronic device. Thus, the lifetime estimation of power semiconductor devices involves several stages and not a straightforward task. The following assumptions are made.

(a) Although the bond-wire liftoff and the soldering cracks between the different layers occur frequently in power modules due to fatigue [107], a unified failure mechanism was assumed in this study.

(b) The Miner's rule was used for the lifetime calculation, which means that a linear damage accumulation in the fatigue was assumed, and the component parameters will seldom deviate along with the system operation.

(c) As most of the manufacturers cannot provide the numbers of power cycling with small temperature swing and high cycling frequency, extended data are obtained through the Bayerer's lifetime model [106].

3.3 Results

The B_{10} lifetime of the IGBT and diode can be estimated by summing the long-term and short-term thermal cycle based component lifetime. This is because for the long-term thermal cycle, the wind speed is regarded as a constant value between two adjacent sampling points. Considering the limitation of the measurement equipment, minimum sampling period is usually at least several minutes. However, owing to the alternating current through the DAB, high frequency junction temperature fluctuation exists on the smooth junction temperature profile obtained by the short-term thermal cycle, and the frequency of these fluctuations is related to the fundamental current applied to the DAB medium frequency transformer.

3.3.1 Long-term thermal cycles

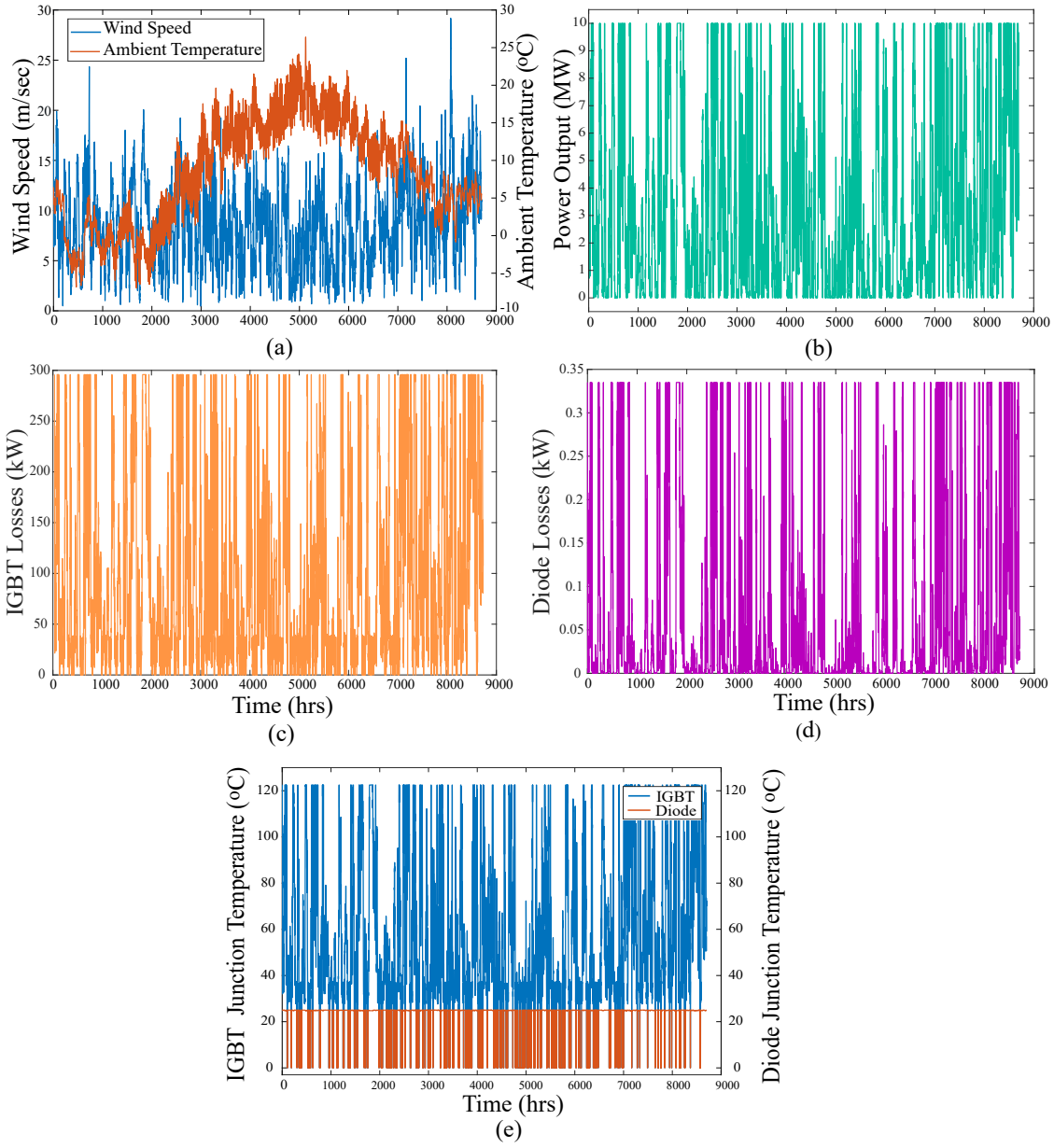

Fig. 3.6. Results of the long-term thermal cycle based lifetime estimation: (a) Wind speed and ambient temperature; (b) Turbine output power; (c) Total loss for IGBT; (d) Total loss for diode; (e) Junction temperature for IGBT and diode.

Fig. 3.6, illustrates the results of the long-term thermal cycle based lifetime estimation of dcWT. The total semiconductor losses of IGBT is relatively larger compared to the diode due to higher conduction time with higher switching frequency and modulation method used. This was also reflected with the lower junction temperatures fluctuations of the diode compared to the IGBT for the same mission profile as shown in Fig. 3.6(e).

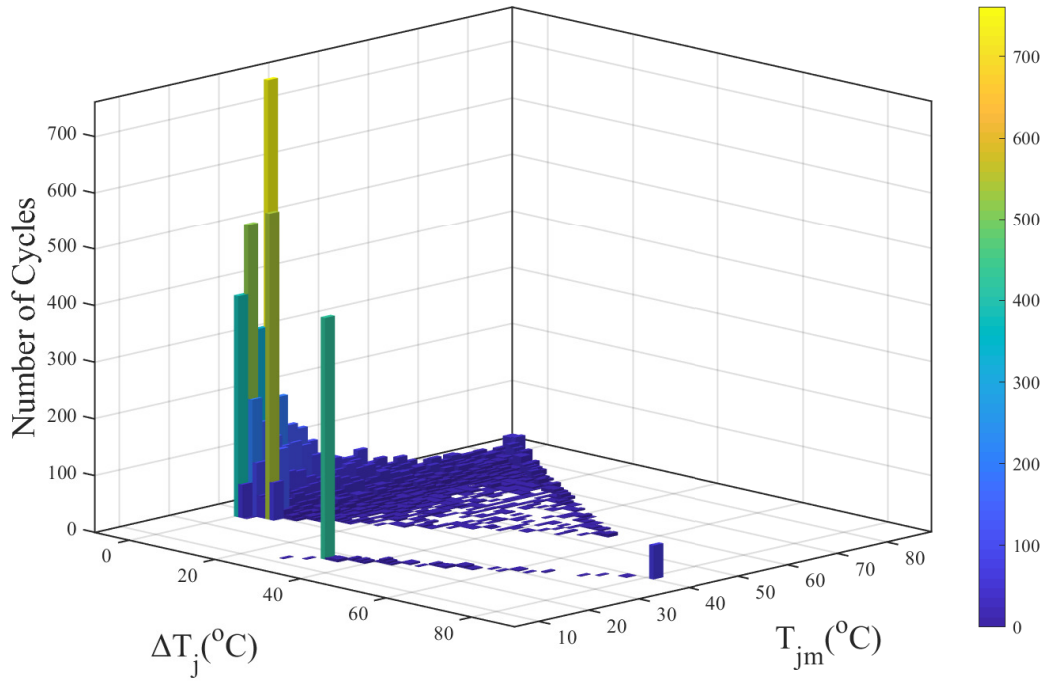

Fig. 3.7. Rainflow counting results for IGBT.

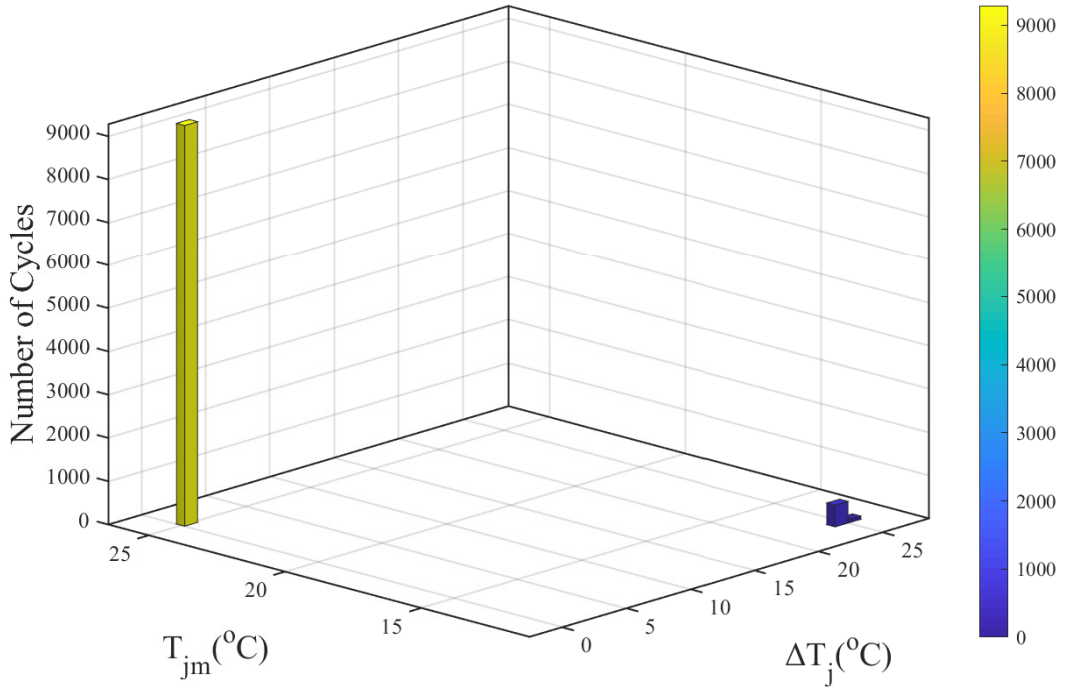

Fig. 3.8. Rainflow counting results for diode.

The corresponding mean junction temperatures, junction temperature fluctuations and thermal cycle periods of the IGBT and diode can be extracted using the Rainflow counting algorithm as shown in Fig. 3.7 and Fig. 3.8. Notably, the distribution of mean junction temperatures, junction temperature fluctuations of IGBT is quite wider compared to the diode. One reason is the conduction time of diode with high frequency switching is quite lower compared to the IGBT and hence the junction temperature fluctuations are quite low. There are 10382 and 9866 total thermal cycles of the IGBT and the diode, respectively.

Similarly, the damage due to short-term thermal cycles cab be obtained with the method discussed in Section 3.2.5.

3.3.2 Calculation of Accumulated Damage

There are various kinds of cumulative damage models in the literature for the reliability engineering assessment, as discussed in [108]. For the lifetime prediction of IGBT modules, the most widely used one is the Miner's rule, which is a linear cumulative damage model. The assumption of Miner's rule is that the damage of the IGBT modules is independent of the stresses experienced during its life cycle, that is, the order of the cyclic thermal stresses.

To calculate the accumulated damage due to long-term temperature cycles, Rainflow method can be used as discussed in Section 3.2.4. Since the wind speed does not follow a repetitive pattern in terms of amplitude and duration, the cycle counting principle was applied in this study. The linear cumulative damage model was applied to obtain the lifetime consumption due to low-frequency thermal cycling given by:

$$\text{Damage}_{\text{LT}} = \sum_i \frac{n_{i,\text{LT}}}{N_{i,\text{LT}}} \tag{3.2}$$

where $n_{i,\text{LT}}$ is the number of cycles due to long-term thermal cycling and $N_{i,\text{LT}}$ is the number of cycles to failure for the same cycle type and same stress as n_{LT}.

Similarly, the accumulated damage due to short-term power cycles at the frequency of 10 kHz was obtained by:

$$\text{Damage}_{\text{ST}} = \sum_i \frac{n_{i,\text{ST}}}{N_{i,\text{ST}}} \tag{3.3}$$

where $n_{i,ST}$ is the number of temperature cycles due to the short-term cycling and $N_{i,ST}$ is the number of cycles to failure for the same cycle type and same stress as $n_{i,ST}$. The number of cycles to failure has been calculated based on (3.1) considering the load variations coming from the given wind mission profile. The junction temperature and its

fluctuation were extracted from the mission profile for each measurement point. Finally, the total damage was calculated with:

$$\text{Total Damage} \;=\; \text{Damage}_{\,LT} + \;\text{Damage}_{\,\text{ST}} \tag{3.4}$$

Table 3.3 summarises the accumulated damage and lifetime consumption of IGBT and diode of dcWT DAB-MSC.

Table 3.3. Accumulated damage per year due to power cycling and thermal cycling.

Component	**Accumulated Damage**	**Lifetime Consumption**
IGBT	0.00718	0.718%
Diode	0.00083	0.083%

3.3.3 Variances in Parameters

Although all these coefficients are statistically fitted and chosen as constants to simplify the calculations, uncertainties for these parameters still exist. It was assumed that all these coefficients were under a standard normal distribution and have 5% variations to their centre values; thus, the probability density functions (PDFs) of parameters A, β_1, β_2, and β_3 in (3.1) as shown in Fig. 3.9 were referred [106].

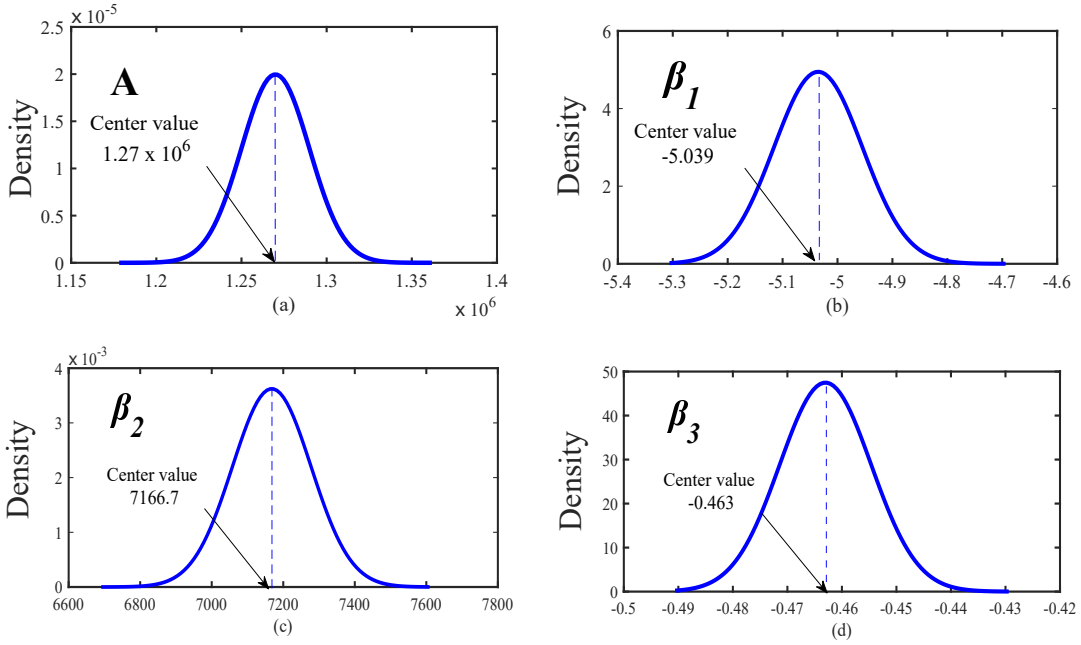

Fig. 3.9. Normal PDFs for coefficients in Bayerer's lifetime model (a) A, (b) β_1, (c) β_2, (d) β_3.

The variations of mean junction temperature T_{jm} and junction temperature fluctuation dT_j in Bayerer's lifetime model (related to the thermal stress parameters) are induced by the manufacturing process. In this analysis, normal distributions with 5% variations were also applied to describe temperature related parameters in IGBT and diode as shown in Fig. 3.10.

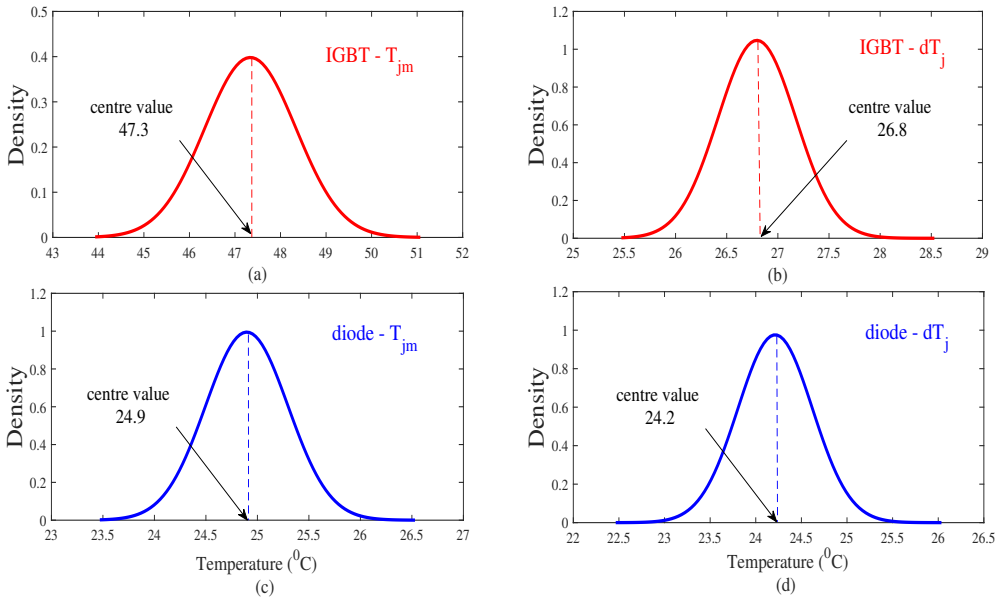

Fig. 3.10. Normal PDFs for thermal stress related parameters in Bayerer's lifetime model (a) mean junction temperature for IGBT, (b) junction temperature fluctuation for IGBT, (c) mean junction temperature for diode, (d) junction temperature fluctuation for diode.

Considering variations of all the parameters into account, a 10,000 sampling Monte Carlo method was utilised to analyse the failure and lifetime distributions for IGBT and diode. The annual damages for one IGBT component and one diode component can be obtained by referring to (3.4). Based on the aforementioned calculations, the lifetime consumption for IGBT and diode under both long-term and short-term thermal cycles are 0.00718 and 0.00083, respectively. Moreover, Weibull distributions are universally used to describe the failure and lifetime (reciprocal of the failure rate) data for power semiconductors. The component-level reliability profiles for IGBT and diode of dcWT-DAB can be illustrated as Fig. 3.11.

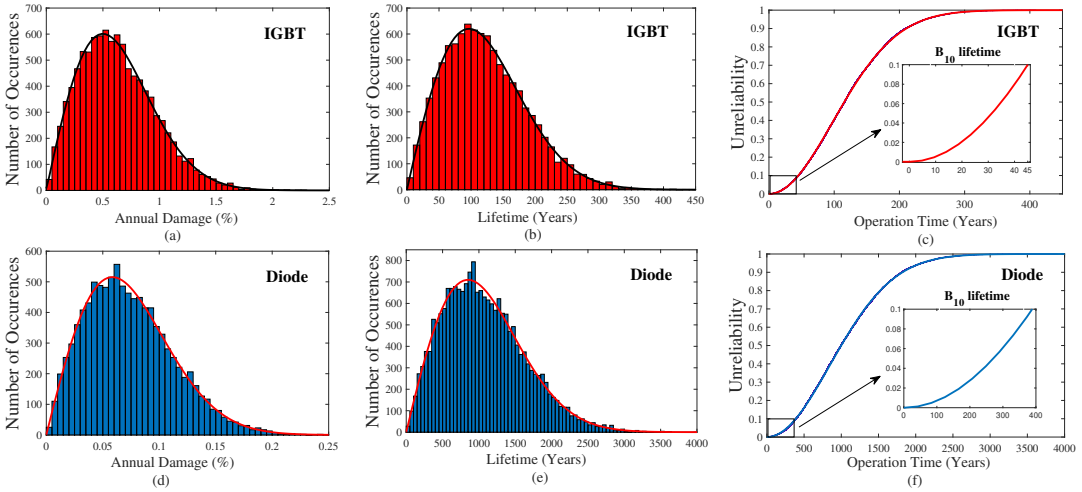

Fig. 3.11. (a) Annual damage Weibull distribution for IGBT; (b) lifetime Weibull distribution for IGBT; (c) unreliability for IGBT; (d) annual damage Weibull distribution for diode; (e) lifetime Weibull distribution for diode; (f) unreliability for diode.

In Fig. 3.11(c) and (f), the failure rate cumulative distribution functions for IGBT and diode were obtained integrating the damage PDFs of diode and IGBT in Fig. 3.11(a) and (d), respectively. It can be observed that for IGBT and diode, the B_{10} lifetime were about 45 years and 384 years, respectively, which are highly over the typical life of an OWF.

3.3.4 Impact of Switching Frequency

To observe the variation of B_{10} lifetime with respect to switching frequency of DAB, the same methodology was repeated form 10 kHz to 1 kHz. As shown in Fig. 3.12, with the decrease of the switching frequency, the expected lifetime of both IGBT and diode of DAB-MSC have been increased. This is due to the fact that, at lower switching frequencies the mean junction temperature variations were relatively lower compared to that of higher switching frequencies.

The B_{10} lifetime of IGBT at 8 kHz and 4 kHz are 68-years and 86-years, respectively. For the same switching frequencies the diode B_{10} lifetime are 563-years and 831-years, respectively. Notably, at 1 kHz the lifetime of IGBT and diode was improved by a factor of 2.5 and 2.9, respectively.

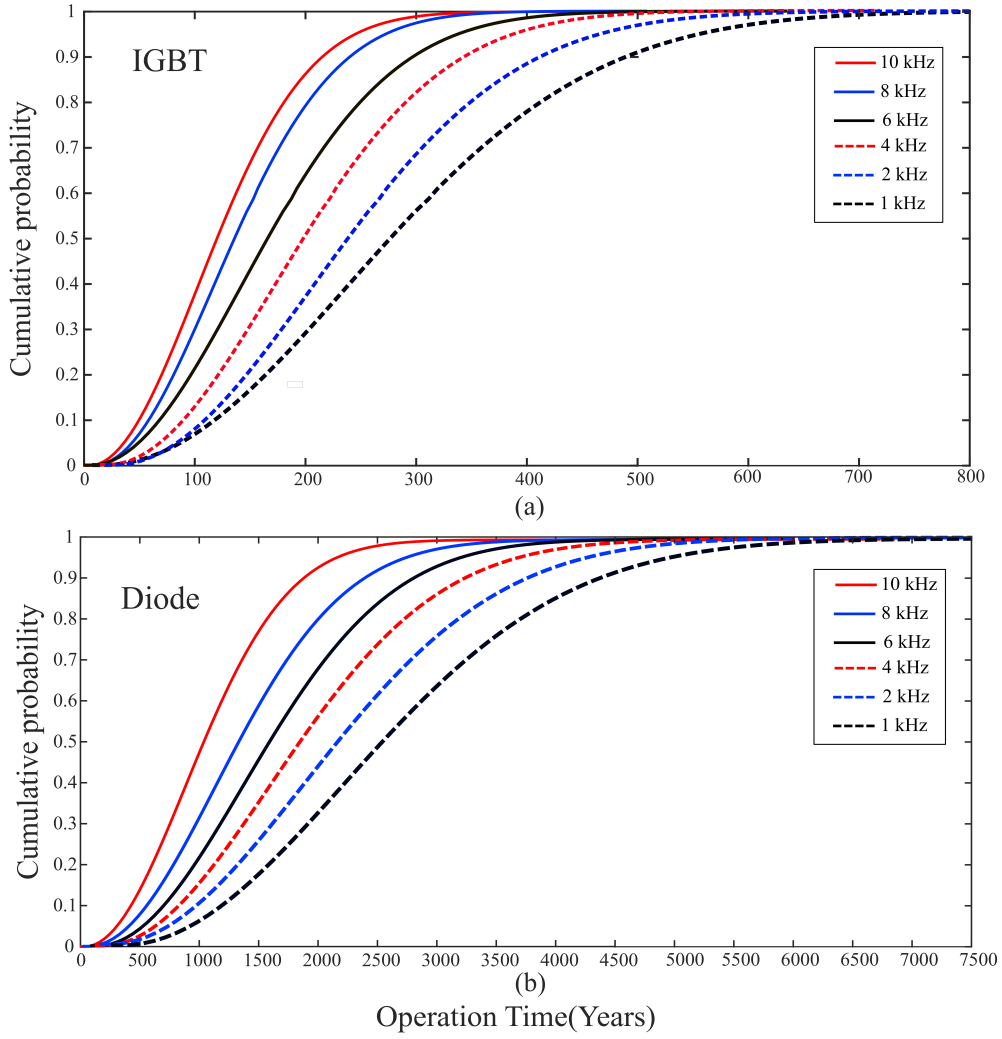

Fig. 3.12. Unreliability of semiconductors over different switching frequencies (a) IGBT; (b) diode.

3.4 Summary

In this chapter, the lifetime of a dual active bridge based dcWT semiconductors was investigated. A methodology based on long- and short- term thermal cycles under a specific mission profile was proposed to estimate B_{10} lifetime of IGBT and diode of machine side converter of DAB. First, the translation from the mission profile to power output was achieved based on of dcWT modelling. Afterwards, a simplified approach to calculate the loss profile and the thermal profile was used to determine the most stressed power semiconductors (the IGBT and/or the freewheeling diode). Finally, according to the modelling of the B_{10} lifetime power cycles, the lifespan of semiconductors were deduced. The results showed that the use of lower switching frequencies improves the lifespan of semiconductors significantly.

Chapter 4

Selection of Multi-Level MVdc Converters for Offshore DC Collection Systems based on Reliability and Cost

4.1 Introduction

The dc technology has gained considerable interest in the medium voltage applications due to the benefits over the ac counterpart. However, to utilise the full capacity of this development, the selection of a suitable power electronic converter topology is a key aspect. From the pool of VSCs, it is unclear which topology is suitable for multi-megawatt applications at MVdc levels. In Chapter 3, the reliabilities of key building blocks of a dcWT at their component-level was investigated. In this chapter, a selection guideline based on reliability and optimum redundancy levels of VSCs at different MVdc voltage levels at OWF dc collection system level is proposed. This will be combined with other functional factors such as operational efficiency and return-on-investment. Further, in the converter topology assessment, redundancy level needs to be considered due to higher repair times and capital investment. Thus, the identification of the optimal redundancy level is important.

The primary motivation of this study is to investigate the feasibility of utilising suitable multi-level VSC topologies at different MVdc voltage levels. Three candidate multi-level

topologies namely three-level neutral point clamped converter (3L-NPC), modular multi-level converter (MMC) and cascaded 3L-NPC (which is being used for the first MVdc link in the U.K.) have been evaluated over two-level-VSC from ±10 kV to ±50 kV.

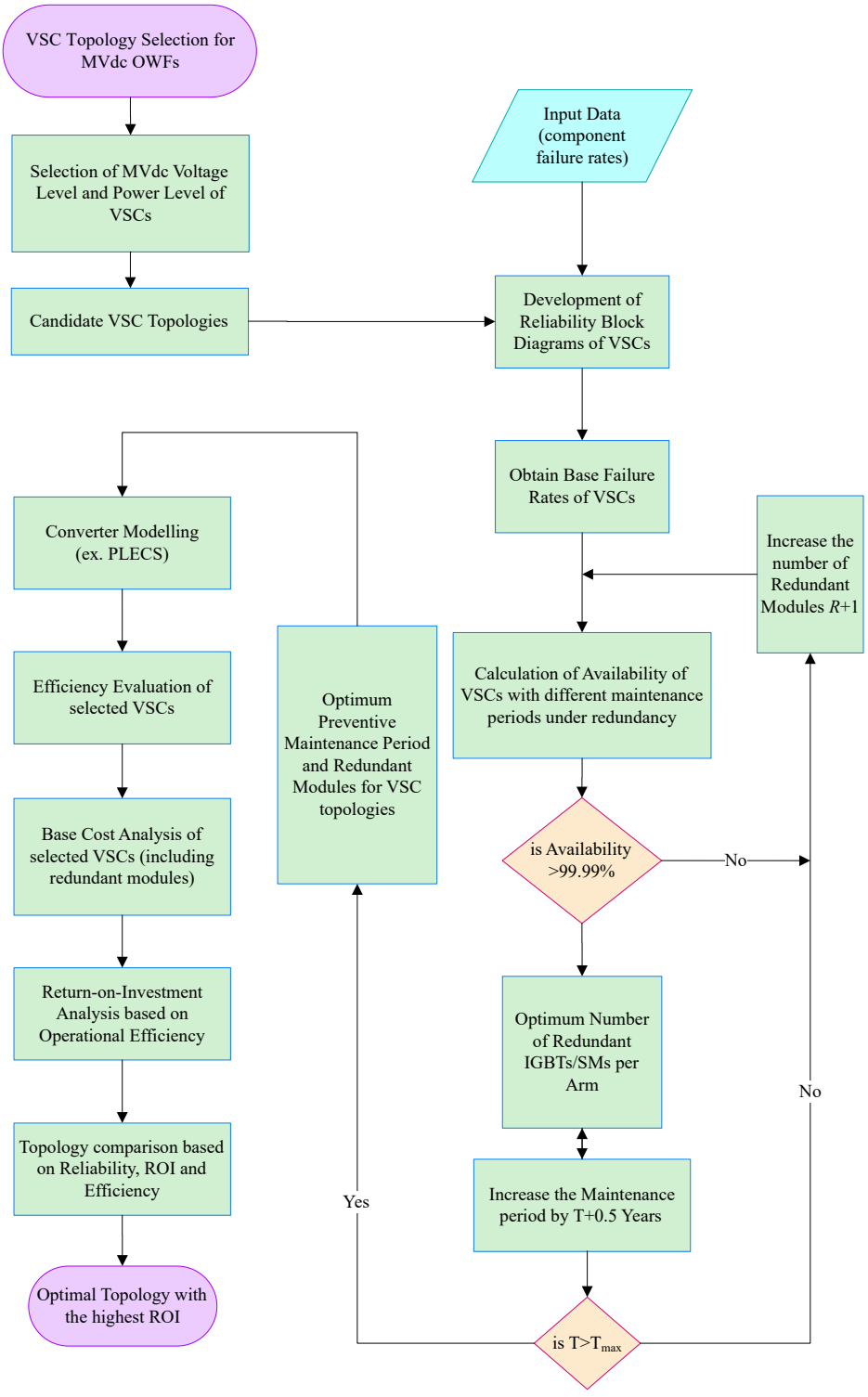

Fig. 4.1. Proposed MVdc topology selection methodology.

4.2 Methodology

As shown in Fig. 4.1, the proposed selection criterion is based on the optimal redundancy level with the consideration of the VSC reliability, preventive maintenance interval, operational efficiency, the total cost of ownership (TCO) and return on investment (ROI). First, the mathematical modelling framework to obtain the optimum number of redundant components of VSCs is introduced. Then, the detailed cost calculation procedure is presented to identify the most appropriate VSC topology at different voltage and power levels.

4.2.1 Reliability of MVdc Converter Topologies

4.2.1.1 Two-level and Three level-NPC

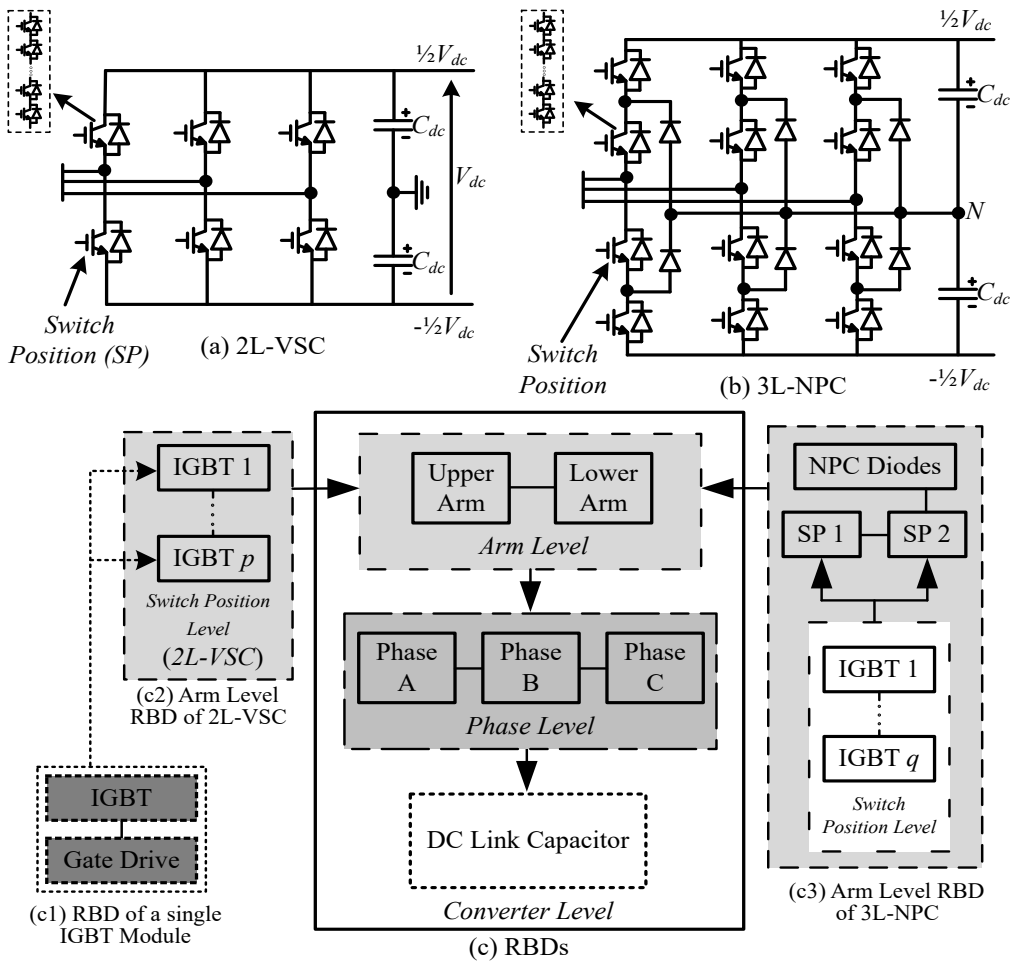

Fig. 4.2. Converter topologies and RBDs of 2L-VSC and 3L-NPC. (a) 2L-VSC; (b) 3L-NPC; (c) RBDs.

For 2L-VSC and 3L-NPC at MVdc voltage levels, the pole-to-pole voltage cannot be withstood by a single IGBT. Thus, series-connected IGBTs are required. Press-pack IGBTs are used for series connection of IGBTs with active redundancy where all the IGBTs are sharing the load [109]. In this study, active redundancy was chosen considering industry practice and concerns over the passive scheme. In this study, the series-connected IGBT group in the arms of 2L-VSC and 3L-NPC is defined as switch position (SP), as shown in Fig. 4.2. Considering the 2L-VSC and 3L-NPC shown in Figs. 4.2(a) and (b), the minimum number (k) of the required IGBT modules per SP can be calculated as:

$$k = \left\lfloor \frac{V_{dc}}{\alpha \times V_{IGBT}} \right\rfloor, \tag{4.1}$$

where V_{dc} is the converter pole-to-pole voltage, α is the number of SPs per arm with α=1 and α=2 refer to 2L-VSC and 3L-NPC, respectively. The IGBT nominal voltage V_{IGBT} is defined as:

$$V_{IGBT} = \eta \times V_D, \tag{4.2}$$

where η and V_D are IGBT module de-rating factor and withstand voltage, respectively. The dc-link capacitor C_{dc} is estimated by:

$$C_{dc} = \frac{2 \times S_{VSC} \times E_S}{V_{dc}^2}, \tag{4.3}$$

where S_{VSC} is the converter MVA rating, E_S is the energy-to-power ratio which is normally between 10-50 kJ/MVA [110].

The converter reliabilities can be obtained using the RBDs. Fig. 4.2(c) shows the hierarchical RBD models of the two topologies. There are different hierarchical levels in the RBDs: SP level, arm-level, phase-level and converter-level. According to the topology of the two converters, all components are required to be in a healthy state for the normal operation. Therefore, all the blocks are in series from the reliability point of view.

4.2.1.2 Cascaded 3L-NPC

Such as cascaded 2L-VSC (used in HVdc applications), 3L-NPC can also be connected in cascaded configuration as shown in Fig. 4.3. One of the practical examples of such configuration is the ANGLE-DC project. It comprises of 12 cells (pole-to-pole), each of which is a 3L-NPC. Each cell is rated for 2.55 MVA with the dc-link voltage of 4.5 kV [111].

A high impedance dc grounding is applied at the converter mid-point to protect the C3L-NPC from earth faults [112]. Therefore, this is a rigid bipolar system without a monopolar operation mode. The required number of components and dc-link capacitance

of each cell can be calculated using (4.1) - (4.3). The hierarchical structure of the RBD of the C3L-NPC is shown in Fig. 4.3.

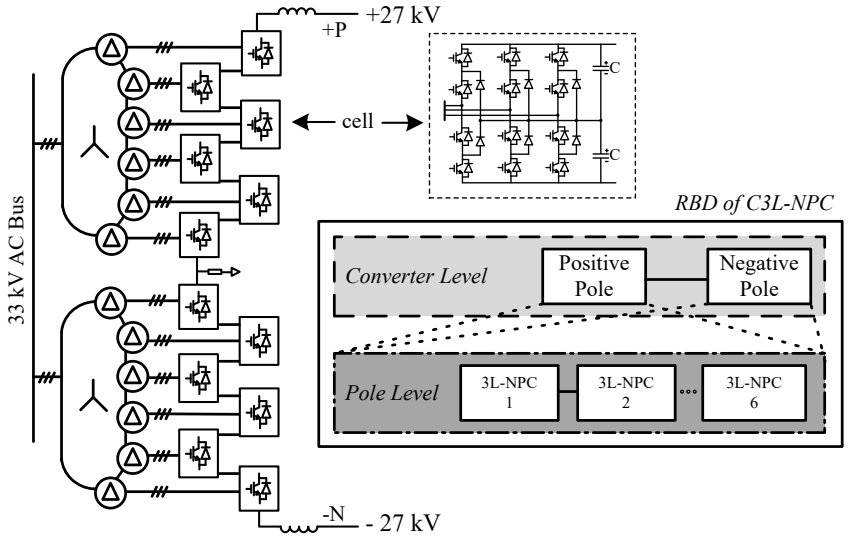

Fig. 4.3. Cascaded 3L-NPC topology and corresponding RBD.

4.2.1.3 MMC

The use of MMC at MVdc voltage level needs to be further justified in terms of reliability, efficiency and return on investment. As the capital cost and power losses of the full-bridge (FB) MMC are higher than the half-bridge (HB) MMC, the FB-MMC may not be an optimal option for MVdc applications. Therefore, only the HB-MMC is investigated in this study, as shown in Fig. 4.4. As illustrated in the RBD of the HB-MMC, the redundant SMs are added at the arm level. To model the reliability of the HB-SM, the reliability blocks of the IGBTs and SM capacitor are connected in series irrespective of the physical configuration.

The minimum number of SMs (k_{SM}) required per arm can be calculated as:

$$k_{SM} = \left\lfloor \frac{V_{dc}}{V_{SM}} \right\rfloor, \tag{4.4}$$

where V_{dc} is the MMC pole-to-pole voltage and V_{SM} is the SM nominal voltage. As defined in [113], the SM capacitance C_{SM} can be calculated as:

$$C_{SM} = \frac{2 \times S_{MMC} \times E_{MMC}}{6 \times n \times V_{SM}^2}, \tag{4.5}$$

where S_{MMC} is the nominal capacity of the MMC; E_{MMC} is the nominal energy per MVA stored in the MMC; n is the number of SMs in each arm.

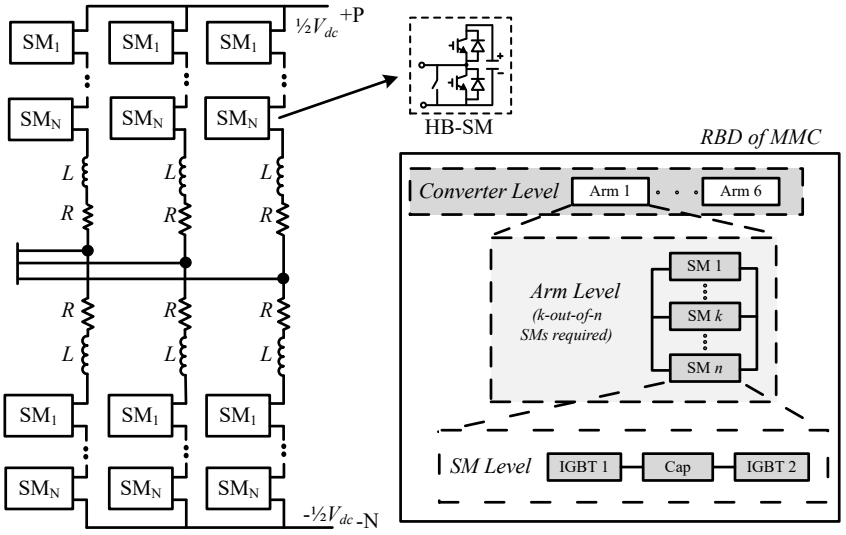

Fig. 4.4. MMC topology and corresponding RBD.

4.2.2 Reliability Modelling

In converter level reliability analysis, the stochastic failure nature of power electronic (PE) devices can be represented by the well-known "bathtub" curve [76, 83]. In this study, the intrinsic failure period is assumed considering the typical project lifetime of an OWF. Mathematically, the reliability function $R(t)$ of any PE device with a failure rate $\lambda(t)$ is defined as:

$$R(t) = e^{-\int_0^t \lambda(t)dt}. \tag{4.6}$$

Assuming the useful life period is characterised by a constant value, the reliability function is calculated

$$R(t) = e^{-\lambda t}. \tag{4.7}$$

Unscheduled outages are associated with high costs due to the long repair time and the high amount of energy not served. These uncertain outages can be reduced with redundant designs. However, more redundant modules will increase capital investment. Therefore, an optimal redundancy level for a specific project is required. There are two main redundancy schemes which can be utilised in PE converters: (a) the active, and (b) passive (standby) mode [114]. In the passive redundancy, redundant modules are kept idle and disconnected (or bypassed) until an operating module fails. Whereas in the active redundancy, the total dc bus voltage is shared by all the n IGBTs/modules until k minimum required modules are in operation. In this study, active redundancy is chosen from a practical point of view.

According to the RBDs shown in Figs. 4.2 $\sim$ 4.4, the reliability $R_a(t)$ of an SP (2L-VSC, 3L-NPC) or an arm (MMC) or pole (C3L-NPC) can be calculated with the probability theory applied for *k-out-of-n* systems [76].

$$R_a(t) = \sum_{i=k}^{n} C_n^i [R_y(t)]^i [1 - R_y(t)]^{n-i}. \tag{4.8}$$

In (4.8) $R_y(t)$ is defined as

$$R_y(t) = \begin{cases} R_{IGBT}(t) & 2L\text{-}VSC,\ 3L\text{-}NPC \\ R_{SM}(t) & MMC \\ R_{cell}(t) & C3L - NPC \end{cases} \tag{4.9}$$

where

$$R_{SM}(t) = R_{IGBT,1}(t) \times R_{IGBT,2}(t) \times R_{cap,SM}(t). \tag{4.10}$$

In (4.9), $R_{IGBT}(t)$ is the IGBT module reliability and $R_{cell}(t)$ is the reliability of the 3L-NPC which is used for the C3L-NPC. In (4.10), $R_{IGBT,1}(t)$ and $R_{IGBT,2}(t)$ are the reliabilities of IGBTs within the SM. $R_{cap,SM}(t)$ is the MMC SM capacitor reliability. Once $R_a(t)$ is calculated, the phase-level $R_{ph}(t)$ and converter level $R_{VSC}(t)$ reliabilities can be calculated as below.

$$R_{ph}(t) = [R_a(t)]^{2\alpha} \tag{4.11}$$

$$R_{VSC}(t) = [R_{ph}(t)]^3 \times [R_{cap}(t)]^{\gamma} \times [R_{npc-d}(t)]^{\mu} \tag{4.12}$$

where $R_{cap}\,(t)$ and $R_{npc\text{-}d}\,(t)$ are the reliabilities of dc-link capacitor and NPC diode respectively. The term α is the number of SPs. At present, no single dc capacitor or NPC diode is able to withstand the MVdc voltage levels discussed in this study. Thus, series connections of dc capacitors are required. The terms γ and μ stand for the number of series-connected dc capacitors and NPC diodes. To obtain the reliability of the MMC, (4.12) can be used with $\gamma = \mu = 0$ and $\alpha = 1$ since the failure rate of the SM capacitor has already been included in (4.10). The reliability $R_{C3L}(t)$ of the C3L-NPC can be obtained once the cell level reliability $R_{cell}(t)$ is obtained following the same methodology discussed for the 3L-NPC.

4.3 Availability and Maintenance Requirements of MVdc Converters

The availability of a converter relies on the frequency of maintenance and repair time. At HVdc levels, periodic preventive maintenance is performed to keep operational costs low because planned outages attract much lower penalty payments than unplanned outages [115]. For example, the Crown Estate licenses for offshore wind farms around the UK require that the HVdc converter availability must be above 98% (including planned maintenance) [116]. The same maintenance approach can be used for MVdc applications.

In this study, the analysis is mainly confined to the comparison of MVdc converter topologies. The availability of the cooling system and the power supply system are assumed to be the same. Further, compared to the failure rate of a converter topology which comprises of a large number of power electronics devices, the failure rate of the interfacing transformer is very low [117]. Hence, the converter transformer is assumed failure-free for the lifetime considered in this analysis. A stringent availability level of 99.99% is maintained for the SP (2L-VSC, 3L-NPC), arm (MMC) and pole (C3L-NPC) level so that the total converter availability can be maintained above 99.99% as of [114].

To calculate the availability of a converter SP/arm/pole A_a using the individual availability of IGBTs/SMs/cells, the *k-out-of-n* model is used as shown in (13), where A_b is the base availability of the arm/pole with no redundancy, N is the total number of IGBTs/SMs within an SP/arm/pole and M is the number of redundant modules.

$$A_a = \sum_{i=0}^{M} \frac{N!}{i!(N-i)!} A_b^i \left(1 - A_b\right)^{(N-i)} \tag{4.13}$$

$$A_b = e^{-\lambda_b T_M} \tag{4.14}$$

$$\lambda_b = -\frac{d\left[\ln R_a(t)\right]}{dt} \tag{4.15}$$

The parameter T_M in (4.14) defined as the preventive maintenance interval (in years). In reliability theory, the base failure rate is defined as the system failure rate without redundancy. The base failure rate of converter SP/arm/pole λ_b was calculated as shown in (4.15) following (4.9) and (4.10) with $n = k$ in (4.8).

4.3.1 VSC Availability and Redundancy Analysis with Different Maintenance Intervals for ± 27 kV

The base failure rates of candidate VSCs for ±27 kV MVdc voltage level can be calculated using (4.15) with the parameters given in Table 4.1. The IGBT used for this analysis is ABB 5SNA 1300K450300 with a de-rating factor of 56% [109]. The gate drive unit SCALE-1SC0450E and dc capacitor of 2.7 kV and 1.5 mF from EPCOS-B25750H2448k004 with the failure rates given in [114] are used. The selected NPC diode is ABB-5SDF13H45014 with the nominal dc voltage of 2.8 kV [118].

Table 4.1. System parameters and base failure rates.

Symbols	**Item**	**Value**
S_{VSC}	Converter Rating	30 MVA
V_{dc}	MVdc voltage level	±27 kV
V_{IGBT}	withstand voltage of IGBT	4.5 kV
η	derating factor of IGBT module	56%
V_{nom}	nominal voltage of IGBT module	2.52 kV
E_s	Energy stored in the VSC	20 kJ/MVA
λ_{IGBT}	IGBT failure rate	0.001752 occ/yr [119]
λ_{cap}	dc capacitor failure rate	0.000876 occ/yr [120]
λ_{GD}	failure rate of IGBT gate drive	0.004380 occ/yr [114]
λ_{npc-d}	NPC diode failure rate	0.000438 occ/yr [118]

It is worth noting that the failure rate of IGBT gate drive unit was an estimated value which was based on the discussion had with GE Grid Solutions as mentioned in [114].

The calculated minimum required components and base failure rates of converters are given in Table 4.2. Due to the higher number of components, MMC shows the highest base failure rate. The C3L-NPC shows the lowest failure rate due to its lower component count. However, due to the inclusion of NPC diodes in 3L-NPC configuration, its failure rate is higher than that of 2L-VSC even though the same number of IGBTs and dc-link capacitors are used in both.

Table 4.2. Required min. number of components and base failure rates.

Topologies	**Component Count** $(n = k)$			**Base Failure**
	IGBTs	**Capacitors**	**NPC Diodes**	**Rates (occ/yr)**
2L-VSC	132	240	-	1.2299
3L-NPC	132	240	66	1.2588
C3L-NPC	144	168	72	1.2089
MMC	264	264	-	1.8501

After obtaining the base failure rates of VSCs, the availability is calculated over different redundancy levels and maintenance intervals for half-year and one-year as shown in Figs. 4.5 and 4.6. The required redundant modules (which corresponds to 99.99% availability) for each topology can be obtained using the same and summarised in Table 4.3. It can be noted that even though the base failure rate of C3L-NPC is the lowest, it requires a higher number of redundant cells to keep the same availability level ($> 99.99\%$) because its per-pole availability is the lowest amongst these VSCs due to its physical configuration.

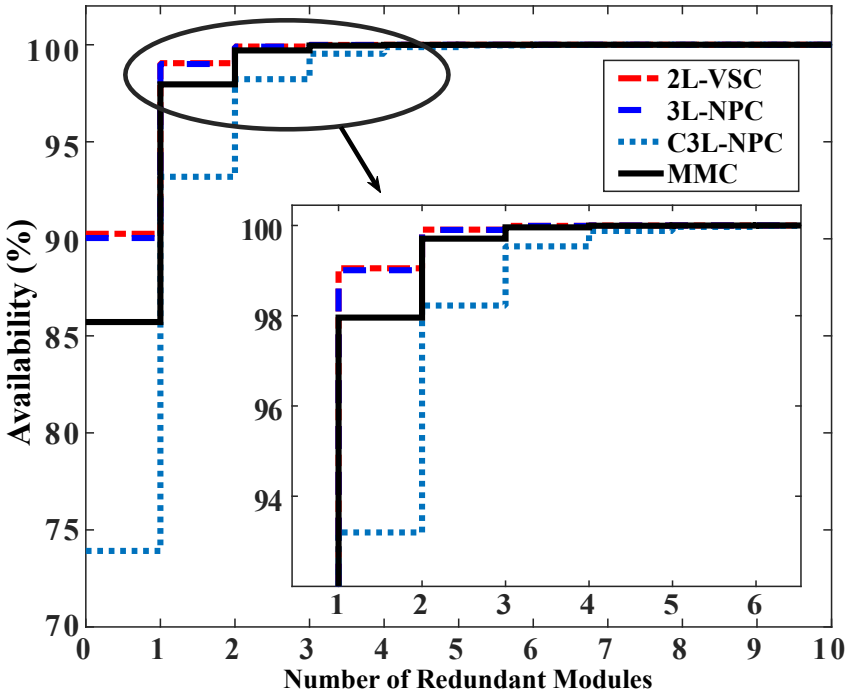

Fig. 4.5. Availability of ± 27 kV VSCs over redundancy for $T_M = 0.5$.

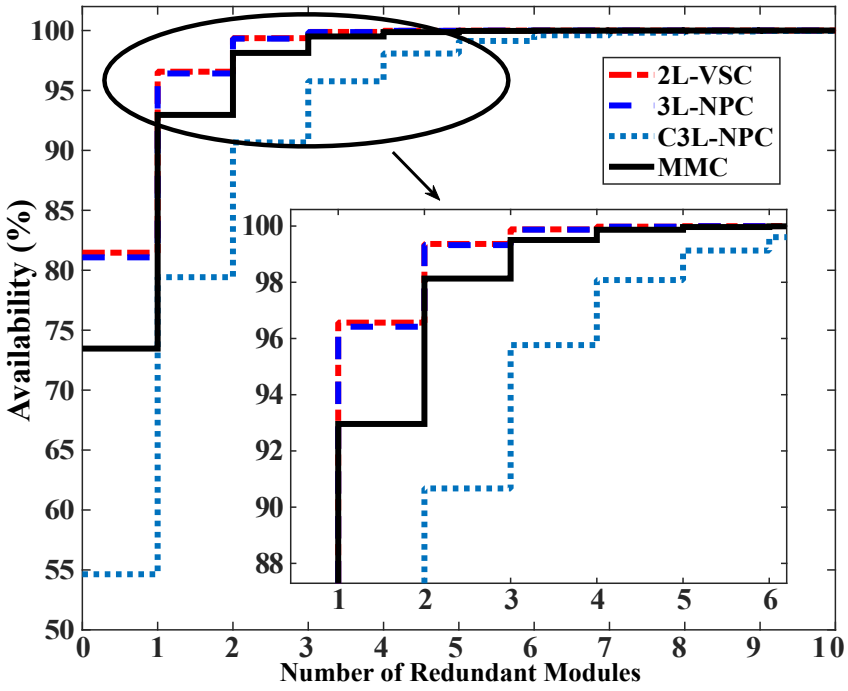

Fig. 4.6. Availability of ±27 kV VSCs over redundancy for $T_M = 1$.

Table 4.3. Redundancy level of VSCs with different maintenance intervals.

Topologies	**Minimum modules/ cells per arm**	**Redundant modules**	
		T_M**=0.5**	T_M**=1**
2L-VSC	22	4 (18%)	6 (27%)
3L-NPC ∗	11	2 (18%)	3 (27%)
C3L-NPC ♯	06	5 (83%)	12 (200%)
MMC	22	5 (22%)	7 (31%)

∗ required IGBTs per SP ♯ required cells per pole ( )-redundancy %

Notably, with the increase of preventive maintenance interval, the redundancy level should also be increased to maintain the same availability level. Hence, the capital investment and power losses of converters may increase unnecessarily. Therefore, T_M=0.5 year has been selected as the best preventive maintenance interval in the analysis.

The variation of VSC reliability for half-year maintenance interval is shown in Fig. 4.7. To compare VSC reliabilities on a common ground the B_{10} life can be used [83]. In reliability engineering calculations, the B_{10} life is defined as the time taken to reach 90% of the reliability of a system. It can be noted that B_{10} life of MMC is the highest with

5.9 years which is more reliable compared to other topologies. The 2L-VSC and 3L-NPC have lower B_{10} life values with 0.68 years and 0.64 years respectively. Although the MMC has the highest base failure rate, its B_{10} life is the highest after redundancy is added. The reason is, due to the cascaded structure of MMC, the capacitors are placed at SM level. When redundant SMs are added it provides additional redundancy compared to 2L-VSC and 3L-NPC which makes MMC more reliable.

Fig. 4.8 shows the variations of failure rate for the four topologies with different redundancy levels. It is notable that, even though the number of redundant modules is increased after the selected redundancy level, the failure rate does not increase significantly before the B_{10} life. For instance, consider the failure rates of MMC with different redundant SMs in Fig. 4.8(d). The failure rates correspond to B_{10} life show that below the selected optimal redundancy level (in here R_{SM} <5) the MMC is more prone to fail.

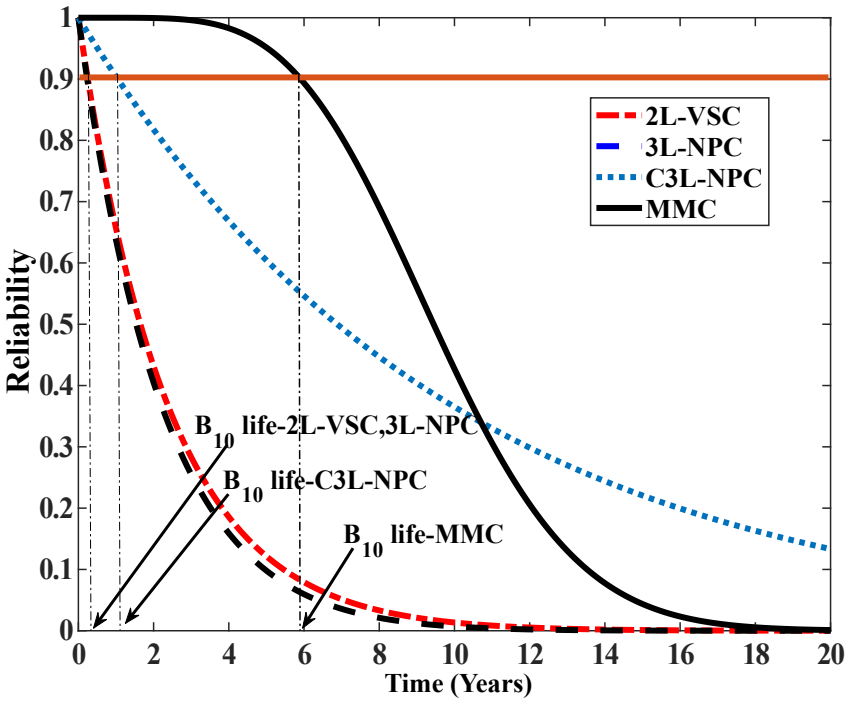

Fig. 4.7. Reliability of ±27 kV VSCs for $T_M = 0.5$ years.

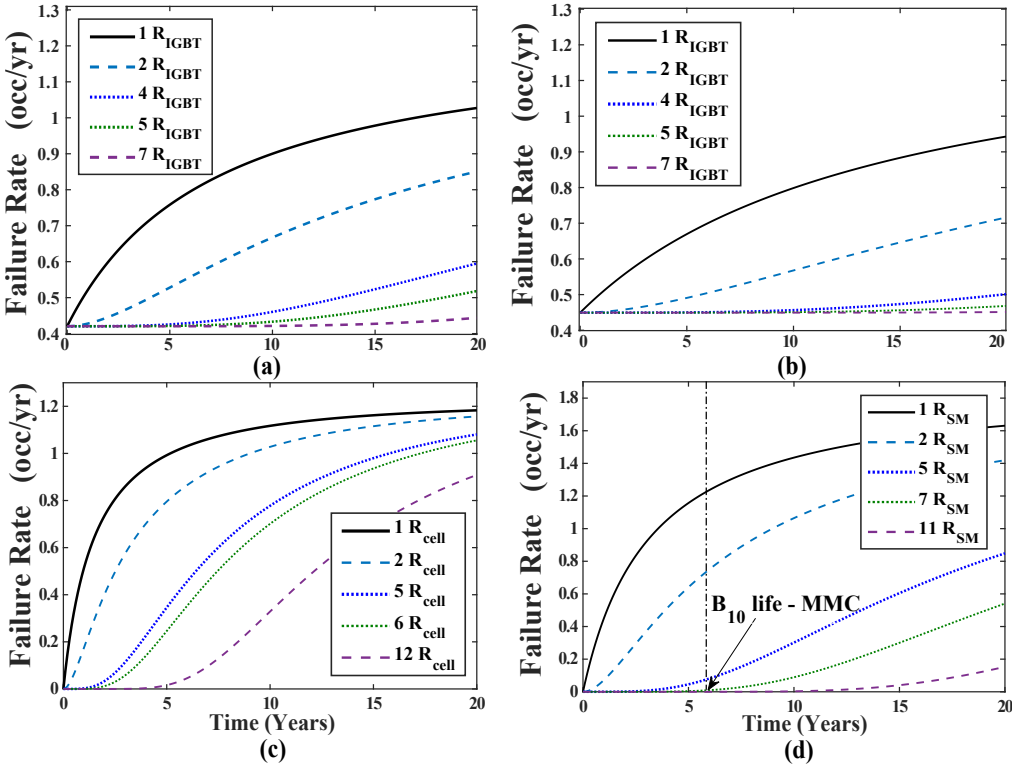

Fig. 4.8. Failure rates of (a) 2L-VSC; (b) 3L-NPC; (c) C3L-NPC; (d) MMC with different redundancy level for ±27 kV with $T_M = 0.5$ years.

4.4 Analysis of operational efficiency, total cost of ownership and return on investment

Apart from reliability and redundancy, the efficiency and lifetime cost of the VSC (i.e. TCO) are two main factors should be considered in the selection of VSCs. In [73], two types of 3L-NPC topologies are compared with the 2L-VSC for the grid integration of the type-4 wind turbine considering capital investment and operational efficiency. However, depending on the application, voltage and powers level, the associated VSC losses will change. For example, the accumulated annual energy losses of a converter utilised in MVdc distribution networks may differ from an MVdc converter applied in the offshore dc collection system.

4.4.1 Operational Efficiency

To analyse the VSCs on common ground with the general grid code requirements defined by IEEE 519 Std., the switching frequencies have been adjusted to meet the maximum current harmonic distortion limits defined in [74]. Thus, the switching frequencies of the

VSCs considered for this analysis are 2.5 kHz/2L-VSC, 2 kHz/3L-NPC, 1 kHz /C3L-NPC and 100 Hz/MMC.

To evaluate the switching and conduction losses of each VSC, the PLECS software tool has been used which is based on multi-dimensional lookup tables on manufacturer information at various semiconductor junction temperatures [121]. For all the losses analysis conducted, the ambient temperature was maintained at 25°C. Fig. 4.9 shows the percentage losses of VSCs at its rated power for ±27 kV with different maintenance intervals for selected redundancy levels. When the maintenance interval is increased, the losses are also increased due to the utilisation of more redundant modules. At T_M=0.5 years, the C3L-NPC (1.52%) shows lower losses compared to 3L-NPC (1.81%) which is notable. However, due to the utilisation of a greater number of redundant cells (to maintain the same availability) at T_M=1 year, the losses are slightly higher than 3L-NPC. The 2L-VSC shows the highest power losses with $P_{l_{2L-0.5}}$=2.95% and $P_{l_{2L-1}}$=3.17%. MMC presents the lowest power losses, $P_{l_{MMC-0.5}}$=0.69% and $P_{l_{MMC-1}}$=0.61% for both maintenance intervals.

From the perspective of mitigating converter power losses, having a lower preventive maintenance period is beneficial. Thus, for the rest of the analysis, the VSC redundancy level corresponds to T_M=0.5 years has been selected.

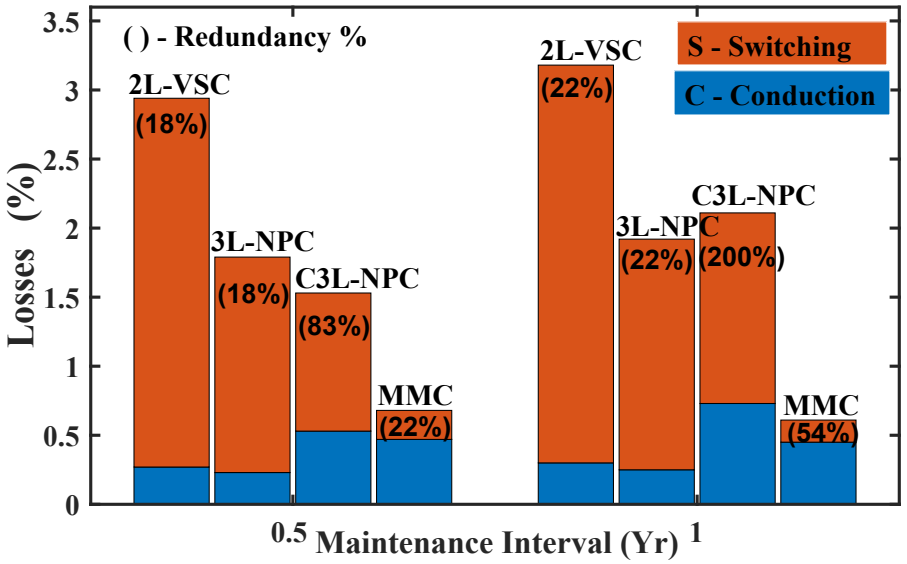

Fig. 4.9. VSC power losses for ±27 kV with different maintenance intervals and redundancy.

4.4.2 Annual Energy Production

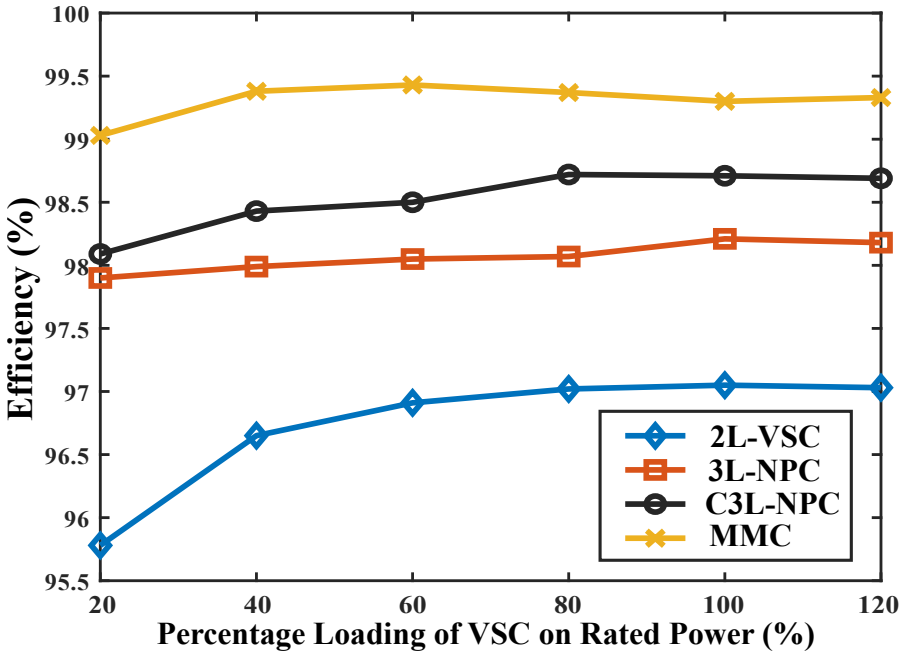

Fig. 4.10. The efficiency of VSCs over different loading conditions for ±27 kV with $T_M = 0.5$ years.

Due to variations in the wind power profile, VSCs connected to OWF MVdc systems may not always operate at their rated power. Thus, efficiency evaluation only at rated power may not reflect the actual efficiency of the VSC. The converter efficiencies related to different loading conditions have been obtained by varying the load current of each VSC. Obtained PLECS simulation results are shown in Fig. 4.10. According to Fig. 4.10, MMC shows the highest efficiency (above 99%) at all the loading conditions. Notably, the C3L-NPC has higher efficiency than 3L-NPC. However, at low load conditions, the converter efficiency is lower compared to the rated power due to relatively higher turn-on and turn-off losses.

To obtain a reasonable value for annual energy produced by each VSCs, a method based on the normalised power duration curve is proposed. Fig. 4.11 shows the normalised power duration curve for Anholt offshore wind farm [122] and its clustered 11-segment step graph. A summary of normalised power output and their duration per annum are summarised in Table 4.4. The number of clusters have been obtained by referring to the Jenks natural breaks clustering algorithm discussed in Section 5.3.1 of Chapter 5.

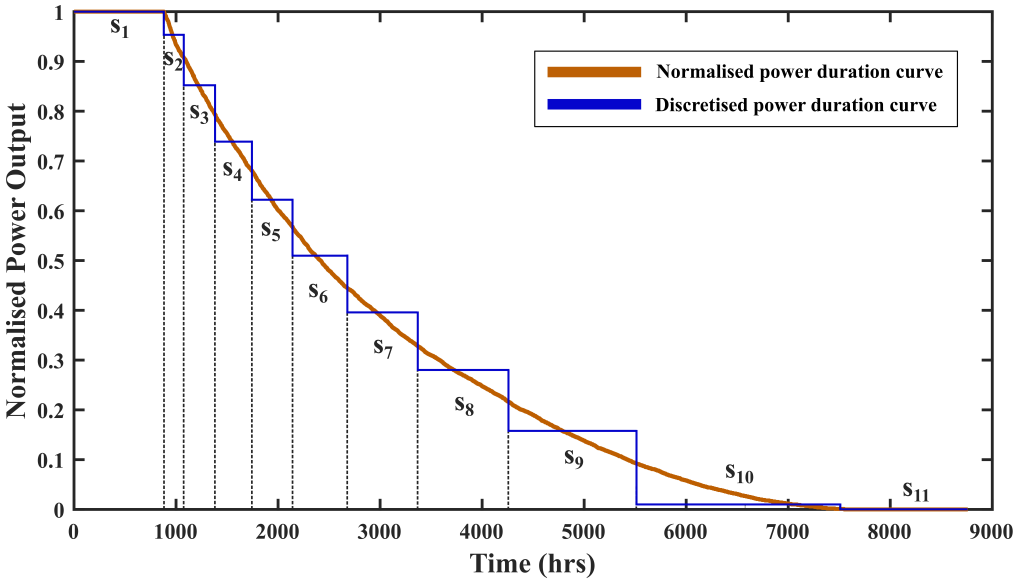

Fig. 4.11. Normalised and discretised 11-segment wind power duration curve of Anholt wind farm.

Table 4.4. Discretised wind power output clusters and their duration per annum.

Segment Number	Normalised Power	Duration (hrs)
S_1	1.000	882
S_2	0.954	82
S_3	0.851	258
S_4	0.739	328
S_5	0.627	370
S_6	0.511	443
S_7	0.397	598
S_8	0.279	769
S_9	0.157	1060
S_{10}	0.047	1370
S_{11}	0.000	2760

In the operational efficiency analysis of VSCs, instead of using a single average value, this discretised method based on data clustering provides accurate information to calculate the annual energy produced. The corresponding efficiencies with respect to the loading of the VSCs can be obtained by referring to Figs. 4.9 and 4.10. Accordingly, the annual energy losses E_{l_X} (in kWh) of each VSC (where x defines the corresponding VSC) is calculated.

$$E_{l_X} = \left\{ \sum_{b_i=1}^{n_{cl}} \left(100 - \eta\left(b_i\right)\right) \times t\left(b_i\right) \right\} \times P_{VSC} \times 10. \tag{4.16}$$

where $\eta\left(b_i\right)$ and $t\left(b_i\right)$ define the efficiency and time (in hours) of the VSC related to the corresponding segment $b_i = 1, 2 \ldots n_{cl}$. The terms n_{cl} and P_{VSC} (in MW) are defined as total number of clusters and the rated power of the converter, respectively. Table 4.5 shows the cumulative energy losses for each VSC per annum for $T_M = 0.5$ years. Due to the lower efficiency of 2L-VSC, the energy losses of each segment is relatively higher than other VSCs.

Table 4.5. Cumulative annual energy losses of each VSC (in MWh).

	2L-VSC	**3L-NPC**	**C3L-NPC**	**MMC**
E_{l_X}	7,297.82	4,070.60	3,177.13	1,882.11

4.4.3 Total Cost of Ownership (TCO)

Depending on the VSC topology, the capital cost, and the operation and maintenance (O&M) costs are varying. The term TCO includes initial investment costs and the O&M cost. However, in this analysis, the O&M cost is assumed the same for each VSC considering the same preventive maintenance interval and simplicity.

To perform cost calculations, up-to-date market prices have been obtained through cross-referencing via various manufacturers and distributors [123]. The IGBT unit price is roughly £1648 for a minimum order quantity of 25 units and the 3L-NPC diodes are £73/unit. Moreover, the gate drive unit cost of £148 is accounted per channel and the capacitor energy price is around £100/kJ [123]. Table 4.6 summarises the TCO of each VSC including redundant components.

The cost of the 3L-NPC is higher than the 2L-VSC due to the additional NPC diodes. Due to more redundant cells in C3L-NPC, (to maintain the same availability) the cost is 69% higher than that of 3L-NPC. The TCO of the MMC is the highest among the four VSCs due to higher part counts.

It is worth mentioning that the actual cost of these VSCs may deviate from the above values due to various non-technical reasons such as confidentiality of cost data and pricing strategies of different manufacturers, time-dependency of component costs due to varying raw material prices and economies of scale. However, project engineers can use their know-how to include more precise component cost factors.

Table 4.6. Total cost of ownership of VSCs (in £).

Components	**2L-VSC**	**3L-NPC**	**C3L-NPC**	**MMC**
IGBT	257,106	257,106	435,103	533,990
Gate Drive	24,395	24,395	41,284	50,667
Heat Sink	29,451	29,451	49,841	61,168
Total Capacitance	66,241	66,241	111,825	134,204
Power Supply	17,217	17,217	29,137	35,759
Sensors	1,596	1,596	1,596	1,596
Control Board	872	872	872	1308
NPC diode	N/A	4848	9,696	N/A
TOTAL	396,881	401,729	679,357	818,695

4.4.4 Return on Investment (ROI)

In any industrial application, the investment decision is made on how much profit can be gained over its capital investment. This is equally valid in the selection of VSCs which provides a quantitative implication for the financial investment made. The ROI is a quantitative indication of how much profit each pound invested into that VSC is producing. Thus, a higher ROI is preferred. The topology which shows the highest ROI is selected as the optimal one. To measure the performance of VSCs in terms of ROI, accumulated cost savings relative to 2L-VSC is determined first. The present value of the future cost savings due to energy saving of a VSC can be calculated by:

$$S_n = \sum_{i=1}^{n} \frac{S_i}{(1+k)^i} \tag{4.17}$$

$$S_i = \sum_{b_i=1}^{n_{cl}} \Delta E_{b_i} \times P_t \tag{4.18}$$

where S_n is the accumulated cost savings in present value for a period of n years. The term S_i is the cost-saving in year i and k is the annual interest rate. The parameter ΔE_{b_i} (kWh) in (4.18) defines as the relative energy saving of segment b_i compared to the 2L-VSC. The term P_t (£/kWh) is the unit of the electricity selling price. For this analysis, P_t=0.155 £/kWh in the UK for the year 2019 has been used [124]. Finally, the ROI is used (4.19) to measure the VSC investment return (over 2L-VSC), relative to their capital cost.

$$ROI = \frac{S_n}{TCO} \tag{4.19}$$

Table 4.7 shows the calculated ROI of each VSC with respect to operational years n=1,5 and 10 assuming a constant annual interest rate of 5% [73]. The topology which shows the highest ROI is selected as the optimal one. Table 4.7 shows that MMC has the highest ROI at ±27 kV. Even though the initial investment is nearly double of 2L-VSC (as shown in Table 4.6), MMC accounts for the highest energy saving compared to other VSCs. Following the MMC, 3L-NPC shows the second most suitable VSC to be used at ±27 kV. However, the sensitivity analysis carried out for C3L-NPC shows that, instead of 5 redundant cells, if 4 redundant cells are used (at the expense of lower availability) the ROI=0.89 for n=1. By doing so, the TCO of C3L-NPC can be reduced by 23% which is significant and competitive compared to the MMC.

Table 4.7. Return on investment of VSCs (±27 kV).

Operational Years	**ROI over 2L-VSC**		
	3L-NPC	**C3L-NPC**	**MMC**
n=1	0.78	0.69	0.99
n=5	3.54	3.17	4.47
n=10	6.33	5.65	8.80

4.5 Impact of Rated dc Voltage and Current on Topology Selection

4.5.1 Impact of dc Voltage Level

As discussed in Section 4.2.2, the selection method of redundant modules for a VSC (to keep the availability above a certain level) is a non-linear process. The required minimum modules and level of redundancy are also different depending on the dc voltage. Thus, the ROI will be different due to variations in TCO and operational efficiencies. In order to observe the impact of dc voltage on topology selection, analyses have been performed from ±10 kV to ±50 kV with a fixed rated current of 500 A. Thus, the power rating varies from 10 MVA to 50 MVA.

Table 4.8 shows the required minimum (k_{min}) and redundant modules (k_R) for each VSC for some selected MVdc voltage levels with the consideration of the targeted availability level of 99.99%. It can be noted that with the increase of dc voltage level the redundancy level also increases to keep the same availability. However, as k_{min} is increased the reliability of the VSC decreases over time due to the stochastic failure nature of PE devices. At low voltage levels, the B_{10} life is high due to the utilisation of a fewer components.

Table 4.8. Level of redundancy required with the change of DC voltage.

Voltage	**3L-NPC** $*$		**C3L-NPC** $\sharp$		**MMC**	
	k_{min}	k_R	k_{min}	k_R	k_{min}	k_R
±10 kV	4	2	3	3	8	4
±15 kV	6	2	4	3	12	4
±25 kV	10	3	6	5	20	5
±35 kV	14	3	8	7	28	6
±45 kV	18	3	10	8	36	6
±50 kV	20	3	10	8	40	7

$*$ required IGBTs per SP $\sharp$ required cells per pole

To observe the voltage ranges in which a particular VSC is the most suitable, variations of ROI against the MVdc voltage are shown in Fig. 4.12. According to Fig. 4.12, between ±10 kV and ±20 kV (R-1) use of 3L-NPC VSC is more economical than the use of other VSCs. This is because, within these power levels (10 - 20 MVA), and dc voltage levels 3L-NPC require only a few redundant modules and capital costs do not increase significantly. This makes the increase in capital cost of 3L-NPC does not depend on the redundancy level. Between ±10 kV and ±15 kV the ROI of all the VSCs increase due to the use of the same k_R as of ±10 kV level. However, at ±15 kV the ROI difference between 3L-NPC over C3L-NPC and MMC is relatively higher. This indicates if C3L-NPC or MMC are used at this dc voltage level it will take much longer time to recover the investment. Notably, after ±15 kV the ROI values of C3L-NPC and MMC decrease due to the increase of k_R and relative energy saving is less significant.

Finally, beyond ±20 kV (R-2) MMC shows the highest ROI compared to other VSCs owing to the fact that improved efficiencies. This is because at higher MVdc voltage levels more MMC SMs are available to select in the switch selection algorithm. Further, after about ±33 kV C3L-NPC also shows better performance than 3L-NPC, but still inferior to MMC. It should be mentioned that these intersection points may vary depending on the sensitivity of the data.

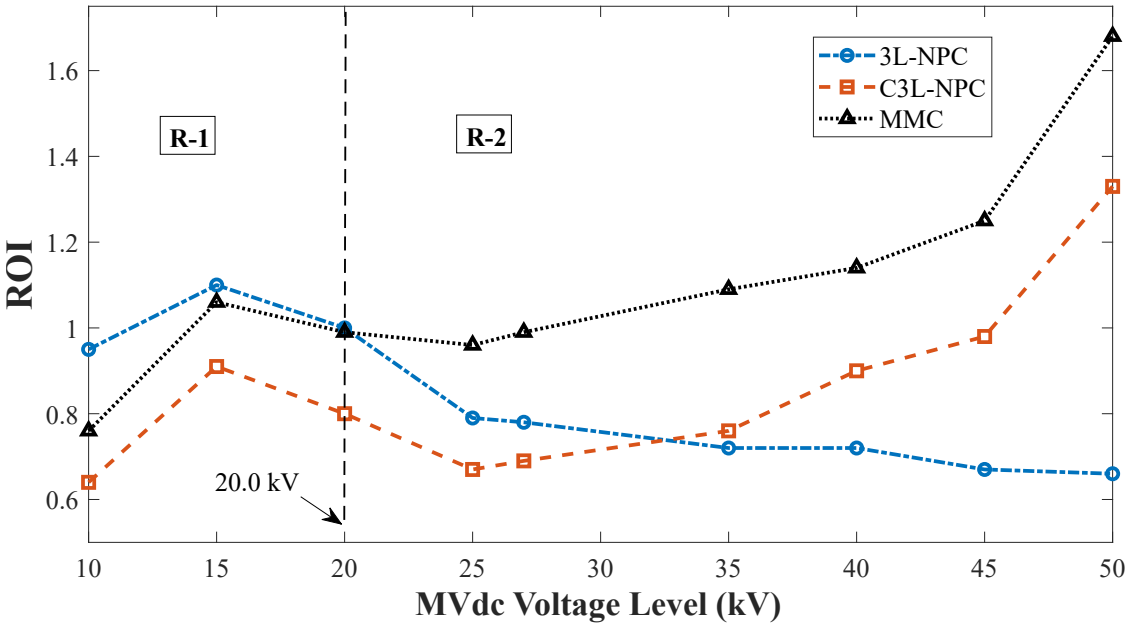

Fig. 4.12. Variation of ROI with MVdc voltage level (at the rated current of 500 A).

4.5.2 Impact of Rated Current

The selection of VSC topologies at different MVdc voltage levels for a fixed rated capacity has been discussed in the above section. Further analysis in identifying a suitable VSC topology with the variation of its rated current has been carried out in this section. In this study, the 3L-NPC, C3L-NPC and MMC are selected as the candidates. As shown in Fig. 4.13, the converter rated current has been changed from 100 A to 1000 A and the same MVdc voltage class (from ±10 kV to ±50 kV) has been considered. This corresponds to a broader spectrum of analysis of converter power ratings which ranges from 2 MVA to 100 MVA.

From Fig. 4.13, it can be observed that irrespective of the MVdc voltage level, the ROI increases with the increase of converter rated current. This is due to the fact that, at higher current levels converter exports more energy than at lower current levels. This results in higher accumulated cost savings for the considered period . The general trend for 3L-NPC is that the ROI decreases with the increase of the voltage level irrespective of the converter rating. On the contrary, the ROI of MMC and C3L-NPC shows an increasing trend. For the current range considered in this analysis, between ±30 kV and ±35 kV, C3L-NPC crosses over 3L-NPC. However, as mentioned in Section 4.5.1, its ROI is still lower compared to MMC.

Fig. 4.14 summarises different MVdc crossover voltage levels in which a candidate VSC topology is suitable under a specific rated current. At current levels below 300 A and

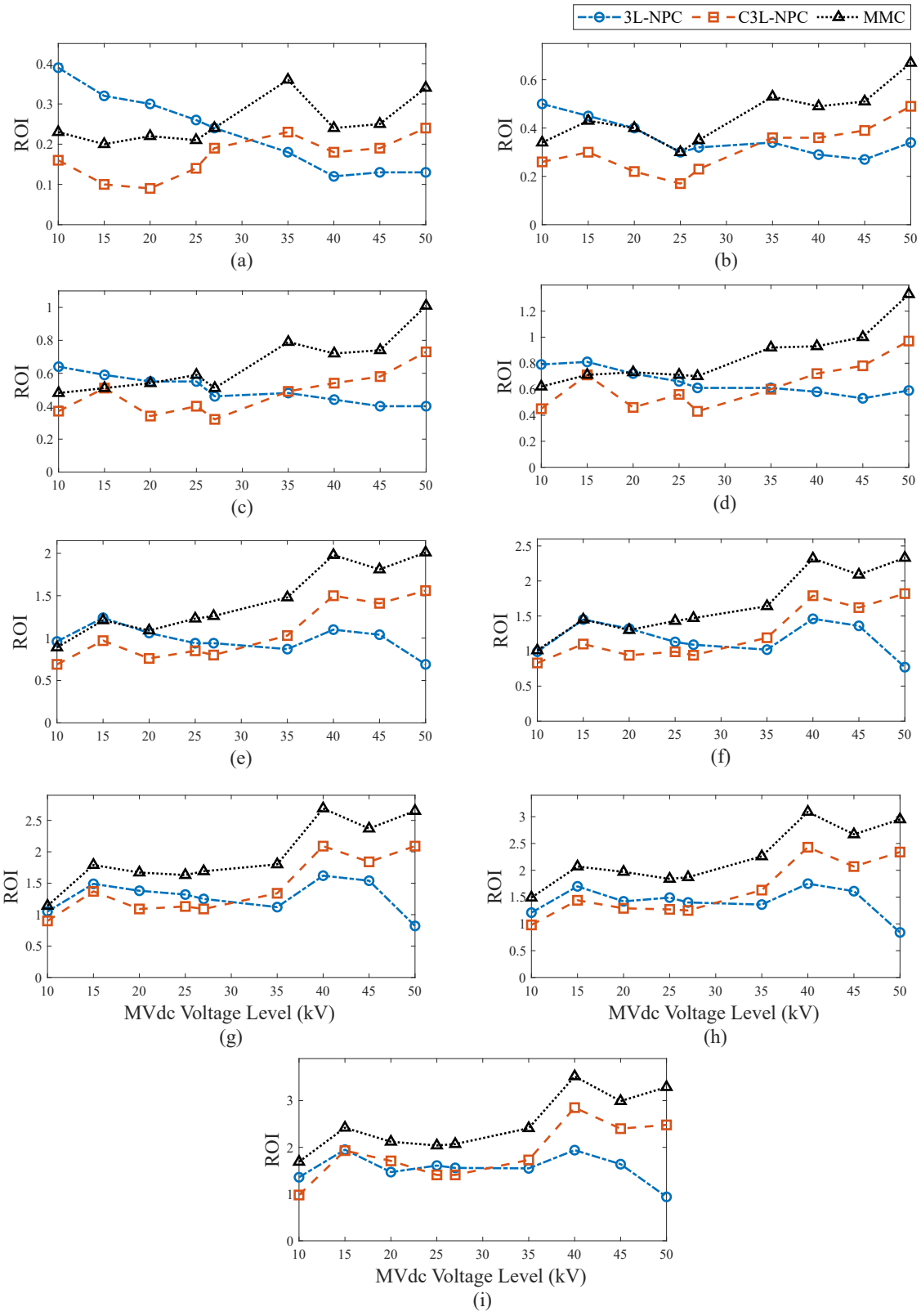

Fig. 4.13. Variation of ROI with the change of rated current at different MVdc voltage levels (a) 100 A; (b) 200 A; (c) 300 A; (d) 400 A; (e) 600 A; (f) 700 A; (g) 800 A; (h) 900 A; (i) 1000 A.

voltage level below ±20 kV, the use of 3L-NPC is more beneficial. Beyond 800 A, the use of MMC is more economical for the whole MVdc voltage spectrum discussed here.

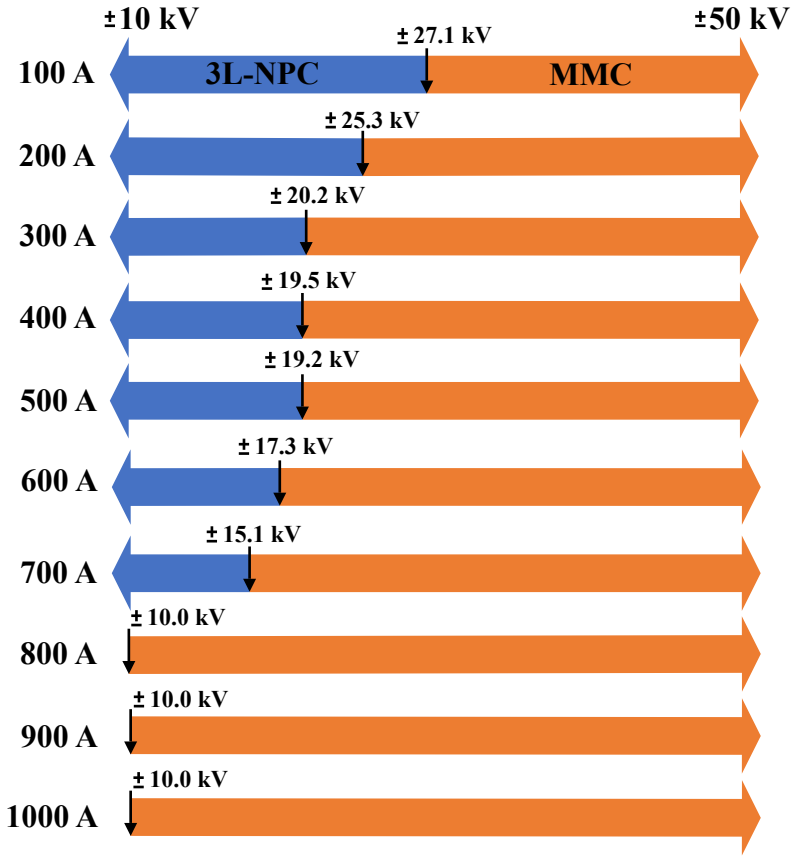

Fig. 4.14. Variation of voltage crossover points with the change of rated currents.

4.6 Summary

To obtain overall techno-economic benefits from MVdc technology, a suitable converter topology is required. This analysis presents a systematic criterion to select multi-level VSC for MVdc offshore collection systems taking the reliability, redundancy, efficiency and economic feasibility factors such as TCO and ROI into account. To obtain the optimum redundancy level for VSCs, a preventive maintenance based approach was used with a pre-defined availability level. A method based on normalised wind power duration curve was introduced to assess the operational efficiencies and thereby to evaluate feasibilities of VSCs at different MVdc voltage levels.

Three candidate multi-level topologies namely 3L-NPC, MMC and cascaded 3L-NPC (which is being used for the first MVdc link in the UK) have been evaluated over 2L-VSC from ±10 kV to ±50 kV with current levels of 100 A to 1 kA. Results show that with the increase of MVdc voltage level MMC shows better performance whereas at low MVdc voltage levels 3L-NPC is the prominent topology.

Chapter 5

Selection of Offshore Wind Power DC Collection Systems based on Reliability and Economic Factors

5.1 Introduction

As discussed in Section 2, with the increasing capacity of the single WT and larger distances to the shore, the use of dc technology at the collection system level is beneficial. In Chapter 3 and Chapter 4, the reliabilities of key building blocks of the dc collection system at component- and converter- level were investigated. To select a suitable dc collection system topology, this chapter presents a comprehensive analytical reliability evaluation method at (system-level) based on UGF technique together with associated economic factors.

This strategy combines the stochasticity of wind with multiple power output states of a single WT. The corresponding state probabilities for a finite number of output states have been obtained using Jenks natural breaks clustering algorithm. The relationship between the output states and corresponding state probabilities of WTs are combined using the UGF technique considering the network structure. Twelve different case studies have been performed using four dc collection system options with three different WT capacities (10 MW, 8 MW and 5 MW) for a 400 MW OWF. Finally, the investment cost and operating costs (which includes network losses) are incorporated to identify the best topology.

5.2 Network Topologies for DC Collection Systems

Different dc collection system options were briefly discussed in Section 2.3.1. Among the pool of proposed configurations, three different radial topologies, and series-parallel (SP) topology is used for this analysis considering different qualitative and quantitative advantages discussed in the literature [15, 17, 84]. The matrix topology is an improved version of the SP topology [86]. However, it uses additional switchgear which is more complex to control, and the investment is also higher compared to SP topology hence opt from this analysis. In the following configurations, the MVdc and HVdc pole-to-pole voltage levels were set to ±10 kV and ±100 kV, respectively.

5.2.1 Radial-1 Topology (R-1)

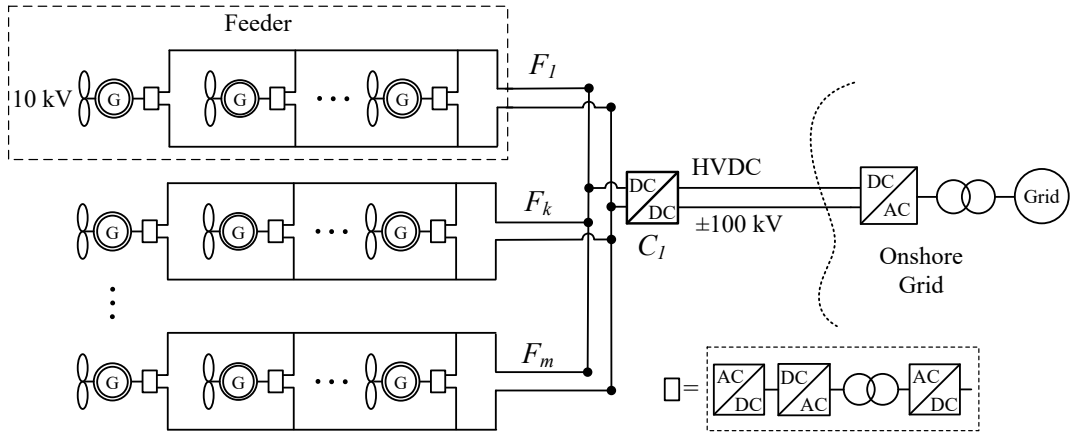

Fig. 5.1. Radial-1 topology.

In any radial configuration, at least one centralised dc/dc converter is required to boost the voltage to the HVdc transmission voltage level. The configuration shown in Fig. 5.1 uses a single collection system platform. The number of WTs connected to each feeder is decided by the optimised network layout under multiple factors, such as the current carrying capacity of cables, network losses, etc. In the radial configuration, the use of a reduced number of voltage conversion stages is beneficial to minimise the capital cost. To improve the reliability of the centralised dc/dc converter station, modular designs can be used [125].

Among the candidate dc/dc converters available for high power applications, the DAB converter looks promising in terms of flexibility in power flow control [42, 126]. One drawback of this configuration is that it requires a higher voltage gain to boost the voltage from the MVdc level to the HVdc level. However, to overcome this issue, modular designs, such as MMC with input-parallel, and output-series (IPOS) connections with a lower transformation ratio, can be used at the expense of capital investment [126].

5.2.2 Radial-2 Topology (R-2)

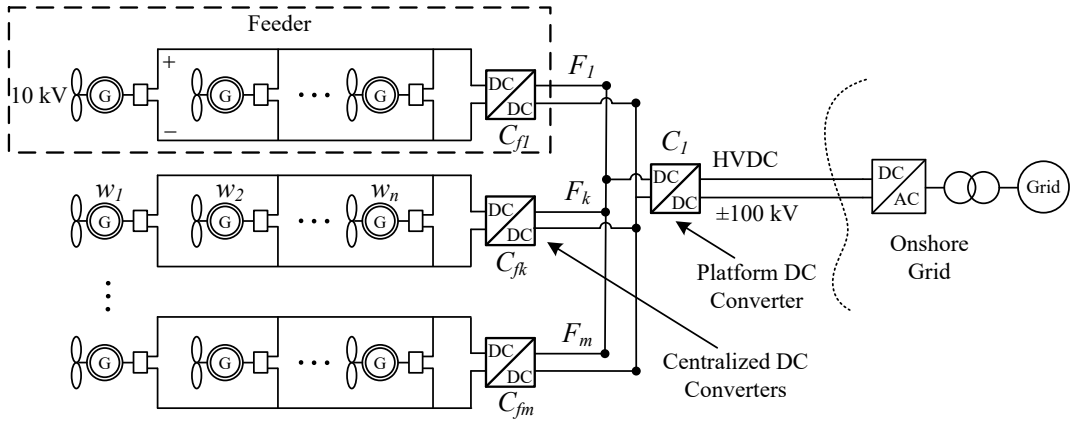

Fig. 5.2. Radial-2 topology.

Fig. 5.2 shows a radial configuration that comprises an individual collection system platform per feeder. This topology is more suitable for OWFs, where the centralised collection system platform is located far away from the OWF collection system. Another advantage of this topology is the ability to use lower voltage transformation ratios. The dc output voltage of WTs is first boosted by the intermediate dc/dc converter and then a higher MVdc voltage level than the voltage in Radial-1 topology is used, at the centralised collection system. However, due to the utilisation of multiple dc/dc converters, the capital cost is higher than the Radial-1 topology.

5.2.3 Radial-3 Topology (R-3)

The feeder configuration of the Radial-3 topology is shown in Fig. 5.3. This configuration is almost the same as Radial-2, except for the intermediate dc/dc converter voltage levels. In this configuration, the intermediate platforms are connected in series to build up the required HVdc voltage level. One advantage of this topology is the elimination of the platform converter, which enables reducing the capital investment. However, the inherent drawbacks of SP topology, which are discussed in Section 5.2.4, are also associated with this topology.

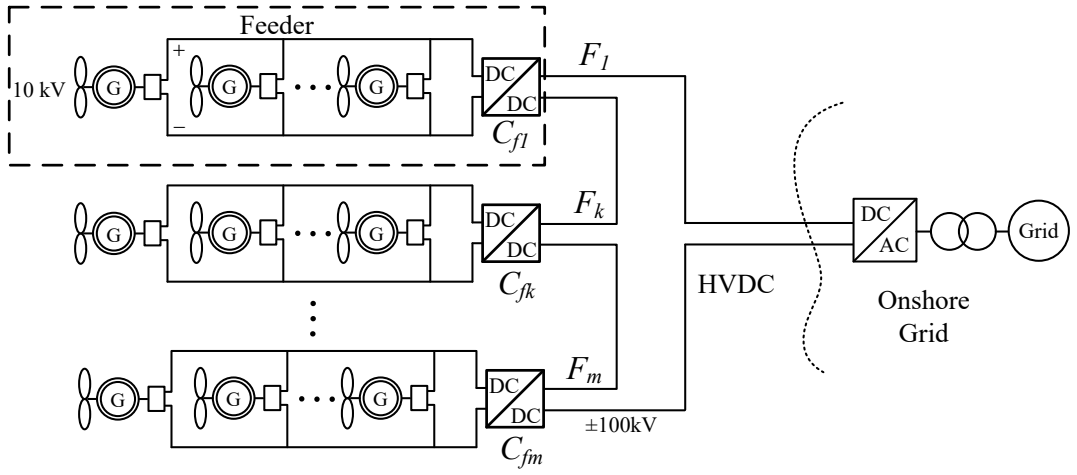

Fig. 5.3. Radial-3 topology.

5.2.4 Series-Parallel Topology (SP)

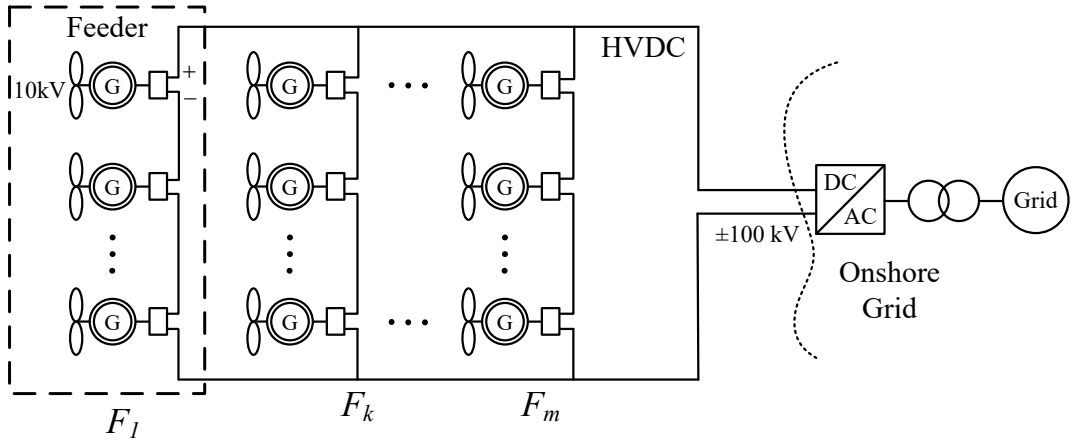

Fig. 5.4. SP topology.

In the series or SP topology (Fig. 5.4), the WTs are connected in series to build up the HVdc transmission voltage. However, in the series topology, there is only one feeder/branch and it has a lower wind farm output capacity than the SP topology, hence, it was eliminated from the analysis. The main advantage of SP topology is that it requires no intermediate platforms to boost the voltage to the transmission level. This helps to minimise capital investment.

The main drawback of this topology is that, upon failure of multiple WTs, the healthy units are required to maintain the pole-to-pole HVdc voltage level [127]. However, if the allowable voltage limits are exceeded by individual units (typically 10% of the rated voltage), the entire string is required to implement a forced-shutdown. Further, additional requirements such as (a) proper insulation coordination between each series-connected WT, and (b) special insulation designs for each unit are some other drawbacks of this SP topology.

5.3 Methodology

In general, a physical component operates with binary states, i.e., working or failed state, with their associated probabilities. However, due to the stochastic nature of wind speed, the WT power output is always coupled with the probability distribution of the wind. Although the WT is in a healthy operational condition (with a certain probability), its power output always correlates with the corresponding state probabilities of wind speed. Thus, this can be considered to be a multi-state system that is driven by a single source, i.e., wind. In the OWF reliability assessment, the variability of wind speed is required to be incorporated. The established methods based on RBDs or COPT tables to evaluate such systems with a large number of components is inherently complex. To overcome this computational complexity with different network structures and their dependency on external constraints, the proposed UGF technique can be easily adapted. Compared with other analytic methods, the required reliability results can be obtained with a fewer calculation step.

5.3.1 Clustering of Wind Turbine Power Output

To evaluate OWF reliability, first, it is required to obtain corresponding state probabilities of WT power output from the measured time-series wind speed data (typically between 1–10 min sampling interval) for a certain period (typically 1 year). However, accounting for all state probabilities of time-series data (e.g., 52,560 state probabilities in 10 min average) with very low probabilities, only increases the computational time. Therefore, the clustering of WT power output into a finite number of states will enhance the computational efficiency when analytical techniques are used.

The intermittent and randomness of wind speed result in different states of WT power output. To obtain the corresponding WT power output for a certain wind speed, it is required to refer to the WT power curve provided by the manufacturer's data sheet. This is given by:

$$P_w\left(v_w\right) = \begin{cases} 0 & v_w < v_{ci} \\ P_r \cdot \frac{(v_w - v_{ci})}{(v_r - v_{ci})} & v_{ci} \leq v_w < v_r \\ P_r & v_r \leq v_w < v_{co} \\ 0 & v_{co} \leq v_w \end{cases} \tag{5.1}$$

where $P_w(v_w)$ is the power generated at wind speed v_w (m/s), v_{ci} is the cut-in wind speed, and v_{c0} is the cut-out wind speed. P_r is the rated power of the wind turbine, and v_r is the rated wind speed. It can be seen from (5.1) that the relationship between the instantaneous wind speed and instantaneous power output of WT is non-linear.

Among the different clustering techniques available in the literature, this study used the Jenks Natural Breaks method to quantify the time-series wind power output data into a finite number of states [128, 129]. The classification principle of this method is based on grouping similar sized data. The variance of the data is used to measure the classification effect, i.e., to determine the number of clusters. First, it calculates the variance of each category, and then the sum of the variances of all categories are calculated. The smaller the sum of variance, the better the classification effect. Therefore, first, the number of clusters K must be determined. The calculation process for obtaining the objective function i.e., Goodness of Variance Fit (GVF) is mathematically represented by (5.2)-(5.4), as follows:

$$SDAM = \frac{1}{N}\sum_{i=1}^{N}(z_i - \bar{z})^2 \tag{5.2}$$

$$SDCM = \sum_{j=1}^{K}\frac{1}{N_j}\sum_{i=1}^{N_j}(z_{ij} - \bar{z}_j)^2 \tag{5.3}$$

$$GVF = 1 - \frac{SDCM}{SDAM} \tag{5.4}$$

where $SDAM$ (Sum of Squared Deviations from the Array Mean) is the variance of all data, which is a fixed value. N is the number of data, z_i is the ith data point, $\bar{z}$ is the average value of the data set, $SDCM$ (Sum of Squared Deviations of Class Mean) is the sum of the variances when data are divided into K categories. N_j is the number of data in the jth category, z_{ij} is the ith data in the jth category, and $\bar{z}_j$ is the average value of the jth category. $SDCM$ is related to the value of K. $SDCM$ decreases with an increase in K. The larger the GVF, the better the classification effect.

5.3.2 Reliability Modelling

5.3.2.1 Failure Rate Calculation of dcWT

The dcWT used in this analysis considered to be an extension of Type-4 acWT, which replaces the GSC with a DAB dc/dc converter [17]. The operating status of the WT is determined by the availability of each sub-system, such as the generator, converter, gearbox, etc. It was assumed that all components were independent and hold Markov properties [87]. In the Markovian context, the status of a component/sub-system was represented by the binary state-space model, as shown in Fig. 5.5.

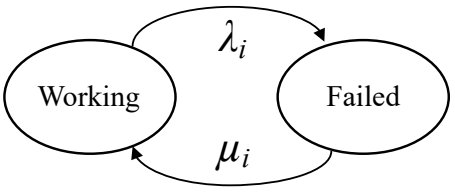

Fig. 5.5. State transition diagram of a wind turbine ith subsystem.

The average failure rate $\bar{\lambda}$ and repair rate $\bar{\mu}$ of the dcWT can be calculated using (5.5) and (5.6), with the knowledge of its subsystems as follows:

$$\bar{\lambda} = \sum_{i=1}^{r} \lambda_i \tag{5.5}$$

$$\bar{\mu} = \frac{\bar{\lambda}}{\sum_{i=1}^{r} \lambda_i \mu_i^{-1}} \tag{5.6}$$

where λ_i and μ_i are the failure and repair rates of the dcWT ith subsystem, which has r number of total subsystems. The availability A_{WT} of the whole system, i.e., the probability of being in the working state can be calculated as (5.7), and the unavailability level U_{WT} is defined as (5.8):

$$A_{WT} = \frac{\bar{\mu}}{\bar{\lambda} + \bar{\mu}} \tag{5.7}$$

$$U_{WT} = \frac{\bar{\lambda}}{\bar{\lambda} + \bar{\mu}} \tag{5.8}$$

5.3.2.2 The Universal Generating Function

In this section, the UGF technique is briefly introduced. Suppose there are n discrete random vectors $G_1, G_2, G_3, \cdots, G_n$, where the probability distribution of G_i can be represented by two vectors g_i and p_i. The vector g_i represents the possible value of G_i and the vector p_i represents the probability corresponding to the value of G_i:

$$\begin{aligned} g_i &= \{g_{i,1}, g_{i,2}, g_{i,3}, \cdots, g_{i,m_i}\} \\ p_i &= \{p_{i,1}, p_{i,2}, p_{i,3}, \cdots, p_{i,m_i}\} \end{aligned} \tag{5.9}$$

where:

$$p_{i,j} = \Pr\{G_i = g_{i,j}\} \quad j = 1, 2, \cdots, m_i \tag{5.10}$$

For a random variable G_i, the polynomial form of its z-transformation is defined as:

$$U_i(z) = p_{i,1} z^{q_{i,1}} + p_{i,2} z^{q_{i,2}} + \cdots + p_{i,m_i} z^{q_{i,m_i}} = \sum_{j=1}^{m_i} p_{i,j} z^{q_{i,j}} \tag{5.11}$$

where z is just a symbolic notation. The index $q_{i,j}$ represents the value of the variable, and the coefficient $p_{i,j}$ represents the probability when the variable value is $q_{i,j}$. Therefore, the z- transformation for the system consisting of n random variables can be represented as:

$$\begin{aligned} U(z) &= \underset{f}{\otimes}(U_1(z), U_2(z), \cdots, U_n(z)) \\ &= \underset{f}{\otimes}\left(\sum_{j_1=1}^{m_1} p_{1,j_1} z^{q_{1,j_1}}, \sum_{j_2=1}^{m_2} p_{2,j_2} z^{q_{2,j_2}}, \cdots, \sum_{j_n=1}^{m_n} p_{n,j_n} z^{q_{n,j_n}}\right) \\ &= \sum_{j_1=1}^{m_1}\sum_{j_2=1}^{m_2}\cdots\sum_{j_n=1}^{m_n}\left(\prod_{i=1}^{n} p_{i,j_i} z^{f\left(q_{1,j_1}, q_{2,j_2}, \cdots, q_{n,j_n}\right)}\right) \end{aligned} \tag{5.12}$$

where $U(z)$ is the UGF of the function and $\underset{f}{\otimes}$ is the combination operator of UGF. For instance, if the system contains two components in series, the UGF of the system is given by:

$$U(z) = \underset{f}{\otimes}(U_1(z), U_2(z))) \quad = \sum_{j_1=1}^{m_1}\sum_{j_2=1}^{m_2}\left(\prod_{i=1}^{n} p_{i,j_i} z^{min\left(q_{1,j_1}, q_{2,j_2}\right)}\right) \tag{5.13}$$

Thus, the $\underset{f}{\otimes}$ combination operator is the minimum value of q_1 and q_2 of system variables under the governing constraints. Similarly, for a system with two components in parallel, the UGF can be represented as (5.14), where the combination operator is the addition of q_1 and q_2.

$$U(z) = \underset{f}{\otimes}(U_1(z), U_2(z))) \quad = \sum_{j_1=1}^{m_1}\sum_{j_2=1}^{m_2}\left(\prod_{i=1}^{n} p_{i,j_i} z^{\left(q_{1,j_1}+q_{2,j_2}\right)}\right) \tag{5.14}$$

5.3.2.3 The UGF Model for Radial Topology

In the radial topologies presented in Figs. 5.1 - 5.3, assume that there are n WTs per feeder and m total number of feeders. Consider the states of the WT as operating at power level P_x MW or failed state, i.e., 0 MW with corresponding state probabilities p_1 and $p_2(=1-p_1)$, respectively. For the time being, assume that the probability of power output level P_x is p_x=1. The UGF of the ith WT $U_i(z,x)$ can then be represented by:

$$U_i(z,x) = p_1 z^{P_x} + p_2 z^0 \tag{5.15}$$

For n WTs in parallel, the UGF function for kth feeder U_{Fk} is represented by:

$$\begin{aligned} U_{Fk}(z,x) &= \underset{\oplus}{\otimes}\left(U_1(z), U_2(z), \cdots, U_i(z), \cdots, U_n(z)\right) \\ &= \prod_{i=1}^{n}\left(p_1 z^{P_x} + p_2 z^0\right)^i = \left(p_1 z^{P_x} + p_2 z^0\right)^n \\ &= a_0 z^0 + a_1 z^{P_x} + a_2 z^{2P_x} + \cdots + a_i z^{iP_x} + \cdots + a_n z^{nP_x} \end{aligned} \tag{5.16}$$

Define the UGF of the platform dc/dc converter C1 with the corresponding state probabilities of perfect functioning as p_{c1} and failure as p_{c2} by:

$$U_{C1} = p_{c1} z^{nmP_x} + p_{c2} z^0 \tag{5.17}$$

Similarly, the UGF of the kth centralised dc/dc converter $\mathrm{CF_k}$ $(k = 1, 2, \cdots, k, \cdots, m)$ with corresponding state probabilities of perfect functioning as p_{cf1} and failure as p_{cf2} is defined as:

$$U_{CF_k} = p_{cf1} z^{nP_x} + p_{cf2} z^0 \tag{5.18}$$

Detailed calculations of UGFs of Radial-1, Radial-2 and Radial-3 topologies are reserved for Appendix A.

5.3.2.4 The UGF Model for Series–Parallel Topology

In SP topology, WTs are connected in series to build up a feeder and then the feeders are connected in parallel. Consider a feeder as a subsystem here. In this subsystem, when a single WT fails and is by-passed, the pole-to-pole voltage of the feeder must still be within the allowable voltage limits. However, the terminal voltages of healthy WTs increase to match the pole-to-pole voltage of the entire string. In this situation, if multiple WTs trip, healthy units experience overvoltages at their terminals beyond their maximum limits. Thus, as a safety measure, the entire feeder is required to implement a forced shutdown. Therefore, a feeder in the SP topology can be considered as a *k-out-of-n(G)* system.

Consider the feeder-F1 in Fig. 5.4 where n WTs are connected in series per feeder and there are m feeders in parallel. Assuming the power output of WTs is aggregated into n_{cl} clusters, the UGF of the feeder at the xth state can be represented as:

$$\begin{gathered} UGF_{F1}(z,x) = \sum_{i=0}^{n-k} C_n^i p_1^{(n-i)} p_2^i z^{P_x \times (n-i)} + \sum_{i=n-k+1}^{n} C_n^i p_1^{n-i} p_2^i z^0 \\ x = 1, 2, \cdots, n_{cl} \end{gathered} \tag{5.19}$$

where all variables are denoted as in Section 5.3.2.3. Assuming the negligible impact of the wake effect, the UGF of SP topology with m-parallel feeders can be defined as:

$$\begin{aligned} UGF_{SP}(z,x) &= p_{wt\_x} \times \underset{f}{\otimes} (UGF_{F1}(z,x), UGF_{F2}(z,x), \cdots, UGF_{Fm}(z,x)) \\ &= p_{wt\_x} \times UGF_{F1}(z,x) \times UGF_{F2}(z,x) \times \cdots \times UGF_{Fm}(z,x) \\ &= h_0 z^0 + h_1 z^{P_x} + h_2 z^{2P_x} + \cdots + h_{nm} z^{nmP_x} \end{aligned} \tag{5.20}$$

where p_{wt_x} is the probability of P_x being in the xth state. Finally, considering all n_{cl} cluster states, the UGF of SP topology can be obtained as follows.

$$UGF_{OWF\_SP}(z,x) = \sum_{x=1}^{n_{cl}} UGF_{SP}(z,x) \tag{5.21}$$

5.3.2.5 Reliability Indices

To evaluate the associated availability levels of different dc collection systems, the EENS and GRA [130] are used. The EENS is the energy the system that is not able to export to the point of connection due to uncertainties of the system. This can be expressed as:

$$EENS = \sum_{i=1}^{N} p_i \times (P_{OWF\,\max} - P_{OWFi}) \times 8760 \tag{5.22}$$

where p_i is the probability that the whole system is in the ith power output state, P_{OWFmax} is the rated capacity of the OWF, P_{OWFi} is the power output of the whole system in the ith state. The total number of states N is the product of the number of WTs n_{wt} and the number of WT power output clusters n_{cl}.

The GRA refers to the probability of at least a certain percentage (defined as Generation Ratio Criterion-GRc) of electrical energy that could be delivered to the grid. Let the column matrix V be defined by:

$$V = \begin{bmatrix} V_1 \\ V_2 \\ \vdots \\ V_x \\ \vdots \\ V_{n_{cl}} \end{bmatrix}_{n_{cl} \times 1} ; x = 1, 2, \cdots, n_{cl} \tag{5.23}$$

where $V_x = [a_0, a_1, a_2, ..., a_{nm}]$ is a row matrix with a_0, a_1, a_2,..., a_{nm} that denotes the corresponding state probabilities of the respective collection system and remains in a certain power output level P_x. GRA(GRc) represents the ratio of power generation availability under the condition of at least i working wind turbines:

$$GRA\,(GR_c) = \sum_{j=2}^{n_d} \sum_{h=i}^{nm} V(j,h) \quad ; GR_c = \frac{i}{n \times m} \times 100\% \tag{5.24}$$

5.3.3 Lifetime Cost Estimation

When identifying a suitable dc collection system option for an OWF, life cycle costs of candidate topologies are required to be considered. Cost estimation is as important as reliability evaluation. To fully reflect the economics of different topologies, both the initial investment costs and costs incurred due to network losses during its operational life cycle is incorporated. The initial investment cost mainly includes the cost of WTs, cables, and converters, while the costs associated with operational losses mainly include the cables and converter losses.

5.3.3.1 Capital Investment

1. **WT Cost**
   The dcWT concept is still at the research and development stage. Therefore, the capital cost was estimated, based on the available prices for acWTs of the same rated capacity, with required modifications. A detailed cost-breakdown of different components for a fully-rated, power-converter-based offshore acWT (Type-4) can be found in [131]. As discussed in Section 5.2.1, a DAB-based dcWT topology was considered in this analysis. This could be considered as an addition of an ac/dc converter to the acWT front-end, and the cost of ac/dc converter was 8667.4 £/MW. The required capital costs of 10 MW, 8 MW, and 5 MW dcWTs are shown in Table 5.1.

Table 5.1. Cost of dcWTs with different capacities.

WT Capacity (MW)	**Cost per WT (£)**
10	1,366,674
8	1,149,339
5	823,337

2. **dc/dc Converter Costs**
   The capital cost per unit capacity (£/MW) of a centralised dc/dc converter and platform dc/dc converter was different, due to various techno-economic factors. The cost of the centralised and the platform dc/dc converters were taken as 120 £/kVA [50], and 0.22 M£/MW [132], respectively.

3. **DC Cable Cost**
   To calculate the capital cost of dc cables with different current carry capacities, the following formula was considered, as discussed in [132, 133]:

$$\begin{aligned} C_{\text{cable}} &= \text{Rate} \times (A + BP_n) \times l_{\text{cable}} \\ P_n &= U_n I_n \end{aligned} \tag{5.25}$$

   where P_n is the rated power of the cable (W), U_n is the rated pole-to-pole dc voltage of the cable (V), and I_n is the rated current of the cable (A). The term *Rate* is the exchange rate of Swedish krona to the British pound, l_{cable} is the cable section length (km), and A and B are coefficients shown in Table 5.2.

Table 5.2. Coefficients for the dc cables

Voltage Levels (kV)	**A** ($\times 10^6$)	**B**
±10.0	-0.320	0.0850
±12.5	-0.320	0.0850
±20.0	-0.314	0.0618
±25.0	-0.314	0.0618
±40.0	0.0	0.0280
±100.0	0.079	0.0120

5.3.3.2 Costs Associated with Energy Losses

1. **Cable Losses (Radial Topology)**
   The current flow of a radial WT feeder is shown in Fig. 5.6. Notably, the upstream cable sections were required to carry more currents than the downstream sections.

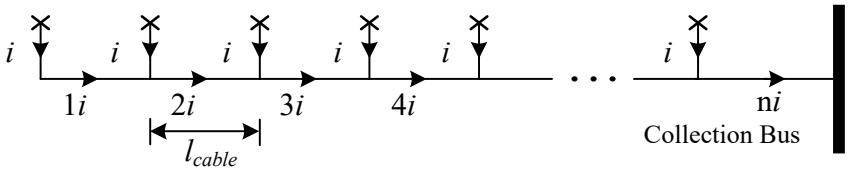

Fig. 5.6. Current flow in a radial feeder.

The total power loss for a certain rated current I (kA) can be obtained as follows [84]:

$$\begin{aligned} P_{\text{loss -cable}} &= \left(I^2 + (2I)^2 + (3I)^2 + \cdots + (nI)^2\right) R_{\text{cable}} \\ I &= \frac{P_w\left(v_w\right)}{U_{\text{cable}}} \\ R_{\text{cable}} &= Rl_{\text{cable}} \end{aligned} \tag{5.26}$$

where R is the cable resistance for a unit length (Ω/km), and l_{cable} is the cable length (km), as shown in Fig. 5.6. The distance between the wind turbines in the same feeder and adjacent feeders were set to $9D$, where D denotes respective rotor diameters of WTs [134].

2. **Cable Losses (SP Topology)**
   In SP topology, the current flowing through each section along the feeder is the same. Therefore, to obtain the cable losses of the SP topology the following can be used:

$$P_{\text{loss - cable}} = \left(I^2 + I^2 + \cdots + I^2\right) R_{\text{cable}} \tag{5.27}$$

3. **Converter Losses**
   Converter losses include both the centralised dc/dc converter and platform dc/dc converters. The required converter losses with different MVdc voltage levels and power levels were obtained using the PLECS simulations.

4. **Cost of Losses**
   The total annual energy losses of each dc collection system E_{loss} can be obtained by:

$$E_{\text{loss}} = \sum_{t_s}^{T} \left(P_{\text{loss - cable}} + P_{\text{loss - converter}}\right) t_s \tag{5.28}$$

where $P_{loss-cable}$ is the time-varying losses of dc cables that changes with wind speed and t_s is the corresponding sampling time, i.e., wind speed measurement interval. The term T is the total period considered (typically one year). Finally, the cost of losses during the life cycle C_{loss} can be obtained as follows:

$$C_{loss} = \frac{E_{loss} \times \text{ energy price}}{i}\left(1 - \frac{1}{(1+i)^{T_{ije}}}\right) \tag{5.29}$$

where i denotes the annual interest rate and T_{life} is the average life of an OWFs.

5.4 Case Study

5.4.1 Obtaining Optimal Number of Wind Power Output Clusters and Other Parameters

As discussed in Section 5.3, first it is required to obtain an optimal number of wind power output clusters with their corresponding state probabilities. Initially, the time series wind speed data is converted to corresponding power output using (5.1). In this analysis, 10-min average wind speed data available with FINO2 offshore weather station is used [135]. Table 5.3 summarises the nameplate data for selected WTs, with their capacities for three scenarios 10 MW (S1), 8 MW (S2), and 5 MW (S3). It is worth noting that the nameplate data provided in Table 5.3 were obtained from commercially available acWTs. They were used to refer to the corresponding power curves of dcWTs with the same capacity and to define the inter-turbine distances.

Table 5.3. Wind turbine nameplate data.

Capacity (MW)	Model	Rated Wind Speed (m/s)	Cut-in Speed (m/s)	Cut-out Speed (m/s)	Rotor Diameter (m)
10 (S1)	V164-9.5 [136]	14	3.5	25	164
8 (S2)	V164-8.0 [137]	13	4.0	25	164
5 (S3)	HTW5.0-126 [138]	13	4.0	25	126

Using the Jenks Natural Breaks clustering method, the WT power output for each rated capacity was clustered into a finite number of states. The optimum number of clusters were selected with the objective function value, which is defined as GVF in (5.4). Fig. 5.7 illustrates the corresponding GVF values for different number of clusters for 10 MW dcWT.

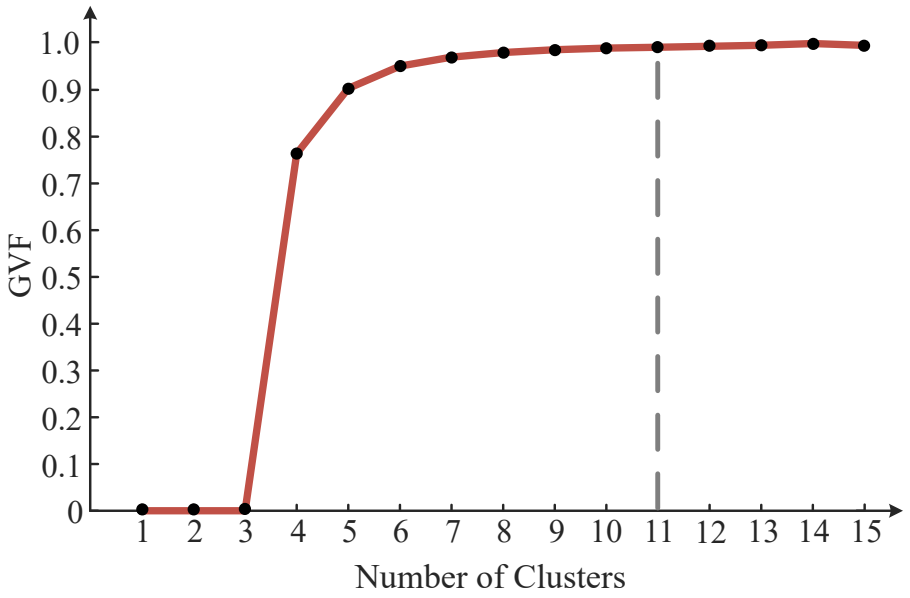

Fig. 5.7. Objective function value with the number of clusters for 10 MW wind turbine.

Notably, for this time-series data set, the GVF difference between adjacent clusters was less significant after 11 clusters. Therefore, 11 clusters were selected to represent the stochastic behaviour of the WT output. Table 5.4 summarises the cluster centre values with their corresponding state probabilities for 10 MW dcWT.

Table 5.4. OWF collection system options: advantages and disadvantages.

Cluster Number	**Cluster Centre (MW)**	**State Probability**
1	0.000	0.0700773
2	0.474	0.0422715
3	1.572	0.0756075
4	2.796	0.0811175
5	3.967	0.0929224
6	5.113	0.0934911
7	6.267	0.0968191
8	7.390	0.0924218
9	8.506	0.0869786
10	9.540	0.0664654
11	10.000	0.2018278

The failure and repair rates of different sub-assemblies of typical offshore WT is considered and summarised in Table 5.5. The failure rate of the dc/dc converter was obtained using the methodology presented in [139]. Notably, compared to other sub-assemblies, the failure rates of power converters were relatively higher due to the greater intrinsic failures of semiconductor devices. The availability level of 98% was considered for the platform dc/dc converters in complying with the specified availability levels of Crown Estate licensed offshore wind farms around the UK [116].

Table 5.5. Failure and repair rates of dcWT different sub-assemblies.

WT Component	**Failure Rate (occ/yr)**	**Repair Time (h)**
Generator [140]	0.1000	
dc breaker [141]	0.0250	
ac/dc converter [142]	0.1000	240
dc/dc converter [142]	0.6132	
Transformer [141]	0.0131	

To calculate the accumulated energy losses for different topologies, losses of dc/dc converters are required to be considered, as they are one of the key building blocks of the dc collection systems. The total switching and conduction losses of the dc/dc converters at different MVdc voltage levels and power levels are required to be first calculated. The accumulated energy losses of different topologies were obtained through PLECS simulation and are shown in Table 5.6. The notations R-1,2,3 denote the radial topologies shown in Figs. 5.1 $\sim$ 5.3, with their corresponding dc/dc converters C1 and C_{fl}.

Table 5.6. dc/dc converter parameters.

Rated Power (MW)	**Converter Type and Scenario**	**Input and Output Voltage Levels (kV)**	**Percentage Losses**
40	R-3 (C_{fl}); S2	$\pm 10/\pm 20$	1.79%
40	R-2 (C_{fl}); S2	$\pm 10/\pm 40$	1.88%
50	R-3 (C_{fl}); S3	$\pm 10/\pm 12.5$	1.53%
50	R-3 (C_{fl}); S1	$\pm 10/\pm 25$	1.68%
50	R-2 (C_{fl}); S2	$\pm 10/\pm 40$	1.65%
400	R-2 (C1); S1, S2, S3	$\pm 40/\pm 100$	1.31%
400	R-1 (C1); S1, S2, S3	$\pm 10/\pm 100$	1.44%

5.4.2 Reliability of DC Collection Systems

In general, EENS and GRA indices are used to evaluate reliabilities for different dc collection system options, which do not depend on load demand at the point of common coupling. It can be seen from Fig. 5.8 that irrespective of the topology, the larger the WT capacity, the larger the EENS. This is because the failure of a single WT with a higher rated power loses more energy as compared to a smaller WT that has the same failure probability. Among all four topologies, the Radial-3 configuration accounts for the largest EENS, whereas the Radial-1 topology shows the lowest for all the three WT scenarios.

Notably, for the 8 MW and 5 MW cases for Radial-1,2, and SP topologies, the EENS difference was about 0.1%. In this analysis, the same number of WTs (i.e., 10 WTs per feeder) was used for all scenarios, irrespective of the WT capacity. Therefore, the use of the same failure rates for each case results in lower EENS for lower WT capacity. This is one possible reason for this negligible EENS difference between the 8 MW and 5 MW cases.

The GRA for the whole range of GRc (from 1% to 100%) for all topologies of 10 MW (S1) is shown in Fig. 5.9. At higher GRc levels, the Radial-1 topology provides higher availability levels than the other three topologies. For instance, at GRc (90%), the Radial-1 topology shows a 90.6% availability level, followed by Radial-3 with 85.3%. The SP topology shows the lowest with an 81.8% availability level. It is worth noting that for the same GRc, different topologies represent different GRA levels. This is because, at

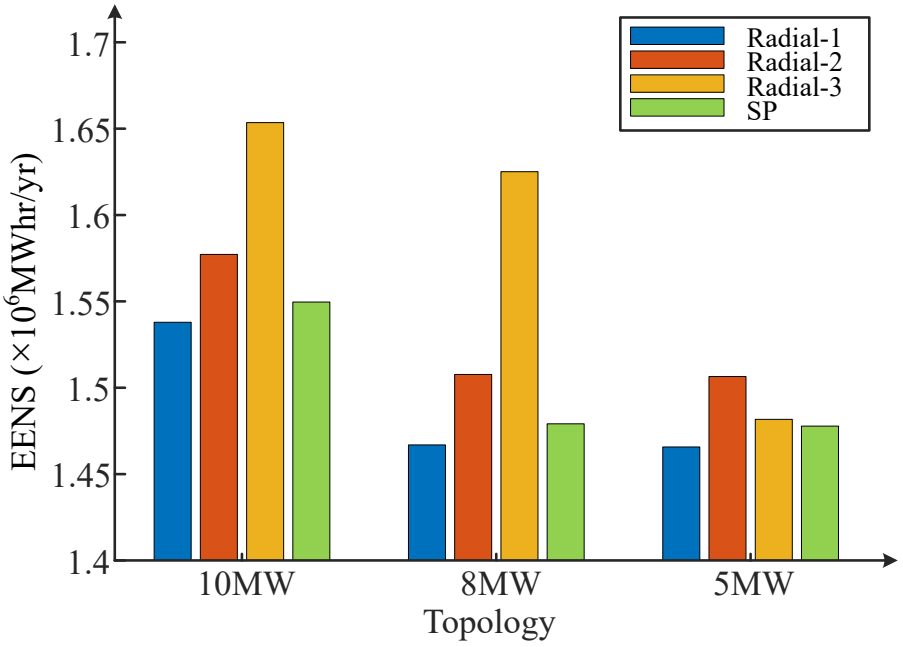

Fig. 5.8. EENS for different dc collection system options.

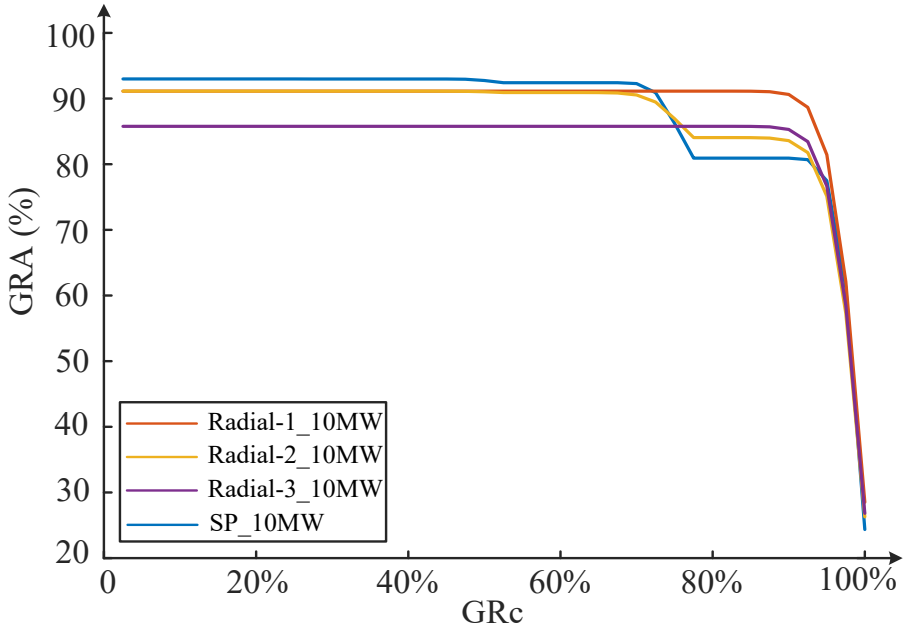

Fig. 5.9. GRA of candidate dc collection system options for the 10 MW WT case.

the same GRc of 90%, S1, S2, S3 requires at least 36, 45, and 72 WTs to be in healthy operating conditions, respectively. Thus, their state probabilities are different, and the availability levels vary, depending on the configuration.

Although the Radial-3 topology shows the second-highest availability level at GRc of 90%, until GRc of 75.4%, it shows the lowest availability level among the four topologies, making it the least reliable.

Similarly, Figs. 5.10 and 5.11 illustrate the GRA variation for different availability criterion related to 8 MW (S2) and 5 MW (S3) WT Cases. Similar to the previous case (S1), the GRA variation of S2 in Fig. 5.10 shows a similar pattern. However, the GRA of Radial-3 topology remained the lowest at GRA of 82.3%, until GRc up to 79.9%. At GRc of 90%, Radial-1 topology showed an availability level of 89.1%, which was 1.5% lower compared to S1.

Notably, for the S3 case until GRc of 73%, all the DC collection system options showed a similar GRA of about 90%, as shown in Fig. 5.11. This is because when the number of system components increases, it requires a relatively higher number of WTs to remain in a healthy operation condition at lower availability levels, as compared to cases S1 and S2. However, at higher GRc levels, failure of multiple WTs (to maintain the same availability ratio) will result in lower GRA values under the same WT failure rates. In this case, at GRc of 90%, Radial-1, 2, and 3 topologies showed 89.3%, 75.9%, and 77.5% GRA levels. Similar to other cases, SP topology showed the lowest availability level with 70.4%.

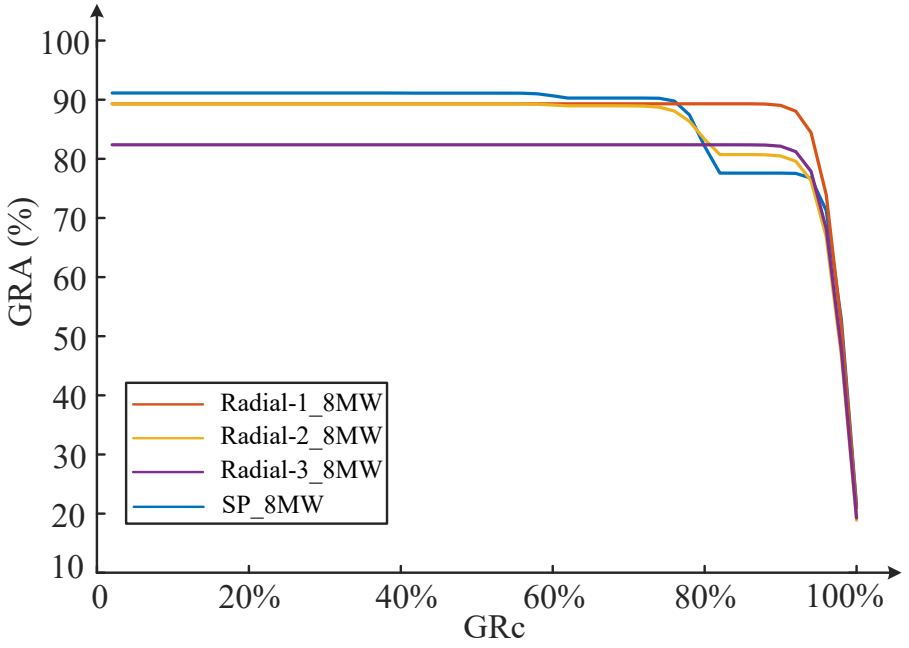

Fig. 5.10. GRA of candidate dc collection system options for the 8 MW WT case.

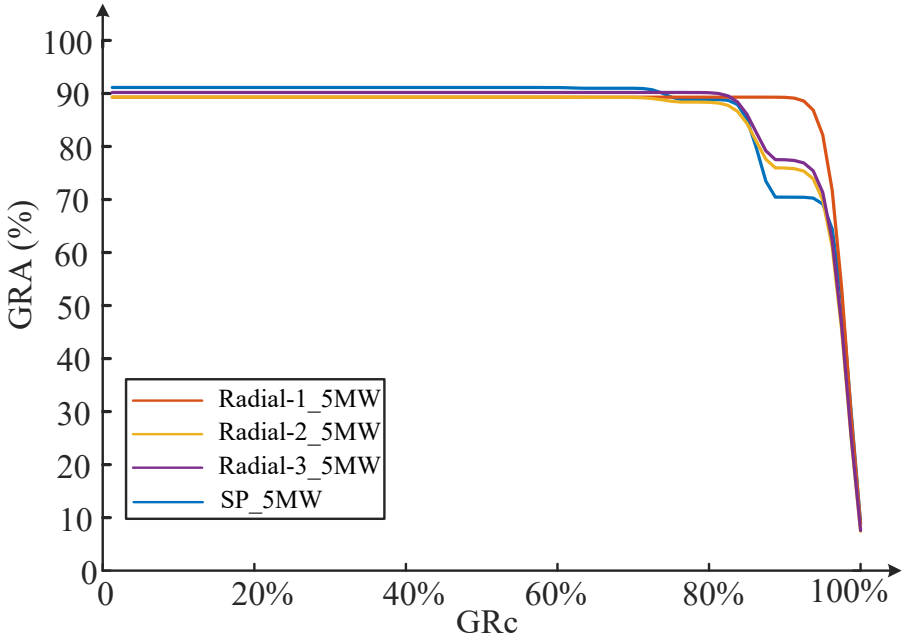

Fig. 5.11. GRA of candidate dc collection system options for the 5 MW WT case.

To observe the variation of GRA with different WT capacities with the available data, this study considered the same WT failure rate for all cases. As shown in Fig. 5.12 when all dc/dc converters were failure-free, the GRA variation of Radial-1, 2, 3 was the same, since the collection system configuration was radial. This also highlighted the importance of maintaining higher availability levels of dc/dc converters located at

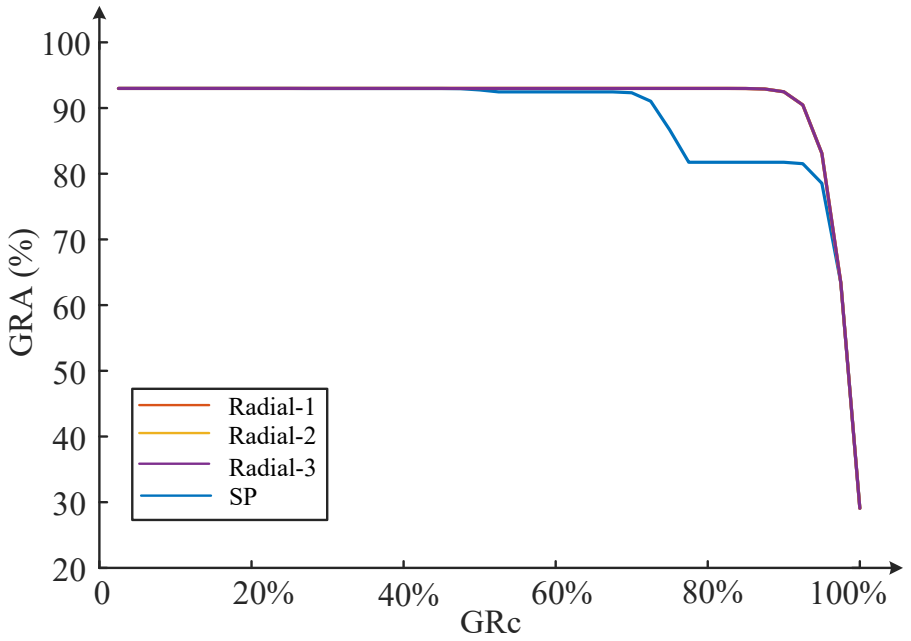

Fig. 5.12. GRA of different topologies with all dc/dc converters working perfectly.

different positions, for each radial configuration. However, the SP topology showed a different variation, since the WT connection was different.

5.4.3 Economic Evaluation of Candidate DC Collection Systems

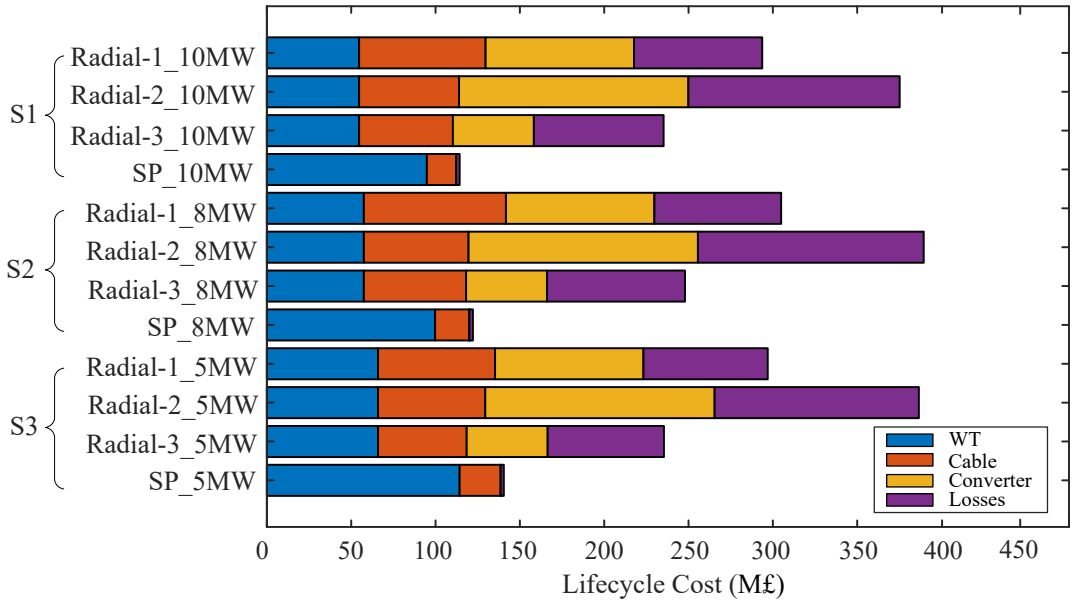

Fig. 5.13. Cost of 12 dc collection system schemes.

To assess the economies of scale of different candidate dc collection systems, the capital and operational costs of each topology were calculated, based on the methodology discussed in Section 5.3.3. As shown in Fig. 5.13, the capital cost included WT cost, cable cost, and converter cost, and the operational losses included cable- and converter-losses. For this analysis, the average lifetime of the offshore wind farm was considered as 25 years [25] and for electrical energy losses calculations, the energy price of 75 £/MWh [16] with a discount rate of 5% was considered [139].

Among the four topologies, the total cost of SP topology was significantly lower than other topologies, due to the elimination of the centralised dc/dc converter. For instance, this cost was about 34% of the lifetime cost of the Radial-1 configuration (S1), which showed better availability. The Radial-2 configuration showed the highest lifetime cost due to the higher capital cost of converters and system losses. For 10 MW and 8 MW dcWT capacities of Radial-1 configuration, the lifetime cost difference was about 11.2 M£.

5.4.4 Overall Assessment of DC Collection System Options

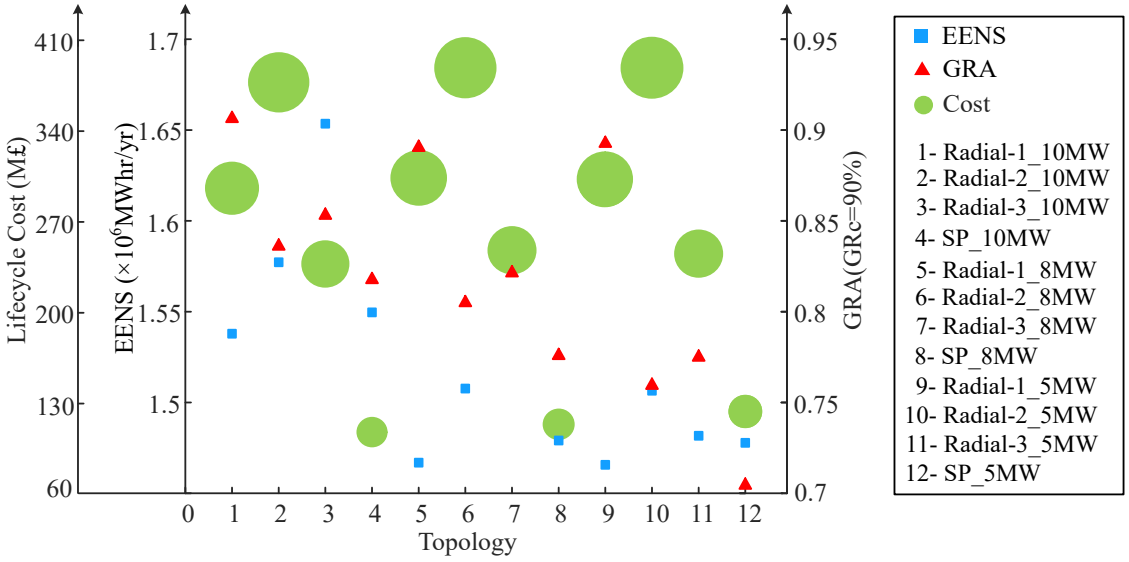

Fig. 5.14. Evaluation of 12 dc collection system schemes.

As discussed above, reliability and life cycle costs need to be considered to identify a suitable dc collection system option. Fig. 5.14 above summarises the three functional factors used to determine the reliable and cost-effective dc collection system option, according to the methodology presented. The ideal topology should be the one with the highest GRA, as well as the lowest EENS and life cycle cost. However, identifying the best topology is not straightforward, due to the inherent characteristics of different topologies.

For example, in SP topology, although the capital investment is lower, its GRA is relatively low, as compared to other radial configurations. Among the three radial configurations, Radial-1 shows the highest GRA with lower EENS for different WT capacities. Hence, it could be considered to be a suitable option for future dc collection systems.

5.4.5 Impact of the DC Voltage Level for the Reliability of Series-Parallel Topology

Although the SP topology does not qualify as a suitable option with the parameters used in the analysis, a sensitivity analysis was performed to assess its GRA variation and EENS with different terminal voltage levels. As summarised in Table 5.7, the dcWT terminal voltage was changed from ±2.5 kV to ±25 kV. This resulted in a different number of series-connected dcWTs per feeder. However, the HVdc pole-to-pole voltage level remained unchanged at ±100 kV. Notably, the ±2.5 kV with 40 WTs connected in series was a special case, as it contained a single feeder. This could be considered as the series topology.

According to Table 5.7, the EENS increased as the terminal dc voltage level increased, which is not favourable. However, in some cases, the use of a higher dc voltage level results in relatively lower EENS than the use of a lower dc voltage level. For instance, consider the ±20 kV and ±25 kV cases that connects 5 and 4 WTs in series. In this case, the use of ±25 kV was economical, since it had a lower EENS of 52,600 MWhr/yr, as compared to ±20 kV case. This was because, for both cases, if a single WT failed, the entire feeder was forced into shut-down; whereas in the ±25 kV case, it contained 10 parallel feeders, making it more reliable than the ±20 kV case with 8 feeders.

Table 5.7. EENS of SP topology with different dcWT voltage.

WT Capacity (MW)	**Terminal Voltage (kV)**	**WTs per Feeder**	**EENS (x10^6 MWhr/yr)**
10	±2.5	40	1.4980
	±5.0	20	1.5015
	±10.0	10	1.5496
	±12.5	8	1.5292
	±20.0	5	1.7179
	±25.0	4	1.6653

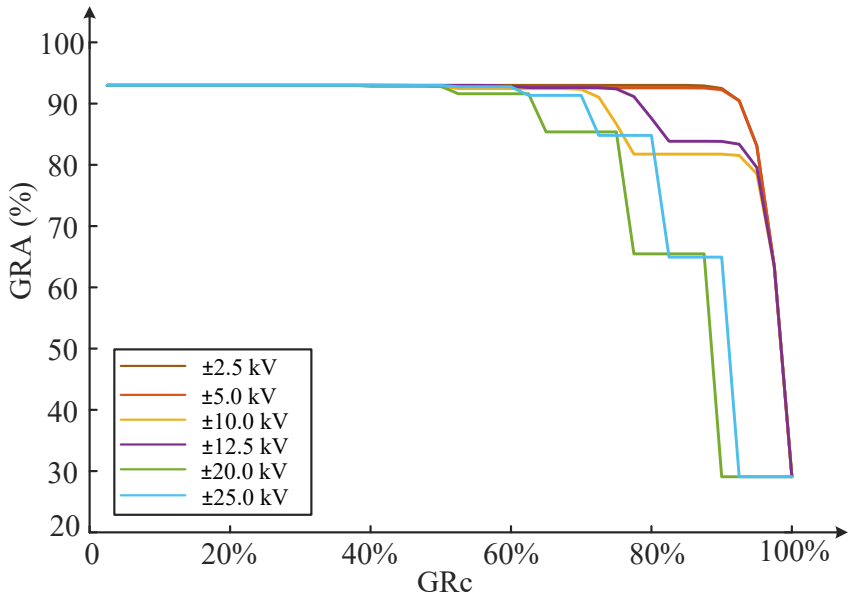

Fig. 5.15. Variation of GRA with the terminal voltage level of SP topology.

Similarly, the GRA variations illustrated in Fig. 5.15 showed better availability levels at higher dc voltage levels, for the same reason as discussed above. However, the use of a lower dc voltage level with a higher number of series-connected dcWTs could provide higher availability levels. For instance, at GRc of 90%, the GRA of ±2.5 kV, ±10 kV, and ±12.5 kV were 92.5%, 81.8%, and 83.8%, respectively.

5.5 Summary

In this analysis, three different WT capacities were used to observe the variation of reliability and economic factors with different dc collection systems. The results suggest that with an increase in dcWT capacity, the GRA of the collection systems increased. Although SP topology showed a significantly lower life cycle cost, the reliability was relatively low due to its series-connected network structure over the other radial topologies. Since there are no dc collection systems under operation at present, several assumptions were made when conducting this study. For instance, the failure rates and costs of components such as dcWT, platform dc/dc converters were calculated by referring to the relevant literature.

The sensitivity analysis conducted to observe the impact of the reliability of dc/dc converters on the overall availability levels of the collection systems revealed the requirement to pay higher attention to improve their reliability levels. However, with field experience and technology advancements, the reliability can be improved, although the high-power dc/dc converter technology is still not mature.

Chapter 6

Availability Assessment of Large-Scale Offshore Wind Farms including their Collector Systems

6.1 Introduction

A detailed availability assessment will assist in obtaining accurate information about the performance of an offshore wind farm. This helps planning preventive maintenance effectively and obtain a clear view of the long-term performance of an offshore wind farm. For a detailed availability assessment, it is required to consider all the key building blocks of the system. However, as discussed in section 2.6, it is required to observe the impact of the inclusion of the network dependency in availability assessment of OWFs irrespective of their lower failure rates.

In Chapter 5, an analytical method was proposed to evaluate the reliabilities of different dc collection system configurations. It was identified that radial-1 topology is relatively reliable than other topologies. In this chapter, a holistic approach combining multi-state Markov processes and the UGF method (presented in Chapter 5) was extended for the reliability assessment of radial large-scale offshore wind farms. With the increase of offshore wind farm size, the use of classical analytical reliability methods becomes computationally intractable. However, the proposed model combines multi-state wind turbine output, wind turbine reliability and inter-array cable reliability models to assess its output at the point of common coupling. A strategy is developed to split the network into its feeders while still accounting for the wind turbine output dependence, significantly reducing the computational burden.

6.2 Methodology

6.2.1 Mathematical Framework

In this section, the stochastic models for the wind farm elements is presented. All elements in a wind farm can be modelled using a time-homogeneous Markov process. Therefore, it is properly introduced before applying it to the specific wind farm elements. The proposed method consists of two parts:

(a) the availability assessment of the individual components using a time-homogeneous multi-state Markov process, and

(b) the wind farm availability assessment at the point of common coupling using an UGF technique, combining the availability of the individual components.

This analysis considered the wind turbine output, wind turbine reliability and the cable reliability. A multi-state system strategy was presented to determine the stochastic output of a wind farm based on the UGF technique. This strategy combines the stochastic performance of its elements and was extended to account for wind turbine output dependency.

6.2.2 Time-Homogeneous Markov Process

The statistical independence among system components and their stochastic behaviour is required to evaluate to qualify to use the UGF. In this regard, one essential feature is that all the random variables are required to hold Markov properties [143]. In general terms it is a process for which predictions can be made regarding future outcomes based solely on its present state and more importantly future and past states are independent [144].

A Markov process is a stochastic process that transit from one state to another within an allowed set of states. A Markov process is characterised by three elements:

1. A state space $\mathcal{S}$, which is a finite or continuous set of values $x \in \mathcal{S}$ that the process is allowed to take.
2. A transition operator $p\left(\mathcal{X}_{t+1} \mid \mathcal{X}_t\right)$ where $t \in \mathcal{T}$ that defines the probability of moving from state $\mathcal{X}_t$ to $\mathcal{X}_{t+1}$.
3. An initial condition distribution $\pi(0)$ which defines the probability of being in any one of the possible states at the initial iteration $t = 0$.

The time index can be discrete or continuous and in this analysis the stochastic nature of all the system components are assumed to fall under the category of continuous-time finite state space.

A continuous-time Markov process is a random process $\{\mathcal{X}(t)\colon t \geq 0\}$ which holds the Markov property and represent the evolution of a system whose behaviour is only probabilistically known. It can be mathematically represented by:

$$p\left(\mathcal{X}(t+s) = j \mid \mathcal{X}(u) = x(u), 0 \leq u < s, \mathcal{X}(s) = i\right) = p\left(\mathcal{X}(t+s) = j \mid \mathcal{X}(s) = i\right). \quad i, j, x(u) \in \mathcal{S} \tag{6.1}$$

This means that the current state (at time instance t) is sufficient to determine the probability of the next state (at time $t+s, \forall s, t \geq 0$). Note that $\mathcal{X}(t) = i$ implies that $\mathcal{X}(u) = i$ for all $u \in [t; t+\epsilon)$, for some $\epsilon > 0$. However, additional information about the past is irrelevant. This memory-less property is formally know as the Markov property.

A Markov process is called time-homogeneous if and only if the transition probabilities are independent of the time. The transition probability p_{ij} from state i to j in time interval t is represented by:

$$p_{ij} = p\left(\mathcal{X}(t+s) = j \mid \mathcal{X}(t) = i\right). \quad \forall s, t \geq 0 \tag{6.2}$$

The probability of the transition is independent when $t \to \infty$. For this reason such Markov processes have stationary transition probabilities. In the following section time-homogeneous Markov property of key components of a OWF collection system is discussed.

6.2.3 Stochastic Behaviour of Wind Farm Components

6.2.3.1 Wind Turbine Output

In order to model the wind turbine output as a time-homogeneous Markov process, two conditions must be met: (a) the sojourn time of any wind speed state needs to follow an exponential distribution, and (b) the continuous wind speed state-space needs to be translated to a discrete one. Condition (a) is met if the non-stationary effects due to seasonal variation can be neglected [95]. This assumption holds for long-term reliability studies and if the wind speed data set is sufficiently large, i.e., longer than one year. Condition (b) is accomplished through clustering of the wind speed data. In this work, the clustering technique proposed in [87] was used. Each data point belongs to a single cluster $s \in \mathcal{S}^{\text{wto}}$ which was selected based on the minimum Euclidean distance to the cluster center. Two special clusters were introduced for a specific wind turbine:

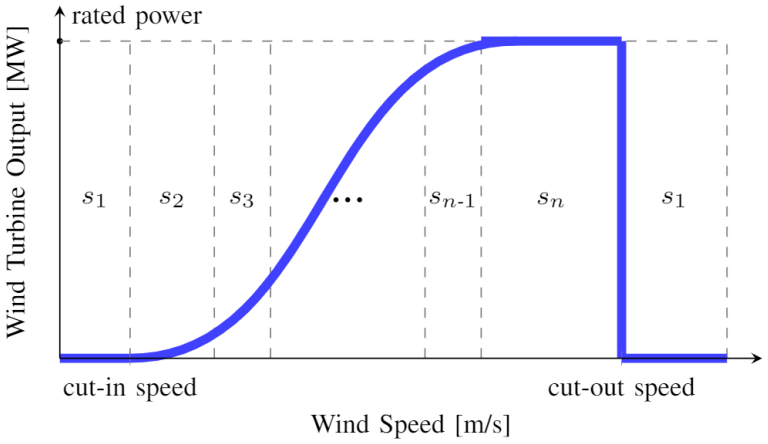

Fig. 6.1. Typical wind turbine power output curve and its discrete state space.

s_1 - groups all wind speed data below its cut-in speed or above its cut-out speed; and

s_n - groups all wind speed data corresponding with its rated speed.

It should be noted that the cluster size does not need to be uniform as shown in Fig. 6.1.

6.2.3.2 Wind Turbine Reliability

The WT reliability model defines the output characteristics of the WT as well as its failure and repair processes. Failures of WTs usually occur due to ageing, wear-out of parts or manufacturing defects. Several studies showed that the size of the WT, operation and environmental factors could lead to different failure modes [145, 146]. Considering failures of WTs as independent events, the stochastic failure nature of a WT can be modelled as Markovian components with two states [87, 95, 98, 99, 101].

In general, the binary states of the WT i.e. the machine is considered fully capable of delivering any output within its limits (up) or it is out of order (down) are defined with known average failure and repair rates, $\bar{\lambda}$ and $\bar{\mu}$ respectively. In here $\bar{\lambda}$ is the failure transition rate from an up state to a down state, where $\bar{\mu}$ is the repair transition rate from a down state to an up state. The averaged failure and repair rates of the binary system relate to those of the multi-state system as [52]:

$$\bar{\lambda} = \sum_{f \in \mathcal{F}^{\text{wtr}}} \lambda_f \tag{6.3}$$

$$\bar{\mu} = \bar{\lambda} / \sum_{f \in \mathcal{F}^{\text{wtr}}} \lambda_f \mu_f^{-1} \tag{6.4}$$

The wind turbine reliability is governed by that of its sub assemblies, e.g., gearbox (b), generator (g) and power converter (pc). Furthermore, each failure is categorised based

on the subsequent corrective maintenance (cost), e.g., minor repair (r_1), major repair (r_2) and replacement (r_3) [147]. Rather than using averaged failure and repair rates, a multi-state system provides a more accurate representation of the failure modes of large-scale OWF [148]. Hence, the failure modes were defined as:

$$\mathcal{F}^{\mathrm{wtr}} = \{f^{\mathrm{b,r_1}}, f^{\mathrm{b,r_2}}, f^{\mathrm{b,r_3}}, f^{\mathrm{g,r_1}}, f^{\mathrm{g,r_2}}, f^{\mathrm{g,r_3}}, f^{\mathrm{pc,r_1}}, f^{\mathrm{pc,r_2}}, f^{\mathrm{pc,r_3}}\}. \tag{6.5}$$

The three subsystems of the WT with respective failure categories have been represented with time-homogeneous Markov models as shown in Fig. 6.2.

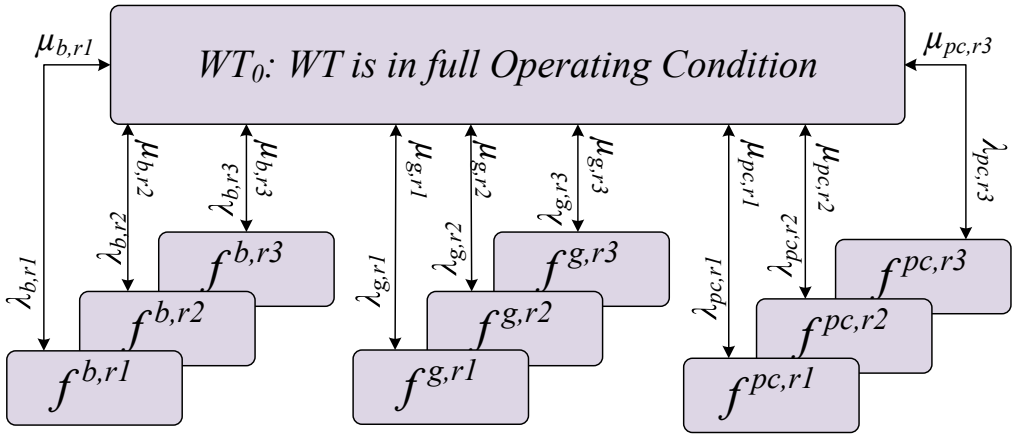

Fig. 6.2. Multi-state Markov model of the wind turbine.

6.2.3.3 Cable Section Reliability

Sub-sea power cables and terminations are continuously subject to electrical, thermal, mechanical, and environmental stresses. Both Crow-AMSAA [149] as the Weibull distribution [150, 151] have been used to predict the reliability of cables. The Crow-AMSAA model only considers the accumulated failures per year while the Weibull model considers the failure rate of each component sub-system. Therefore, the Crow-AMSAA model is more suitable for mixed failure mode analysis with less failure information about sub-systems while the Weibull distribution is more useful for detailed failure mode representation [152].

Like other power systems assets, the lifetime of sub-sea cable also follows the well-known bathtub curve, which consists of a burn-in, useful life and wear-out phase [150]. In this work, it was assumed that the sub-sea cables were in their useful life phase, having constant failure rates [55, 153, 154]. Similar to the wind turbine, a cable system can be divided into sub assemblies: sub-sea cable (c) and its terminations (t). Consequently, its failure modes were defined as:

$$\mathcal{F}^{\mathrm{cbl}} = \{f^{\mathrm{c}}, f^{\mathrm{t}}\}. \tag{6.6}$$

The cable subsystems with respective failure categories have been represented with time-homogeneous Markov models as shown in Fig. 6.3.

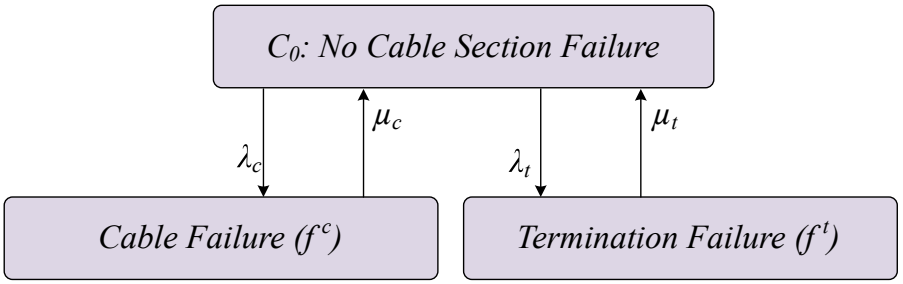

Fig. 6.3. Multi-state Markov model of the cable section.

6.2.4 Universal Generating Function Strategy

In this section, a multi-state system strategy was presented to determine the stochastic output of a wind farm. The strategy combines the stochastic performance of its components, i.e., wind turbines, cables, etc., using the UGF method introduced by Lisnianski [155] but was extended to account for wind turbine output dependency.

Any component $e \in \mathcal{E}$ is represented by its UGF:

$$\omega_e(z) = \sum_{s \in \mathcal{S}_e^{\text{red}}} p_s \cdot z^{v_s}, \quad \forall e \in \mathcal{E}, \tag{6.7}$$

where $\mathcal{S}_e^{\text{red}}$ represents its reduced state-space with unique performances v_s and associated probabilities p_s. The combination performance of multiple components with respect to a specific user $u \in \mathcal{U}$ may be found through its universal generating operator (UGO):

$$\Omega_u\big([\omega_e(z)]_{e\in\mathcal{E}}\big) = \sum_{\gamma \in \Gamma} f^{\text{prb}}(\gamma) \cdot z^{f^{\text{str}}(\gamma)}, \tag{6.8}$$

where Γ denotes the Cartesian product of the relevant components' reduced state space: $\Gamma = \prod_{e\in\mathcal{E}} \mathcal{S}_e^{\text{red}}$. Its elements γ are ordered tuples of states $(s_e)_{e\in\mathcal{E}}$, each corresponding to a specific component's reduced state-space $\mathcal{S}_e^{\text{red}}$. The probability function $f^{\text{prb}}(\gamma)$ gives the product of state probabilities corresponding to a tuple γ:

$$f^{\text{prb}}(\gamma) = \prod_{s_e \in \gamma} p_{s_e}. \tag{6.9}$$

The structure function $f^{\text{str}}(\gamma)$ expresses the resulting performance towards the user corresponding to a tuple γ [155].

Given the large number of components in a realistic wind-farm, it is computationally intractable to solve the entire system directly using the UGF method. To put this into context: a wind farm with 100 binary components, i.e., $|\mathcal{S}_e| = 2$ and $|\mathcal{E}| = 100$, amounts to $2^{100} \approx 1.25e30$ possible combinations. Given the radial nature, the obvious strategy to reduce the computational burden would be to split the wind farm in its feeders $\phi \in \Phi$, evaluate them separately before determining their overall impact on the user's performance. Continuing on the previous example, if the wind farm would consist of ten feeders, the number of combinations would be reduced to $10 \cdot 2^{10} = 10240$. However, this is still impossible to solve due to the wind turbine output dependency, i.e., it should be the same over all feeders which cannot be enforced if the feeders are evaluated separately. The following strategy circumvents this dependency:

1. temporarily replace the wind turbine output UGF by $\omega_w(z) = 1.0 \cdot z^{1.0}$;
2. evaluate the performance of the wind farm as ω^{ntw}, possibly splitting the collector system; and
3. multiply ω^{ntw} with the original wind turbine output UGF.

This strategy holds if all other components are binary components, meaning they are either unavailable of available, and, if available, their capacity exceeds that of the wind turbines connected.

The following radial two-feeder, four-WT and four-cables system shown in Fig 6.4 illiterates the above UGF strategy.

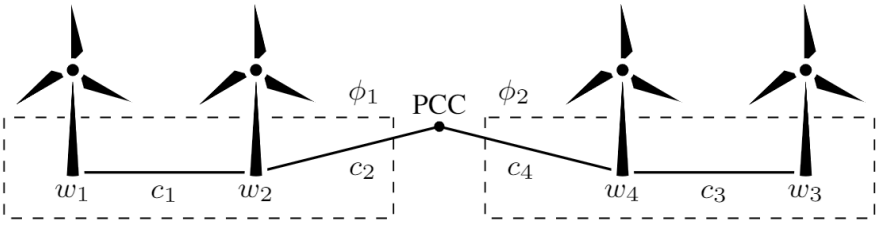

Fig. 6.4. Wind farm with four wind turbines w_1-w_4 and cables c_1-c_4.

The stochastic behaviour of a wind turbine output w and cable c are described by:

$$\omega_w(z) = p_w z^{0\,\text{MW}} + (1 - p_w) z^{P_w\,\text{MW}}, \quad \forall w \in \mathcal{W}, \tag{6.10}$$

$$\omega_c(z) = p_c z^{0\,\text{MW}} + (1 - p_c) z^{P_c\,\text{MW}}, \quad \forall c \in \mathcal{C}, \tag{6.11}$$

where p_w and p_c denotes the failure probabilities of individual wind turbines and cable sections, respectively. The notation P_w denotes the WT rated capacity, and P_c denotes

the current carrying capacity of the cable, where $P_c = 2 \cdot P_w$. The structure function of the wind farm with respect to the PCC is given by:

$$f^{\text{str}}(\gamma) = \min(v_{c_2}, v_w + \min(v_{c_1}, v_w)) + \min(v_{c_4}, v_w + \min(v_{c_3}, v_w)). \tag{6.12}$$

Given the wind turbine output dependence, all wind turbine's performances may be replaced by a single performance v_w. The Cartesian product Γ of the components' state-spaces contains $2^1 \cdot 2^4 = 32$ tuples γ. To put this into context, consider an illustrative example with $P_w = 2$ MW, $P_c = 4$ MW, p_w=0.3 and p_c=0.1. The performance of the wind farm at the PCC is given by: (The full calculation is reserved for Appendix B.1.)

$$\omega^{\text{pcc}}(z) = 0.307 \cdot z^{0\,\text{MW}} + 0.0126 \cdot z^{2\,\text{MW}} + 0.11907 \cdot z^{4\,\text{MW}} + 0.10206 \cdot z^{6\,\text{MW}} + 0.45927 \cdot z^{8\,\text{MW}} \tag{6.13}$$

Alternatively, using the presented strategy, the feeders could be evaluated separately, each using their own structure function:

$$f^{\text{str}}_{\phi_1/\phi_2}(\gamma) = \min(v_{c_2/c_4}, v_w + \min(v_{c_1/c_3}, v_w)). \tag{6.14}$$

Conform the strategy, the UGF of the wind turbine output is temporarily replaced by $\omega_w(z) = 1.0z^{1\,\text{MW}}$. Consequently, given their symmetry, both feeder's UGF $\omega_\phi(z)$ is given by: (The full calculation is reserved for Appendix B.2.)

$$\omega_\phi(z) = 0.1 \cdot z^{0\,\text{MW}} + 0.09 \cdot z^{1\,\text{MW}} + 0.81 \cdot z^{2\,\text{MW}}. \tag{6.15}$$

Combining both feeders ϕ_1 and ϕ_2 results in:

$$\omega^{\text{ntw}}(z) = 0.01 \cdot z^{0\,\text{MW}} + 0.018 \cdot z^{1\,\text{MW}} + 0.1701 \cdot z^{2\,\text{MW}} + 0.1458 \cdot z^{3\,\text{MW}} + 0.6561 \cdot z^{4\,\text{MW}}. \tag{6.16}$$

After combination with the original wind turbine output UGF $\omega_w(z) = 0.3z^{0\,\text{MW}} + 0.7z^{2\,\text{MW}}$, the performance of the wind farm at the PCC becomes:

$$\omega^{\text{pcc}}(z) = 0.307 \cdot z^{0\,\text{MW}} + 0.0126 \cdot z^{2\,\text{MW}} + 0.11907 \cdot z^{4\,\text{MW}} + 0.10206 \cdot z^{6\,\text{MW}} + 0.45927 \cdot z^{8\,\text{MW}} \tag{6.17}$$

Comparing (6.13) with (6.17), it can be seen that the proposed strategy gives the same solution, whereas it only required evaluation of $2 \cdot 2^2 + 3^2 + 2 \cdot 5 = 27$ combinations. Although the difference seems small in this particular case, it circumvents the exponential growth in combinations when the wind farm size becomes realistic.

6.2.5 Reliability Indices

Two indices, i.e., GRA and EENS, were introduced to show the impact of the contributions. GRA was defined as the probability that at least a given percentage of the wind power can be transferred to the PCC [130]. That percentage was referred to as the GRc. For example, for a GRc of 70 % in given wind conditions which result in total wind power output of 200 MW, the corresponding GRA gives the percentage that at least 140.0 MW can be transferred to the PCC. As a result, the GRA is not subject to wind speed variability and therefore is a very appropriate index to show the impact of reliability. The GRA for a given GRc can be determined using ω^{ntw} as:

$$\text{GRA}(\text{GRc}) = \sum_{i \in \mathcal{I} \,:\, \text{cnd}_i} \omega^{\text{ntw}}.p_i, \text{cnd}_i = \omega^{\text{ntw}}.v_i \geq \text{GRc} \cdot \max(\omega^{\text{ntw}}.v), \tag{6.18}$$

where $\mathcal{I}$ gives the set of all elements of UGF ω^{ntw}. The condition cnd_i evaluates whether the corresponding value of the UGF $\omega^{\text{ntw}}.v_i$ is greater or equal to GRc.

The EENS index gives the expected yearly energy that cannot be delivered to the PCC with respect to the maximum yearly energy of the wind farm. In contrast to GRA, EENS incorporates the wind speed variability. The EENS can be determined using ω^{pcc} as:

$$\text{EENS} = 8760 \cdot \sum_{i \in \mathcal{I}} \omega^{\text{pcc}}.p_i \cdot (\max(\omega^{\text{pcc}}.v) - \omega^{\text{pcc}}.v_i) \tag{6.19}$$

6.3 Case Study

In this section, a case study is presented for the Anholt offshore wind farm located between Djursland and Anholt island in Denmark [122]. To demonstrate the effectiveness of the proposed strategy on a real OWF with an uneven network structure, this case study considers a radial ac collection system. However, this methodology can easily be extended to radial dc collection system upon availability of required data.

The Anholt wind farm comprises 111 wind turbines and a collector system consisting of 177 km inter-array cables (Fig. 6.5). First, the impact of the collector system reliability was studied. Second, the impact of modelling each component as a multi-state system was discussed. All analyses in this case study were performed using MultiStateSystems.jl[1], a package developed in Julia to solve multi-state systems [156].

[1] Available at https://github.com/timmyfaraday/MultiStateSystems.jl

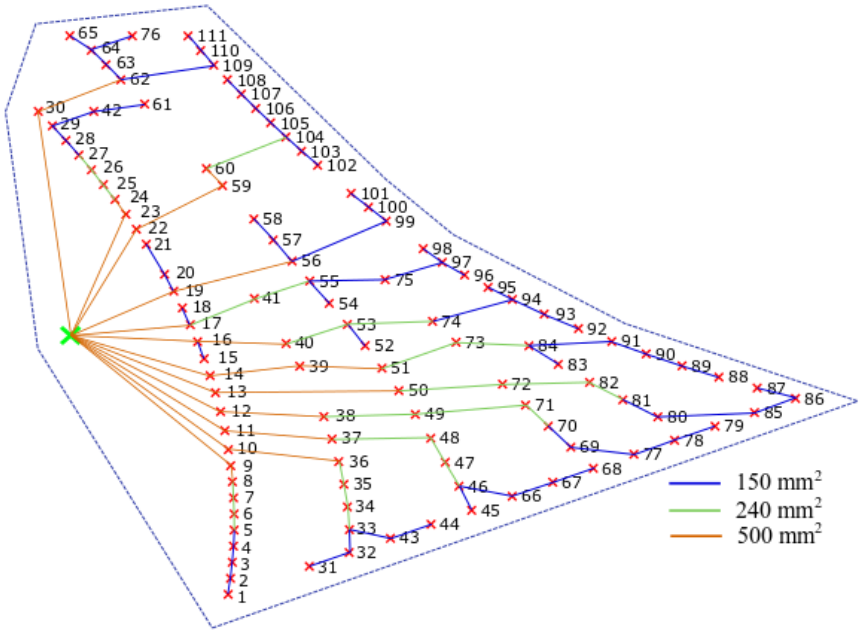

Fig. 6.5. Inter array cable configuration of the Anholt offshore wind farm.

6.3.1 Anholt Wind Farm

The Anholt wind farm includes 111 Siemens SWT-3.6-120 wind turbines with a rated power of 3.6 MW and a rotor diameter of 120 m, amounting to a nameplate capacity of 399.6 MW. All wind turbines have a cut-in speed of 3.5 m/s, rated speed of 14.0 m/s, and cut-off speed of 25.0 m/s. To determine the wind turbine power output, ten minutes averaged wind speed data from the Anholt wind farm was combined with its power curve [105]. This data set comprises one year of wind speed data, i.e., 52 560 wind speed data points. Once the time series of the wind turbine power output was obtained, it was clustered using the method discussed in Section 6.2.3.1. An example of eight clusters is shown in Table 6.1, including the cluster centres and corresponding transition rate matrix.

Table 6.1. Illustration of wind turbine output clustering for eight clusters including their centre and transition rates.

Cl.	**Centre**	**Transition Rates [1/yr]**							
	[MW]	**1**	**2**	**3**	**4**	**5**	**6**	**7**	**8**
1	0.000	0.0	4706.6	27.0	9.0	0.0	0.0	9.0	27.0
2	0.187	2739.6	0.0	3769.5	120.2	10.5	0.0	5.2	0.0
3	0.655	21.5	5229.3	0.0	5601.3	221.8	21.5	14.3	0.0
4	1.224	0.0	136.2	7372.2	0.0	7217.9	326.8	108.9	9.1
5	1.818	0.0	21.7	152.1	9030.1	0.0	7726.2	1075.8	108.7
6	2.361	0.0	0.0	0.0	407.9	12929.3	0.0	11687.8	248.3
7	3.099	11.3	0.0	33.9	90.4	1174.6	7476.9	0.0	7431.7
8	3.600	14.2	0.0	0.0	9.5	33.2	61.7	3141.8	0.0

As discussed in Section 6.2.3.2, wind turbine reliability is governed by that of its sub-assemblies. For the purpose of this case study, the reliability data presented in [147, 148] was used. This data complies with the Anholt wind turbines as it is valid for wind turbines with an output range of 2.0 MW to 4.0 MW and a rotor diameter range of 80 m to 120 m. Table 6.2 summarises the relevant data for each of these sub-assemblies and the corrective maintenance strategies following a specific failure.

Table 6.2. Reliability of wind turbine sub-assemblies.

Sub-Assembly	**Corr. Maintenance**	λ_f **[1/yr]**	μ_f **[1/hr]**
Gearbox (b)	Minor (r_1)	0.059	0.0132
	Major (r_2)	0.042	0.0361
	Repl. (r_3)	0.432	0.0752
Generator (g)	Minor (r_1)	0.007	0.1695
	Major (r_2)	0.024	0.3704
	Repl. (r_3)	0.437	0.0625
Converter (c)	Minor (r_1)	0.077	0.0158
	Major (r_2)	0.338	0.0443
	Repl. (r_3)	0.538	0.0515

The collector system consists of 177 km of inter-array cables. Each cable segment may have a different length and diameter, depending on the number of connected wind turbines. The Anholt wind farm comprises three different cable diameters, i.e., 150, 240 and 500 mm^2, with corresponding failure rates [55, 157, 158]. Table 6.3 summarises the relevant data.

Table 6.3. Reliability of the cable system.

Diameter	**Cable**		**Cable Termination**	
	λ [1/yr/km]	μ [1/hr]	λ [1/yr]	μ [1/hr]
150/240 mm^2	7.43e-3	6.94e-4	1.68e-3	9.26e-4
500 mm^2	9.45e-3	6.94e-4	1.68e-3	9.26e-4

6.3.2 Impact of Collector System Reliability

The collector system of the Anholt wind farm consists of twelve radial feeders, nine feeders with nine wind turbines and three feeders with ten wind turbines. The lay-out of each feeder is different, resulting in a unique structure function for each feeder. The impact of the collector system was determined using the strategy presented in Section 6.2.4. Three scenarios were considered:

1. *fully reliable*, both the wind turbine and cable system reliability are neglected;
2. *including wind turbine reliability*, the wind turbine reliability is considered, the cable system is still neglected; and
3. *including wind turbine and cable system reliability*, both the wind turbine and cable system reliability are considered.

All components were modelled as multi-state systems. Using the strategy presented in Section 6.2.4, the state-space Γ contains 8, 6.14e4 and 4.40e7 elements, respectively. A brute-force approach for the third scenario would result in a state-space Γ containing 5.39e67 elements. Therefore, applying the proposed strategy reduces the state-space Γ with a factor of 1.22e60. A 3.10 GHz Dual-Core MacBook Pro with 16 Gb of memory solved the respective scenarios in 0.98 s, 10.61 s and 150.22 s.

Fig. 6.6 shows the EENS for the three scenarios with respect to the number of wind speed clusters. Two conclusions can be drawn from this figure. First, at least eight clusters are necessary to accurately represent the Anholt wind speed data. Second, not including wind turbine and cable system reliability introduces an error with respect to the EENS: 3.89 GWh/yr (0.2 %) and 19.89 GWh/yr (1.0 %), respectively. To put this into context, using the average Danish electricity price of 36.57 \$/MWh (2017) [159], this amounts to 4.70 M\$ and 24.05 M\$, respectively, over the lifetime of the Anholt wind farm (20 yr) with a discount rate of 5 % [160]. The impact of the collector system reliability significantly exceeds that of the wind turbine reliability, i.e, by a factor five.

Fig. 6.7 shows the GRA for the three scenarios with respect to the GRc. This figure affirms the previous conclusions. For a GRc of 95.0 %, the GRA is reduced to 76.3 %

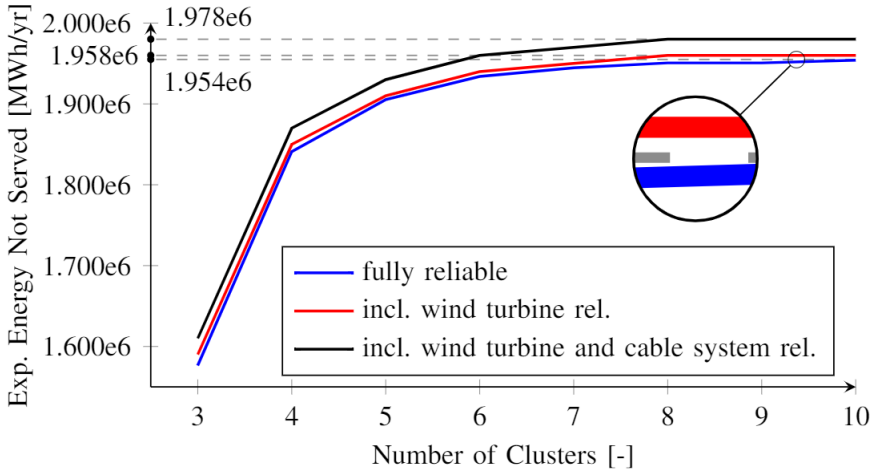

Fig. 6.6. Expected energy not served for the Anholt wind farm in function of the number of wind speed clusters.

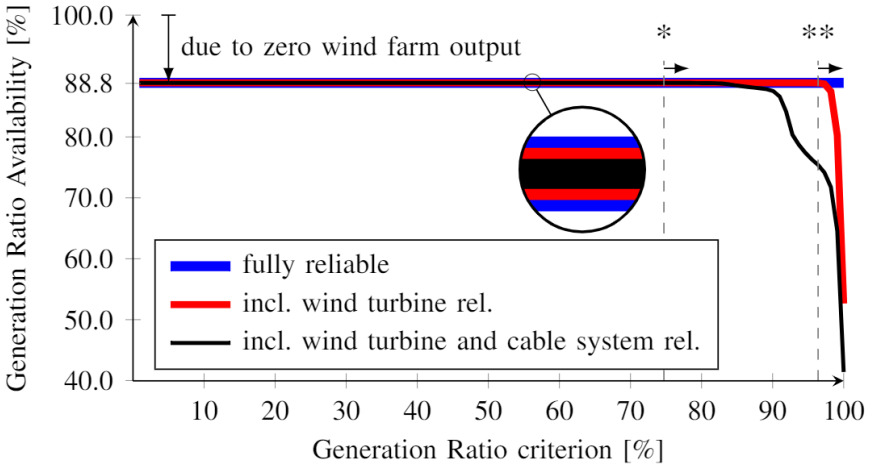

Fig. 6.7. Generation ratio availability for the Anholt wind farm. The GRc at which the impact of the collector system and wind turbine reliability starts is indicated using * and **, respectively.

(-12.0 %) when considering the collector system reliability. Furthermore, the figure shows that the impact of collector system reliability starts from a significantly lower GRc compared to the wind turbine reliability: 74.7 % and 96.4 %, respectively.

Fig. 6.8 presents the probability distribution of the power delivered at the PCC for the two scenarios: (a) including wind turbine reliability, and (b) including wind turbine and cable system reliability, respectively. Each dot represents the probability of the wind farm delivering a specific power at the PCC. It can be seen that including the cable system reliability in addition to the wind turbine reliability has two effects:

1. the average output for a specific cluster is reduced; and

2. the output variance within a specific cluster is increased.

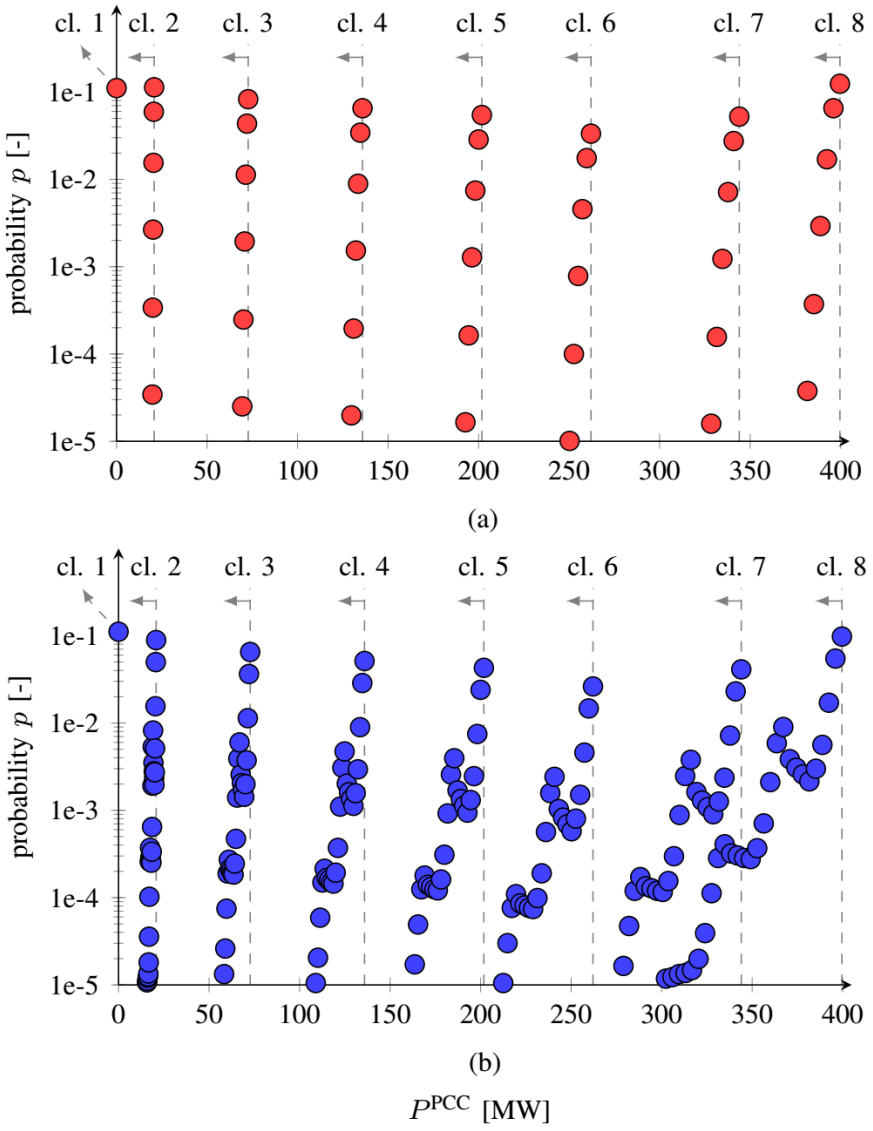

Fig. 6.8. Probability distribution of the power delivered at the PCC for the scenario (a) incl. wind turbine reliability, and (b) the scenario incl. wind turbine and cable system reliability. Each dot represents the probability of the wind farm delivering a specific power at the PCC. All probabilities $p \leq 1e\text{-}5$ are omitted.

Fig. 6.9 shows the difference between both probability distributions and corroborates this.

6.3.3 Multi-State vs. Binary System Reliability

As discussed in Section 6.2.3.2, multi-state systems can be approximated as binary systems with their averaged failure and repair rates (6.3) - (6.4). It should be noted that the failure and repair rates of each sub-assembly are required to determine these averaged rates. To show the difference between multi-state and binary system modelling for

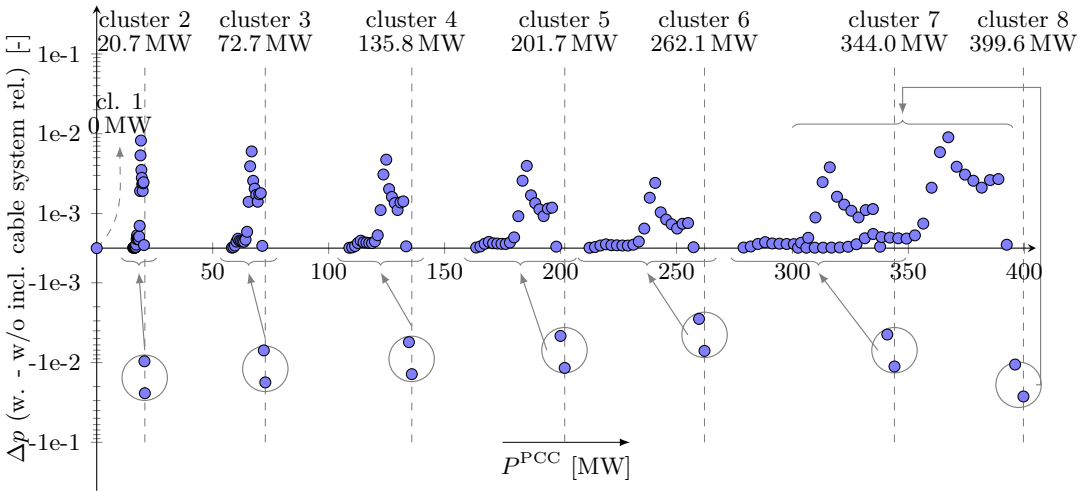

Fig. 6.9. Difference of the probability distributions between the scenario incl. wind turbine and cable system reliability and the scenario incl. wind turbine reliability. Each dot represents the difference in probability between both scenarios of the wind farm delivering a specific power at the PCC. All probability differences $|\Delta p| \leq 1e\text{-}5$ are omitted.

wind farm components in a Markovian context, the latter two scenarios introduced in Section 6.3.2 were considered with eight wind speed clusters.

The difference of EENS between multi-state and binary system modelling was about 1.8 MWh/yr (0.0001 %) for the scenario including wind turbine and cable system reliability. The EENS difference for the scenario which neglects the inter-array cable network was 3.2 MWh/yr (0.0002 %). The GRA values for GRc of 95 % remain unchanged for both scenarios: 88.88 % and 76.32 %, respectively.

Fig. 6.10 illustrates the difference of the probability distributions between multi-state system and binary system modelling for the scenario including wind turbine and cable system reliability. Although there was a variation between the two modelling approaches, the difference was not significant. This was supported by the reliability indices enumerated in the previous paragraph. Accordingly, this analysis suggests that a binary reliability model suffices in a Markovian context to model multi-state OWF components.

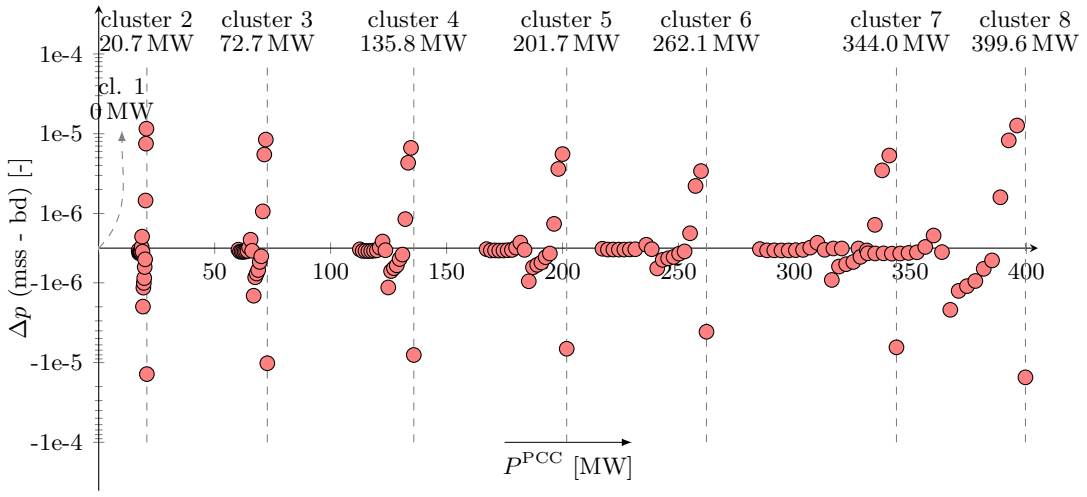

Fig. 6.10. Difference of the probability distributions between modeling the component reliability as a multi-state system and binary system for the scenario incl. wind turbine and cable system reliability. Each dot represents the difference in probability between reliability models of the wind farm delivering a specific power at the PCC. All probability differences $|\Delta p| \leq 1e\text{-}8$ are omitted.

6.4 Summary

This chapter highlights the importance of the inclusion of inter-array cable network reliability in the availability assessment of large-scale offshore wind farms. To evaluate their reliability, an analytical method based on universal generating function combined with multi-state Markov processes is proposed considering its dependencies. This method combines multi-state wind turbine outputs, reliability of different sub-assemblies of wind turbine and cable systems, each with different failure and repair rate characteristics.

The case study carried out for 400 MW Anholt offshore wind farm in Denmark highlights the requirement for the inclusion of inter-array cable network in the reliability evaluation of such electrical networks. Not including the cable network reliability results in a 12 % error in generation ratio availability for generation ratio criterion of 95 %. Furthermore, this could lead to an underestimation in energy not supplied over the operating lifetime of the offshore wind farm worth 24.05 M$. It has been shown that including the cable system reliability is five times more impactful compared to including the wind turbine reliability. In the Markovian context, it has been shown that it is appropriate to represent individual wind farm components using their averaged failure and repair rates.

Chapter 7

Conclusions

7.1 Conclusions

Medium voltage dc technology plays an increasingly important role in integrating renewable energy resources and it provides flexibility to distribution networks. A potential option in future offshore wind power development is to use dc technology at the collection system. At present, it still uses ac technology. On the contrary, the use of dc technology provides additional benefits. However, on top of the technical competencies, reliability is one of the key factors to consider when introducing a new concept.

To this end, this thesis investigated the reliability of the dc collection system concept from the component level to the system level. In particular, how different reliability evaluation techniques can be utilised to analyse and provide pertinent solutions to problems discussed in the thesis.

7.1.1 The Reliability of dc-Wind Turbine

The lifespan of a wind power system is highly influenced by the reliable operation of its power converter. The study in Chapter 3 investigated the B_{10} lifetime and annual consumed damage for a dual active bridge based dcWT.

The study presented a reliability comparison for semiconductors between different thermal cycles and evaluated the component-level (namely, IGBTs and diodes) reliability for a dual active bridge based machine side converter (MSC). Firstly, the total annual damage for IGBT and diode under long-term thermal cycles and short-term thermal cycles were obtained separately and compared. The results showed the damage under both long-term and short-term thermal cycles takes a majority proportion for the IGBT.

Then, based on the Bayerer's lifetime model and the Monte Carlo method, the component-level reliability of dcWT MSC was analysed. The final lifetimes can be obtained from the cumulative distribution functions. Finally, according to the modelling of the B_{10} lifetime power cycles, the lifespan can be deduced and compared. It was observed that B_{10} lifetime for power components in the selected MSC fulfil the industry requirements.

7.1.2 The Selection of a Suitable MVdc Converter Topology

To utilise the full potential from offshore dc collection systems, the selection of a suitable power electronic converter topology is a key aspect. From the pool of voltage source converters, it is unclear which topology is suitable at different MVdc levels.

The study conducted in Chapter 4 proposed a selection criterion based on the optimal redundancy level with the consideration of the VSC reliability, preventive maintenance interval, operational efficiency, the total cost of ownership, and return on investment. Following the proposed selection criterion, the voltage crossover points which the candidate VSCs are suitable were identified for the MVdc spectrum from ±10 kV to ±50 kV. Finally, the practicality of the proposed selection methodology was applied to the ANGLE-DC case and tested.

The analysis performed here revealed that below 300 A and ±20 kV MVdc voltage level, the use of 3L-NPC VSC is much more cost-effective since it provides higher investment return (due to lower capital cost and redundancy). Between 400 A and 700 A and above ±23 kV, the use of MMC is more economical. However, the study suggested that with the increase of MVdc voltage level and higher current levels, the use of MMC is financially beneficial and is also more reliable than other converter topologies. Additionally, beyond about ±35 kV, C3L-NPC can also be considered as an alternative option for MMC.

7.1.3 Topology Selection of Offshore Wind Power DC Collection Systems

To make the correct investment decision, the selection of a suitable offshore wind farm collection system topology is vital at its initial planning phase. Chapter 5 aimed at evaluating the reliability and associated life cycle costs of dc collection system options. Three radial and series–parallel dc collection system configurations were assessed for a 400 MW offshore wind farm. Each had three different dc wind turbine capacity sizes.

An analytical reliability evaluation method called universal generating function (UGF) was proposed to evaluate different reliability indices for these dc collection system options. The use of the UGF technique can greatly improve calculation efficiency for larger

systems. An economic model was also accounted for, to consider the initial investment cost and cost of network losses during the operational life.

The results suggested that with an increase in dcWT capacity, the availability of the collection systems increased. Although the series-parallel topology showed a significantly lower lifecycle cost, the reliability was relatively low due to its series-connected network structure over the other radial topologies. Further, the results showed that the Radial-1 topology is more reliable than the other three topologies, with the smallest EENS and the largest GRA. On the other hand, the Radial-3 topology was the least reliable option, although it eliminates the centralised collection system platform.

Since there are no dc collection systems under operation at present, several assumptions were made when conducting this study. For instance, the failure rates and costs of components such as dcWT, platform dc/dc converters were calculated by referring to the relevant literature. The sensitivity analysis conducted to observe the impact of the reliability of dc/dc converters on the overall availability levels of the collection systems revealed the requirement to pay higher attention to improve their reliability levels. However, with field experience and technology advancements, the reliability can be improved, although the high-power dc/dc converter technology is still not mature.

7.1.4 Impact of Cable Network Reliability on Availability Assessment of Offshore Wind Farms

The work conducted in Chapter 6 presented a tractable methodology for the availability assessment of large-scale offshore wind farms accounting for (a) reliability of individual collector system cables, (b) reliability of individual wind turbines, and (c) output of wind turbines dependent on a single stochastic source: the wind, geographically distributed over the network. Although the edge cases have been thoroughly investigated in the literature, including:

- independent sources, geographically distributed over a network, i.e., including features (a) and (b), and
- dependent sources without considering the network, including features (b) and (c)

this study presented and applied a methodology which considered all three features (a), (b) and (c), i.e., considered the reliability of the network as well as dependent geographically distributed sources.

A direct application of this divide-and-concur strategy in the case with dependent sources, as studied in Chapter 6, was impossible specifically because of that dependency. The main contribution of this study is to propose a strategy that enables the aforementioned

divide-and-concur approach for the case with dependent sources which are geographically distributed over the network. Given this strategy, it becomes feasible to assess the impact of wind speed stochasticity, wind turbine reliability and collector system reliability on the availability of large-scale offshore wind farms.

Additionally, the effect of modelling the individual components as a multi-state system rather than a binary one was investigated in a Markovian context. This was driven by the fact that these components were subject to competing risks, e.g., a wind turbine consists of several subsystems, each with their individual failure and repair rates.

The case study carried out for the 400 MW Anholt offshore wind farm in Denmark highlighted the requirement for the inclusion of the inter-array cable network in the reliability evaluation of such electrical networks. Not including the cable network reliability results in a 12 % error in generation ratio availability for generation ratio criterion of 95 %. Furthermore, this could lead to an underestimation of energy not supplied over the operating lifetime of the offshore wind farm worth 24.05 M$. It was shown that including the cable system reliability five times more impactful compared to including the wind turbine reliability. In the Markovian context, it had been shown that it was appropriate to represent individual wind farm components using their averaged failure and repair rates.

7.2 Thesis Contributions

The main contributions of this thesis can be summarised as follows:

- **Analysis of machine side converter semiconductor reliabilities of dc-wind turbine**: Evaluated lifetime and annual damages of IGBT and diode of dual active bridge based dc-wind turbine.
- **Propose a new selection guideline to identify the most suitable converter for offshore wind power DC collection systems at different voltage levels and power levels**:
  (a) Development of reliability models of different MVdc converters.
  (b) Development of different MVdc converter models for thermal losses calculations.
- **Analysis and identification of reliable and cost effective dc collection system topology**: Evaluated different candidate dc collection system options based on their availability levels, life cycle costs including operational losses.

- **Availability assessment of large-scale offshore wind farms including their collector system**:

  (a) Development of a strategy to incorporate wind stochasticity and failure of different component sub-systems into a single stochastic process for reliability assessment of offshore wind farms.

  (b) Development of an analytical model based on UGF technique for availability assessment of large scale offshore wind farms considering the cable network dependency.

  (c) Investigate the error of modelling wind farm components using a binary Markov model rather than a multi-state model, in a Markovian context.

7.3 Future Work

The following future work is outlined:

7.3.1 Identification of optimum preventive maintenance intervals of converters considering the wear-out phase failure of semiconductor devices

The analysis conducted in Chapter 4 considered the useful-life failure rate of IGBT and diode when identifying the optimum redundancy levels of converters. However, this analysis was based on predefined preventive maintenance intervals, which is the common industrial practice. This methodology can further be extended accounting for the wear-out phase failure of semiconductors (which shows an exponential failure rate) to identify the optimum preventive maintenance interval at the latter stage of the project lifetime. Because with the evolve of time, components are subjected to fail frequently which needs more frequent maintenance than usual to maintain the same availability levels.

7.3.2 Reliability of closed-loop radial topology

As concluded in Chapter 5, the radial-1 topology showed better reliability among the candidate dc collection system topologies. However, one drawback of single-sided radial topology is upon failure of an upstream cable section all the healthy WTs are required to forced shutdown. This can be eliminated with the use of double-sided radial topology where the adjacent feeder is connected with a normally-open bus coupler. The proposed UGF method can be extended to observe the availability levels of double-sided radial topology with necessary alterations to network structure function.

7.3.3 Availability assessment of offshore wind farms under non-Markovian context

In Chapter 6, all the components were assumed to hold Markov properties. However, some of the components could be well represented under the non-Markovian assumption where the present state of a component depends on all or several previous states. For instance, as discussed in section 6.2.1, the cable failure can be modelled as both Crow-AMSAA as the Weibull distribution. With the availability of required data, the proposed UGF technique can be extended to investigate the variation of these different models in the availability assessment of offshore wind farms. This will help to identify the most suitable stochastic process to represent such components for accurate reliability assessment.

List of Publications and Awards

Journal Articles related to this Thesis

- **G. Abeynayake**, T. Van Acker, D. Van Hertem and J. Liang, "Analytical Model for Availability Assessment of Large-Scale Offshore Wind Farms including their Collector System," *in IEEE Transactions on Sustainable Energy*, vol. 12, no. 4, pp. 1974-1983, Oct. 2021, DOI: 10.1109/TSTE.2021.3075182.
- **G. Abeynayake**, G. Li, T. Joseph, J. Liang and W. Ming, "Reliability and Cost-oriented Analysis, Comparison and Selection of Multi-level MVdc Converters," *in IEEE Transactions on Power Delivery*, January 2021. (Early Access), DOI: 10.1109/TPWRD.2021.3051531.
- R. Sun, **G. Abeynayake**, J. Liang, and K. Wang, "Reliability and Economic Evaluation of Offshore Wind Power DC Collection Systems," *Energies*, vol. 14, no. 10, p. 2922, May 2021. (Special issue on Innovative HVDC and MVDC Connection Schemes for Offshore Wind Farms)
- X. Li, **G. Abeynayake**, L.Yao, J. Liang and F. Cheng, "Recent Development and Prospect of Offshore Wind Power in Europe," *Journal of Global Energy Interconnection*, vol. 2, no. 2, pp.116-126, Mar 2019.

Journal Articles (Other)

- **G. Abeynayake**, J. Yu, A. Moon and J. Liang, "Analysis and control of MVDC demonstration project in the UK: ANGLE-DC," *Distribution & Utilization*, vol. 37, no. 10, pp.44-50, Oct 2020.
- **G. Abeynayake** et al., "Long-term and Short-term Mission-profile based Reliability Assessment of dc-Wind Turbine based on Dual Active Bridge," (Under preparation for submission to *IET Renewable Power Generation*).

Conference Proceedings

- **G. Abeynayake**, G. Li, J. Liang and N. A. Cutululis, "A Review on MVdc Collection Systems for High-Power Offshore Wind Farms," *2019 14th Conference on Industrial and Information Systems (ICIIS)*, pp. 407-412, 2019.
- **G. Abeynayake** et al., "Reliability Evaluation of Voltage Source Converters for MVDC Applications," *2019 IEEE Innovative Smart Grid Technologies - Asia (ISGT Asia)*, pp. 2566-2570, 2019.

Awards

- **First Prize**, "IEEE PES UKRI Presentation Competition," Cardiff, 2018.

International Workshops and Colloquium Presentations

- **G. Abeynayake**, "DC Collection Systems for Large Offshore Wind Farms," *Wind Energy Science Conference*, Hannover, Germany, May 2021. (Online)
- **G. Abeynayake**, "DC Collection Systems for Large Offshore Wind Farms," *Wind Energy Science Conference*, Cork, Ireland, June 2019.
- **G. Abeynayake**, "An overview of DC Collection Systems for Large Offshore Wind Farms: from the Reliability Perspective," *KIC-InnoEnergy Master's Class workshop*, Barcelona, Spain, Sep. 2018. (Online)
- **G. Abeynayake**, "Operation and Control aspects of DC Collection Systems," *8th HVDC Doctoral Colloquium*, Barcelona, Spain, Sep. 2018.

Other

- European Energy Innovation Communication Magazine – InnoDC feature contributor, Autumn 2020.
  [Online]. Available: www.europeanenergyinnovation.eu/OnlinePublication/Autumn2020.

Appendix A

Proof of UGFs for Radial Topologies

A.1 Radial-1 Topology

As shown in Fig.5.1, all MVdc feeders are aggregated at the platform dc/dc converter in Radial-1 topology. The UGF of the OWF collection system U_{r1}, which has nxm number of WTs can be defined as:

$$\begin{aligned} U_{r1k}(z,x) &= \underset{\oplus}{\otimes}\left(U_{F1}(z), U_{F2}(z), \cdots, U_{Fk}(z), \cdots, U_{Fm}(z)\right) \\ &= \prod_{k=1}^{m}\left(p_1 z^{P_x} + p_2 z^0\right)^{nk} \\ &= b_0 z^0 + b_1 z^{P_x} + b_2 z^{2P_x} + \cdots + b_{ik} z^{ikP_x} + \cdots + b_{nm} z^{nmP_x} \end{aligned} \tag{A.1}$$

Next, to obtain the UGF of the Radial-1 topology, the UGFs of the collection system and the platform dc/dc converter is combined using the formula:

$$\begin{aligned} U_{Radial-1}(z,x) = & \underset{min}{\otimes}\left(U_{r1}(z,x), U_{C1}(z,x)\right) \\ =& (b_0 z^0 + b_1 z^{P_x} + b_2 z^{2P_x} + \cdots + b_{ik} z^{ikP_x} + \cdots + b_{nm} z^{nmP_x}) \\ & \times (p_{c1} z^{nmP_x} + p_{c2} z^0) \\ =& p_{c1} b_0 z^{min(0,mnP_x)} + p_{c2} b_0 z^{min(0,0)} + p_{c1} b_1 z^{min(P_x,mnP_x)} + p_{c2} b_1 z^{min(P_x,0)} + \\ & p_{c1} b_2 z^{min(2P_x,mnP_x)} + p_{c2} b_2 z^{min(2P_x,0)} + \cdots + p_{c1} b_{ik} z^{min(ikP_x,nmP_x)} + \\ & p_{c2} b_{ik} z^{min(ikP_x,0)} + \cdots + p_{c1} b_{nm} z^{min(nmP_x,nmP_x)} + p_{c2} b_{nm} z^{min(nmP_x,0)} \\ =& c_0 z^0 + c_1 z^{P_x} + c_2 z^{2P_x} + \cdots + c_{ik} z^{ikP_x} + \cdots + c_{nm} z^{nmP_x} \end{aligned} \tag{A.2}$$

In (A.2) the combination operator $\underset{f}{\otimes}$ is the minimum value of corresponding to the state variables. Finally, the UGF of the Radial-1 topology for P_x power, which corresponds to cluster x with the state probability of p_{wt_x} can be obtained as:

$$U_{Radial-1}(z,x) = (c_0 z^0 + c_1 z^{P_x} + c_2 z^{2P_x} + \cdots + c_{ik} z^{ikP_x} + \cdots + c_{nm} z^{nmP_x}) \times p_{wt\_x} \tag{A.3}$$

Considering that all n_{cl} WT power output clusters, the UGF of the Radial-1 topology is given by:

$$UGF_{OWF-Radial-1} = \sum_{x=1}^{n_{cl}} UGF_{Radial-1}(z,x) \tag{A.4}$$

A.2 Radial-2 Topology

Similarly, using (5.16) and (5.18), the UGF of a feeder in Radial-2 topology which combines the n parallel WTs, and the centralised dc/dc converter could be represented as:

$$\begin{aligned}
U_{CF_k}(z,x) =& \underset{min}{\otimes} (U_{Fk}(z,x), U_{CF_k}(z,x)) \\
=& (a_0 z^0 + a_1 z^{P_x} + a_2 z^{2P_x} + \cdots + a_i z^{iP_x} + \cdots + a_n z^{nP_x}) \\
& \times (p_{cf1} z^{nP_x} + p_{cf2} z^0) \\
=& p_{cf1} a_0 z^{min(0,nP_x)} + p_{cf2} a_0 z^{min(0,0)} + p_{cf1} a_1 z^{min(P_x,nP_x)} + p_{cf2} a_1 z^{min(P_x,0)} + \\
& p_{cf1} a_2 z^{min(2P_x,nP_x)} + p_{cf2} a_2 z^{min(2P_x,0)} + \cdots + p_{cf1} a_i z^{min(iP_x,nP_x)} + \\
& p_{cf2} a_i z^{min(iP_x,0)} + \cdots + p_{cf1} a_n z^{min(nP_x,nP_x)} + p_{cf2} a_n z^{min(nP_x,0)} \\
=& d_0 z^0 + d_1 z^{P_x} + d_2 z^{2P_x} + \cdots + d_{ik} z^{ikP_x} + \cdots + d_{nm} z^{nmP_x}
\end{aligned} \tag{A.5}$$

Following (A.1), m-feeders of the Radial-2 topology can be combined as follows:

$$\begin{aligned}
U_{r2}(z,x) &= \underset{\oplus}{\otimes} (U_{F1}(z), U_{F2}(z), \cdots, U_{Fk}(z), \cdots, U_{Fm}(z)) \\
&= \prod_{k=1}^{m} (d_0 z^0 + d_1 z^{P_x} + d_2 z^{2P_x} + \cdots + d_{ik} z^{ikP_x} + \cdots + d_{nm} z^{nmP_x})^k \\
&= e_0 z^0 + e_1 z^{P_x} + e_2 z^{2P_x} + \cdots + e_{ik} z^{ikP_x} + \cdots + e_{nm} z^{nmP_x}
\end{aligned} \tag{A.6}$$

Finally, to obtain the UGF of the Radial-2 topology, the UGFs of the collection system and the platform dc/dc converter could be can using (A.2). The final UGF is obtained using (A.3) and (A.4).

A.3 Radial-3 Topology

In Radial-3 topology, the UGF of the OWF collection system is the same as in the Radial-2 topology defined in (A.5). However, the feeders are connected in series, in which its topology reliability can be considered as a *k-out-of-n(G)* system. The OWF remains connected to the grid until *n–k+1* feeder dc/dc converters fail. The value of k is decided by the allowable over-voltage limit of each dc/dc converter. The technique used to obtain the UGF of a general *k-out-of-n(G)* system was adapted with necessary modifications.

1. Determine the UGF (U_{CFk}) of each feeder dc/dc converter as in (5.18).

2. Obtain the UGF of all m feeders (k = *1,2,. . . ,m*)

$$\begin{aligned} U_{CF}(z,x) &= \underset{\oplus}{\otimes}\left(U_{CF1}(z), U_{CF2}(z), \cdots, U_{CFk}(z), \cdots, U_{CFm}(z)\right) \\ &= \prod_{k=1}^{m}\left(p_{cf1}z^{nP_x} + p_{cf2}z^{0}\right)^{k} \\ &= f_0 z^0 + f_1 z^{P_x} + f_2 z^{2P_x} + \cdots + f_{k-1} z^{(k-1)nP_x} + f_k z^{(knP_x} \cdots + f_m z^{nmP_x} \end{aligned} \tag{A.7}$$

3. Define the value of k_{min}, i.e., the minimum number of centralised dc/dc converters required for a successful operation of the OWF collection system.

4. Obtain the new UGF by replacing all z^{knP_x} with z^0 for $k < k_m in$ in (A.7)

$$\begin{aligned} U'_{CF}(z,x) &= f_0 z^0 + f_1 z^0 + f_2 z^0 + \cdots + f_{k-1} z^0 + f_k z^{knP_x} + \cdots + f_m z^{mnP_x} \\ &= \left(f_0 + f_1 + f_2 + \cdots + f_{k-1}\right) z^0 + f_k z^{knP_x} + \cdots + f_m z^{mnP_x} \end{aligned} \tag{A.8}$$

5. Finally, combine (A.8) with the UGF of the OWF collection system U_r1, which comprises m-feeders and n-WTs per feeder, as defined in (A.1).

$$\begin{aligned} U_{r3}(z,x) &= \underset{min}{\otimes}\left(U'_{CF}(z,x), U_{r1}(z,x)\right) \\ &= \left(\left(f_0 + f_1 + f_2 + \cdots + f_{k-1}\right) z^0 + f_k z^{knP_x} + \cdots + f_m z^{mnP_x}\right) \times \\ &\quad \left(b_0 z^0 + b_1 z_x^{P_x} + b_2 z^{2P_x} + \cdots + b_{ik} z^{ikP_x} + \cdots + b_{nm} z^{nmP_x}\right) \\ &= g_0 z^0 + g_1 z^{P_x} + g_2 z^{2P_x} + \cdots + g_{ik} z^{ikP_x} + \cdots + g_{nm} z^{nmP_x} \end{aligned} \tag{A.9}$$

6. The final UGF for $n_c l$ states can be obtained by referring to (A.3) and (A.4).

Appendix B

Proofs of point of common coupling and feeder UGF

B.1 Proof of UGF at the PCC

$$
\begin{aligned}
\omega^{\mathrm{PCC}}(z) = & \sum_{\gamma\in\Gamma}\prod_{s_e\in\gamma} p_{s_e}\cdot z^{f^{\mathrm{str}}(\gamma)} \\
= & 0.1\cdot 0.1\cdot 0.1\cdot 0.1\cdot 0.3\cdot z^{\min(0,0+\min(0,0))+\min(0,0+\min(0,0))} + \\
& 0.9\cdot 0.1\cdot 0.1\cdot 0.1\cdot 0.3\cdot z^{\min(0,0+\min(4,0))+\min(0,0+\min(0,0))} + \\
& 0.1\cdot 0.9\cdot 0.1\cdot 0.1\cdot 0.3\cdot z^{\min(4,0+\min(0,0))+\min(0,0+\min(0,0))} + \\
& 0.9\cdot 0.9\cdot 0.1\cdot 0.1\cdot 0.3\cdot z^{\min(4,0+\min(4,0))+\min(0,0+\min(0,0))} + \\
& 0.1\cdot 0.1\cdot 0.9\cdot 0.1\cdot 0.3\cdot z^{\min(0,0+\min(0,0))+\min(0,0+\min(4,0))} + \\
& 0.9\cdot 0.1\cdot 0.9\cdot 0.1\cdot 0.3\cdot z^{\min(0,0+\min(4,0))+\min(0,0+\min(4,0))} + \\
& 0.1\cdot 0.9\cdot 0.9\cdot 0.1\cdot 0.3\cdot z^{\min(4,0+\min(0,0))+\min(0,0+\min(4,0))} + \\
& 0.9\cdot 0.9\cdot 0.9\cdot 0.1\cdot 0.3\cdot z^{\min(4,0+\min(4,0))+\min(0,0+\min(4,0))} + \\
& 0.1\cdot 0.1\cdot 0.1\cdot 0.9\cdot 0.3\cdot z^{\min(0,0+\min(0,0))+\min(4,0+\min(0,0))} + \\
& 0.9\cdot 0.1\cdot 0.1\cdot 0.9\cdot 0.3\cdot z^{\min(0,0+\min(4,0))+\min(4,0+\min(0,0))} + \\
& 0.1\cdot 0.9\cdot 0.1\cdot 0.9\cdot 0.3\cdot z^{\min(4,0+\min(0,0))+\min(4,0+\min(0,0))} + \\
& 0.9\cdot 0.9\cdot 0.1\cdot 0.9\cdot 0.3\cdot z^{\min(4,0+\min(4,0))+\min(4,0+\min(0,0))} + \\
& 0.1\cdot 0.1\cdot 0.9\cdot 0.9\cdot 0.3\cdot z^{\min(0,0+\min(0,0))+\min(4,0+\min(4,0))} + \\
& 0.9\cdot 0.1\cdot 0.9\cdot 0.9\cdot 0.3\cdot z^{\min(0,0+\min(4,0))+\min(4,0+\min(4,0))} + \\
& 0.1\cdot 0.9\cdot 0.9\cdot 0.9\cdot 0.3\cdot z^{\min(4,0+\min(0,0))+\min(4,0+\min(4,0))} + \\
& 0.9\cdot 0.9\cdot 0.9\cdot 0.9\cdot 0.3\cdot z^{\min(4,0+\min(4,0))+\min(4,0+\min(4,0))} + \\
& 0.1\cdot 0.1\cdot 0.1\cdot 0.1\cdot 0.7\cdot z^{\min(0,2+\min(0,2))+\min(0,2+\min(0,2))} + \\
& 0.9\cdot 0.1\cdot 0.1\cdot 0.1\cdot 0.7\cdot z^{\min(0,2+\min(4,2))+\min(0,2+\min(0,2))} +
\end{aligned}
$$

$$
\begin{aligned}
&0.1 \cdot 0.9 \cdot 0.1 \cdot 0.1 \cdot 0.7 \cdot z^{\min(4,2+\min(0,2))+\min(0,2+\min(0,2))} + \\
&0.9 \cdot 0.9 \cdot 0.1 \cdot 0.1 \cdot 0.7 \cdot z^{\min(4,2+\min(4,2))+\min(0,2+\min(0,2))} + \\
&0.1 \cdot 0.1 \cdot 0.9 \cdot 0.1 \cdot 0.7 \cdot z^{\min(0,2+\min(0,2))+\min(0,2+\min(4,2))} + \\
&0.9 \cdot 0.1 \cdot 0.9 \cdot 0.1 \cdot 0.7 \cdot z^{\min(0,2+\min(4,2))+\min(0,2+\min(4,2))} + \\
&0.1 \cdot 0.9 \cdot 0.9 \cdot 0.1 \cdot 0.7 \cdot z^{\min(4,2+\min(0,2))+\min(0,2+\min(4,2))} + \\
&0.9 \cdot 0.9 \cdot 0.9 \cdot 0.1 \cdot 0.7 \cdot z^{\min(4,2+\min(4,2))+\min(0,2+\min(4,2))} + \\
&0.1 \cdot 0.1 \cdot 0.1 \cdot 0.9 \cdot 0.7 \cdot z^{\min(0,2+\min(0,2))+\min(4,2+\min(0,2))} + \\
&0.9 \cdot 0.1 \cdot 0.1 \cdot 0.9 \cdot 0.7 \cdot z^{\min(0,2+\min(4,2))+\min(4,2+\min(0,2))} + \\
&0.1 \cdot 0.9 \cdot 0.1 \cdot 0.9 \cdot 0.7 \cdot z^{\min(4,2+\min(0,2))+\min(4,2+\min(0,2))} + \\
&0.9 \cdot 0.9 \cdot 0.1 \cdot 0.9 \cdot 0.7 \cdot z^{\min(4,2+\min(4,2))+\min(4,2+\min(0,2))} + \\
&0.1 \cdot 0.1 \cdot 0.9 \cdot 0.9 \cdot 0.7 \cdot z^{\min(0,2+\min(0,2))+\min(4,2+\min(4,2))} + \\
&0.9 \cdot 0.1 \cdot 0.9 \cdot 0.9 \cdot 0.7 \cdot z^{\min(0,2+\min(4,2))+\min(4,2+\min(4,2))} + \\
&0.1 \cdot 0.9 \cdot 0.9 \cdot 0.9 \cdot 0.7 \cdot z^{\min(4,2+\min(0,2))+\min(4,2+\min(4,2))} + \\
&0.9 \cdot 0.9 \cdot 0.9 \cdot 0.9 \cdot 0.7 \cdot z^{\min(4,2+\min(4,2))+\min(4,2+\min(4,2))} + \\
=&0.00003 \cdot z^0 + 0.00027 \cdot z^0 + 0.00027 \cdot z^0 + 0.00243 \cdot z^0 + \\
&0.00027 \cdot z^0 + 0.00243 \cdot z^0 + 0.00243 \cdot z^0 + 0.02187 \cdot z^0 + \\
&0.00027 \cdot z^0 + 0.00243 \cdot z^0 + 0.00243 \cdot z^0 + 0.02187 \cdot z^0 + \\
&0.00243 \cdot z^0 + 0.02187 \cdot z^0 + 0.02187 \cdot z^0 + 0.19683 \cdot z^0 + \\
&0.00007 \cdot z^0 + 0.00063 \cdot z^0 + 0.00063 \cdot z^2 + 0.00567 \cdot z^4 + \\
&0.00063 \cdot z^0 + 0.00567 \cdot z^0 + 0.00567 \cdot z^2 + 0.05103 \cdot z^4 + \\
&0.00063 \cdot z^2 + 0.00567 \cdot z^2 + 0.00567 \cdot z^4 + 0.05103 \cdot z^6 + \\
&0.00567 \cdot z^4 + 0.05103 \cdot z^4 + 0.05103 \cdot z^6 + 0.45927 \cdot z^8 + \\
=&0.30700 \cdot z^0 + 0.01260 \cdot z^2 + 0.11907 \cdot z^4 + 0.10206 \cdot z^6 + \\
&0.45927 \cdot z^8
\end{aligned}
\tag{B.1}
$$

B.2 Proof of feeder UGF

$$
\begin{aligned}
\omega_\phi(z) =&0.1 \cdot 0.1 \cdot 1.0 \cdot z^{\min(0\,\mathrm{MW},1\,\mathrm{MW}+\min(0\,\mathrm{MW},1\,\mathrm{MW}))} + \\
&0.9 \cdot 0.1 \cdot 1.0 \cdot z^{\min(0\,\mathrm{MW},1\,\mathrm{MW}+\min(4\,\mathrm{MW},1\,\mathrm{MW}))} + \\
&0.1 \cdot 0.9 \cdot 1.0 \cdot z^{\min(4\,\mathrm{MW},1\,\mathrm{MW}+\min(0\,\mathrm{MW},1\,\mathrm{MW}))} + \\
&0.9 \cdot 0.9 \cdot 1.0 \cdot z^{\min(4\,\mathrm{MW},1\,\mathrm{MW}+\min(4\,\mathrm{MW},1\,\mathrm{MW}))} \\
=&0.1 \cdot z^{0\,\mathrm{MW}} + 0.09 \cdot z^{1\,\mathrm{MW}} + 0.81 \cdot z^{2\,\mathrm{MW}}.
\end{aligned}
\tag{B.2}
$$

Bibliography

[1] "World Energy Outlook 2020 – Analysis and key findings," *IEA*, 2020. [Online]. Available: https://www.iea.org/reports/world-energy-outlook-2020

[2] European Union, "Going climate-neutral by 2050 : a strategic long-term vision for a prosperous, modern, competitive and climate-neutral EU economy," Tech. Rep., July 2019.

[3] "UK becomes first major economy to pass net zero emissions law." [Online]. Available: https://www.gov.uk/government/news/uk-becomes-first-major-economy-to-pass-net-zero-emissions-law

[4] "Net Zero - The UK's contribution to stopping global warming," Committee on Climate Change, Tech. Rep., May 2019.

[5] "Reaching Net Zero in the UK." [Online]. Available: https://www.theccc.org.uk/uk-action-on-climate-change/reaching-net-zero-in-the-uk/

[6] Global Wind Energy Council, "Global Offshore Wind Report 2020," Tech. Rep., 2020.

[7] ——, "Global Wind Report 2019," Tech. Rep., July 2020.

[8] "Wind Energy Statistics - UK Wind Energy Database," *Renewable UK*, Dec. 2020. [Online]. Available: https://www.renewableuk.com/page/UKWEDhome/Wind-Energy-Statistics.htm

[9] "A leader in offshore wind, the UK offers a glimpse of a world run on green energy," *The Guardian*, Dec. 2020. [Online]. Available: https://www.theguardian.com/power-of-green/2020/dec/17/uk-offshore-wind-global-renewable-future

[10] K. Johansen, "Wind energy in denmark: A short history [history]," *IEEE Power and Energy Magazine*, vol. 19, no. 3, pp. 94–102, 2021.

[11] J.-A. Pérez-Rúa and N. A. Cutululis, "Electrical cable optimization in offshore wind farms—a review," *IEEE Access*, vol. 7, pp. 85 796–85 811, 2019.

[12] M. Banzo and A. Ramos, "Stochastic optimization model for electric power system planning of offshore wind farms," *IEEE Transactions on Power Systems*, vol. 26, no. 3, pp. 1338–1348, 2011.

[13] A. Cerveira, A. de Sousa, E. J. S. Pires, and J. Baptista, "Optimal cable design of wind farms: The infrastructure and losses cost minimization case," *IEEE Transactions on Power Systems*, vol. 31, no. 6, pp. 4319–4329, 2016.

[14] J.-A. Pérez-Rúa, S. Lumbreras, A. Ramos, and N. A. Cutululis, "Closed-loop two-stage stochastic optimization of offshore wind farm collection system," *Journal of Physics: Conference Series*, vol. 1618, p. 042031, sep 2020.

[15] M. De Prada Gil, J. Domínguez-García, F. Díaz-González, M. Aragüés-Peñalba, and O. Gomis-Bellmunt, "Feasibility analysis of offshore wind power plants with dc collectiongrid," *Renewable Energy*, vol. 78, pp. 467–477, 2015.

[16] P. Lakshmanan, J. Liang, and N. Jenkins, "Assessment of collection systems for hvdc connected offshore wind farms," *Electric Power Systems Research*, vol. 129, pp. 75–82, 2015.

[17] G. Abeynayake, G. Li, J. Liang, and N. A. Cutululis, "A Review on MVdc Collection Systems for High-Power Offshore Wind Farms," in *2019 14th Conference on Industrial and Information Systems (ICIIS)*, Kandy, Sri Lanka, 2019, pp. 407–412.

[18] C. Dincan, "High power medium voltage DC/DC converter technology for DC wind turbines," Ph.D. dissertation, Aalborg Universitetsforlag, 2018.

[19] Shurong, Wei, Yuyao, Feng, Kunlun, Liu, and Yang, Fu, "Optimization of power collector system for large-scale offshore wind farm based on topological redundancy assessment," in *E3S Web Conf.*, vol. 194, 2020, pp. 3–25.

[20] O. Dahmani, S. Bourguet, M. Machmoum, P. Guerin, P. Rhein, and L. Josse, "Optimization and reliability evaluation of an offshore wind farm architecture," *IEEE Transactions on Sustainable Energy*, vol. 8, no. 2, pp. 542–550, 2017.

[21] J.-S. Shin and J.-O. Kim, "Optimal design for offshore wind farm considering inner grid layout and offshore substation location," *IEEE Transactions on Power Systems*, vol. 32, no. 3, pp. 2041–2048, 2017.

[22] A. Fernandez-Guillamon, K. Das, N. A. Cutululis, and A. Molina-Garcia, "Offshore wind power integration into future power systems: Overview and trends," *Journal of Marine Science and Engineering*, vol. 7, no. 11, pp. 2077–1312, 2019.

[23] B. Yang, L. Jiang, L. Wang, W. Yao, and Q. H. Wu, "Nonlinear maximum power point tracking control and modal analysis of DFIG based wind turbine," *International Journal of Electrical Power & Energy Systems*, vol. 74, pp. 429–436, 2016.

[24] F. Blaabjerg, M. Liserre, and K. Ma, "Power electronics converters for wind turbine systems," *IEEE Transactions on Industry Applications*, vol. 48, no. 2, pp. 708–719, 2012.

[25] J. Carroll, A. McDonald, I. Dinwoodie, D. McMillan, M. Revie, and I. Lazakis, "Availability, operation and maintenance costs of offshore wind turbines with different drive train configurations," *Wind Energy*, vol. 20, no. 2, pp. 361–378, 2017.

[26] A. Durakovic, "Vestas Launches 15 MW Offshore Wind Turbine," February 2021. [Online]. Available: https://www.offshorewind.biz/2021/02/10/vestas-launches-15-mw-offshore-wind-turbine/

[27] N. Skopljak, "14 MW GE Haliade-X for third phase of world's largest offshore wind farm," December 2020. [Online]. Available: https://www.offshorewind.biz/2020/12/18/14-mw-ge-haliade-x-for-third-phase-of-worlds-largest-offshore-wind-farm/

[28] C. Ng and L. Ran, Eds., *Offshore Wind Farms : Technologies, Design and Operation*, ser. Woodhead Publishing in energy. London, UK: Woodhead Publishing, March 2016.

[29] A. Hansen and G. Michalke, "Multi-pole permanent magnet synchronous generator wind turbines' grid support capability in uninterrupted operation during grid faults," *IET Renewable Power Generation*, vol. 3, no. 3, pp. 333–348, 2009.

[30] P. Alves Dias, S. Bobba, S. Carrara, and B. Plazzotta, "The role of rare earth elements in wind energy and electric mobility: An analysis of future supply/demand balances," Publications Office of the European Union, EUR - Scientific and Technical Research Reports, 2020.

[31] "Global and China Rare Earth Permanent Magnet Industry Report: 2018-2023," March 2019. [Online]. Available: https://www.reportlinker.com/p05389598/Global-and-China-Rare-Earth-Permanent-Magnet-Industry-Report

[32] A. B. Abrahamsen, N. Magnusson, B. B. Jensen, and M. Runde, "Large Superconducting Wind Turbine Generators," *Energy Procedia*, vol. 24, pp. 60–67, 2012.

[33] H. Kyling, "Results of Ground-Based Tests-D.8.3 EcoSwing Public results of ground based tests at Fraunhofer IWES," 2019. [Online]. Available: https://ecoswing.eu/images/EcoSwing_Results_of_Ground-Based_Tests.pdf

[34] "Superconducting wind turbine chalks up first test success," November 2019. [Online]. Available: https://phys.org/news/2019-11-superconducting-turbine-chalks-success.html

[35] M. P. van der Laan *et al.*, "Power curve and wake analyses of the vestas multi-rotor demonstrator," *Wind Energy Science*, vol. 4, no. 2, pp. 251–271, 2019.

[36] "About INNWIND.EU: Innovative Wind Conversion Systems (10-20 MW) for Offshore Applications." [Online]. Available: http://www.innwind.eu/about-innwind

[37] S. Watson *et al.*, "Future emerging technologies in the wind power sector: A european perspective," *Renewable and Sustainable Energy Reviews*, vol. 113, p. 109270, 2019.

[38] P. Jamieson *et al.*, "Innovative turbine concepts – multi-rotor system," EU INNWIND, Deliverable Report-D1.33, September 2015.

[39] M. d. Prada Gil, "Design, operation and control of novel electrical concepts for offshore wind power plants," Ph.D. dissertation, Departament d'Enginyeria Elèctrica, Universitat Politècnica de Catalunya, 2014.

[40] R. Barrera-Cardenas and M. Molinas, "Comparative study of wind turbine power converters based on medium-frequency ac-link for offshore dc-grids," *IEEE Journal of Emerging and Selected Topics in Power Electronics*, vol. 3, no. 2, pp. 525–541, 2015.

[41] R. W. A. A. De Doncker, D. M. Divan, and M. H. Kheraluwala, "A three-phase soft-switched high-power-density dc/dc converter for high-power applications," *IEEE Transactions on Industry Applications*, vol. 27, no. 1, pp. 63–73, 1991.

[42] C. Meyer, "Key components for future offshore DC grids," Ph.D. dissertation, Institution of Power Generation and Storage Systems, RWTH, Aachen University, Aachen, Germany, 2007.

[43] M. Banzo and A. Ramos, "Stochastic optimization model for electric power system planning of offshore wind farms," *IEEE Transactions on Power Systems*, vol. 26, no. 3, pp. 1338–1348, 2011.

[44] D. Van Hertem, O. Gomis-Bellmunt, and J. Liang, Eds., *HVDC Grids: For Offshore and Supergrid of the Future*, ser. IEEE Press Series on Power Engineering. United States of America: John Wiley & Sons, Ltd, April 2016.

[45] D. Elliott, K. R. W. Bell, S. J. Finney, R. Adapa, C. Brozio, J. Yu, and K. Hussain, "A comparison of ac and hvdc options for the connection of offshore wind generation in great britain," *IEEE Transactions on Power Delivery*, vol. 31, no. 2, pp. 798–809, 2016.

[46] M. Lena, T. Torbjörn, and C. Ola, "Control of a wind farm with an internal direct current collection grid," *Wind Energy*, vol. 15, no. 4, pp. 547–561, 2012.

[47] K. Musasa, N. I. Nwulu, M. N. Gitau, and R. C. Bansal, "Review on dc collection grids for offshore wind farms with high-voltage dc transmission system," *IET Power Electronics*, vol. 10, no. 15, pp. 2104–2115, 2017.

[48] R. Sun, G. Abeynayake, J. Liang, and K. Wang, "Reliability and economic evaluation of offshore wind power dc collection systems," *Energies*, vol. 14, no. 10, 2021.

[49] N. Holtsmark, H. J. Bahirat, M. Molinas, B. A. Mork, and H. K. Hoidalen, "An all-dc offshore wind farm with series-connected turbines: An alternative to the classical parallel ac model?" *IEEE Transactions on Industrial Electronics*, vol. 60, no. 6, pp. 2420–2428, 2013.

[50] M. Parker and O. Anaya-Lara, "Cost and losses associated with offshore wind farm collection networks which centralise the turbine power electronic converters," *IET Renewable Power Generation*, vol. 7, pp. 390–400, 2013.

[51] DC-AS-Executive Summary, "Offshore Wind Accelerator–TWG-E: DC-AS–DC Array System Technology Revisit," Carbon Trust, Tech. Rep, March 2021.

[52] R. Billinton and R. N. Allan, *Reliability Evaluation of Power Systems*, 2nd ed. New York, NY: Plenum Press, 1994.

[53] W. Li, *Risk Assessment Of Power Systems: Models, Methods, and Applications*, 2nd ed. IEEE Press, Wiley, 2005.

[54] S. Distefano and A. Puliafito, "Dependability evaluation with dynamic reliability block diagrams and dynamic fault trees," *IEEE Transactions on Dependable and Secure Computing*, vol. 6, no. 1, pp. 4–17, 2009.

[55] B. W. Tuinema, "Reliability of transmission networks: Impact of EHV underground cables & interaction of offshore-onshore networks," Ph.D. dissertation, TU Delft, 2017.

[56] H. Chung, H. Wang, F. Blaabjerg, and M. Pecht, *Reliability of Power Electronic Converter Systems*, ser. Power and Energy. Institution of Engineering and Technology, 2015.

[57] G. Abeynayake, G. Li, T. Joseph, W. Ming, J. Liang, A. Moon, K. Smith, and J. Yu, "Reliability evaluation of voltage source converters for mvdc applications," in *2019 IEEE Innovative Smart Grid Technologies - Asia (ISGT Asia)*, 2019, pp. 2566–2570.

[58] K. Ma, M. Liserre, F. Blaabjerg, and T. Kerekes, "Thermal loading and lifetime estimation for power device considering mission profiles in wind power converter," *IEEE Transactions on Power Electronics*, vol. 30, no. 2, pp. 590–602, 2015.

[59] L. M. Moore and H. N. Post, "Five years of operating experience at a large, utility-scale photovoltaic generating plant," *Progress in Photovoltaics: Research and Applications*, vol. 16, no. 3, pp. 249–259, 2008.

[60] D. Zhou and F. Blaabjerg, "Converter-level reliability of wind turbine with low sample rate mission profile," *IEEE Transactions on Industry Applications*, vol. 56, no. 3, pp. 2938–2944, 2020.

[61] S. Yang *et al.*, "An industry based survey of reliability in power electronic converters," *IEEE Transactions on Industry Applications*, vol. 47, no. 3, pp. 1441–1451, May 2011.

[62] J. Berner, "Load-cycling capability of HiPak IGBT modules," ABB, ABB Application Note 5SYA 2043-02, 2012.

[63] G. Zhang, D. Zhou, J. Yang, and F. Blaabjerg, "Fundamental-frequency and load-varying thermal cycles effects on lifetime estimation of dfig power converter," *Microelectronics Reliability*, vol. 76-77, pp. 549–555, 2017. [Online]. Available: https://www.sciencedirect.com/science/article/pii/S0026271417302573

[64] D. Zhou, F. Blaabjerg, M. Lau, and M. Tønnes, "Optimized reactive power flow of dfig power converters for better reliability performance considering grid codes," *IEEE Transactions on Industrial Electronics*, vol. 62, no. 3, pp. 1552–1562, 2015.

[65] D. Zhou, F. Blaabjerg, T. Franke, M. Tønnes, and M. Lau, "Comparison of wind power converter reliability with low-speed and medium-speed permanent-magnet synchronous generators," *IEEE Transactions on Industrial Electronics*, vol. 62, no. 10, pp. 6575–6584, 2015.

[66] A. Isidori, F. M. Rossi, F. Blaabjerg, and K. Ma, "Thermal loading and reliability of 10-mw multilevel wind power converter at different wind roughness classes," *IEEE Transactions on Industry Applications*, vol. 50, no. 1, pp. 484–494, 2014.

[67] S. Ye, D. Zhou, and F. Blaabjerg, "System-level reliability assessment for a direct-drive pmsg based wind turbine with multiple converters," *Microelectronics Reliability*, vol. 114, p. 113801, 2020, 31st European Symposium on Reliability of Electron Devices, Failure Physics and Analysis, ESREF 2020.

[68] C. Dincan *et al.*, "A High-Power, Medium-Voltage, Series-Resonant Converter for DC Wind Turbines," *IEEE Transactions on Power Electronics*, vol. 33, no. 9, pp. 7455–7465, 2018.

[69] X. Yang *et al.*, "An Improved Droop Control Strategy for VSC-Based MVDC Traction Power Supply System," *IEEE Transactions on Industrial Electronics*, vol. 54, no. 5, pp. 5173–5186, 2018.

[70] R. M. Cuzner and V. Singh, "Future Shipboard MVdc System Protection Requirements and Solid-State Protective Device Topological Tradeoffs," *IEEE Journal of Emerging and Selected Topics in Power Electronics*, vol. 5, no. 1, pp. 244–259, 2017.

[71] C. Yuan, M. A. Haj-ahmed, and M. S. Illindala, "Protection Strategies for Medium-Voltage Direct-Current Microgrid at a Remote Area Mine Site," *IEEE Transactions on Industry Applications*, vol. 51, no. 4, pp. 2846–2853, 2015.

[72] R. M. Burkart and J. W. Kolar, "Comparative Life Cycle Cost Analysis of Si and SiC PV Converter Systems Based on Advanced η-ρ-σ Multiobjective Optimization Techniques," *IEEE Transactions on Power Electronics*, vol. 32, no. 6, pp. 4344–4358, 2017.

[73] E. Kantar and A. M. Hava, "Optimal Design of Grid-Connected Voltage-Source Converters Considering Cost and Operating Factors," *IEEE Transactions on Industrial Electronics*, vol. 63, no. 9, pp. 5336–5347, 2016.

[74] IEEE Std 519-2014 (Revision of IEEE Std 519-1992), "IEEE Recommended Practice and Requirements for Harmonic Control in Electric Power Systems," Institute of Electrical and Electronics Engineers, IEEE Std., 2014.

[75] G. Li, C. Li, and D. Van Hertem, "Chapter 3: HVDC technology overview," in *HVDC Grids for Offshore and Supergrid of the Future*, D. Van Hertem, O. Gomis-Bellmunt, and J. Liang, Eds. Hoboken, NJ, USA: Wiley IEEE Press, 2016, pp. 45–78.

[76] J. Guo, X. Wang, J. Liang, H. Pang, and J. Gonçalves, "Reliability Modeling and Evaluation of MMCs Under Different Redundancy Schemes," *IEEE Transactions on Power Delivery*, vol. 33, no. 5, pp. 2087–2096, 2018.

[77] G. Abeynayake, J. Yu, A. Moon, and J. Liang, "Analysis and Control of MVDC Demonstration Project in the UK: ANGLE-DC," *Power Supply*, vol. 37, no. 10, pp. 44–50, 2020.

[78] L. Qu *et al.*, "Planning and Analysis of the Demonstration project of the MVDC Distribution Network in Zhuhai," *Frontiers in Energy*, vol. 13, no. 1, pp. 120–130, 2019.

[79] F. Mura and R. W. De Doncker, "Design aspects of a medium-voltage direct current (MVDC) grid for a university campus," in *8th Int. Conf. on Power Electron.-ECCE Asia, Jeju*, 2011, pp. 2359–2366.

[80] Y. Gao *et al.*, "Study on Fault Current Characteristics and current limiting method of Plug-In Devices in VSC-DC Distribution System," *Energies*, vol. 12, no. 3159, 2019.

[81] H. A. B. Siddique *et al.*, "Comparison of modular multilevel and neutral-point-clamped converters for medium-voltage grid-connected applications," in *2016 IEEE*

Int. Conf. on Renewable Energy Research and Applications (ICRERA), Birmingham, 2016, pp. 297–304.

[82] J. Xu, P. Zhao, and C. Zhao, "Reliability Analysis and Redundancy Configuration of MMC with Hybrid Submodule Topologies," *IEEE Transactions on Power Electronics*, vol. 31, no. 4, pp. 2720–2729, 2016.

[83] P. Tu, S. Yang, and P. Wang, "Reliability- and Cost-Based Redundancy Design for Modular Multilevel Converter," *IEEE Transactions on Power Electronics*, vol. 66, no. 3, pp. 2333–2342, 2019.

[84] H. J. Bahirat, B. A. Mork, and H. K. Høidalen, "Comparison of wind farm topologies for offshore applications," in *2012 IEEE Power and Energy Society General Meeting*, 2012, pp. 1–8.

[85] H. J. Bahirat, G. H. Kjølle, B. A. Mork, and H. K. Høidalen, "Reliability assessment of dc wind farms," in *2012 IEEE Power and Energy Society General Meeting*, 2012, pp. 1–7.

[86] S. Chuangpishit, A. Tabesh, Z. Moradi-Shahrbabak, and M. Saeedifard, "Topology design for collector systems of offshore wind farms with pure dc power systems," *IEEE Transactions on Industrial Electronics*, vol. 61, no. 1, pp. 320–328, 2014.

[87] S. Sulaeman, M. Benidris, J. Mitra, and C. Singh, "A wind farm reliability model considering both wind variability and turbine forced outages," *IEEE Transactions on Sustainable Energy*, vol. 8, no. 2, pp. 629–637, 2017.

[88] M. Banzo and A. Ramos, "Stochastic optimization model for electric power system planning of offshore wind farms," *IEEE Transactions on Power Systems*, vol. 26, no. 3, pp. 1338–1348, 2011.

[89] S. Lumbreras and A. Ramos, "Optimal design of the electrical layout of an offshore wind farm applying decomposition strategies," *IEEE Transactions on Power Systems*, vol. 28, no. 2, pp. 1434–1441, 2013.

[90] O. Dahmani, S. Bourguet, M. Machmoum, P. Guerin, and P. Rhein, "Reliability analysis of the collection system of an offshore wind farm," in *2014 Ninth International Conference on Ecological Vehicles and Renewable Energies (EVER)*, 2014, pp. 1–6.

[91] L. He, M. Zhou, F. Guo, and H. Yi, "Comparative study on reliability of wind farm collector systems," in *International Conference on Renewable Power Generation (RPG 2015)*, 2015, pp. 1–5.

[92] H. Chao, B. Hu, K. Xie, H. Tai, J. Yan, and Y. Li, "A sequential mcmc model for reliability evaluation of offshore wind farms considering severe weather conditions," *IEEE Access*, vol. 7, pp. 132 552–132 562, 2019.

[93] Y. Wu, P. Su, Y. Su, T. Wu, and W. Tan, "Economics- and reliability-based design for an offshore wind farm," *IEEE Transactions on Industry Applications*, vol. 53, no. 6, pp. 5139–5149, 2017.

[94] O. Dahmani, S. Bourguet, M. Machmoum, P. Guerin, P. Rhein, and L. Josse, "Optimization and reliability evaluation of an offshore wind farm architecture," *IEEE Transactions on Sustainable Energy*, vol. 8, no. 2, pp. 542–550, 2017.

[95] Y. Guo, H. Gao, and Q. Wu, "A combined reliability model of vsc-hvdc connected offshore wind farms considering wind speed correlation," *IEEE Transactions on Sustainable Energy*, vol. 8, no. 4, pp. 1637–1646, 2017.

[96] N. Barberis Negra, O. Holmstrom, B. Bak-Jensen, and P. Sorensen, "Aspects of relevance in offshore wind farm reliability assessment," *IEEE Transactions on Energy Conversion*, vol. 22, no. 1, pp. 159–166, 2007.

[97] C. MacIver, K. R. W. Bell, and D. P. Nedić, "A reliability evaluation of offshore hvdc grid configuration options," *IEEE Transactions on Power Delivery*, vol. 31, no. 2, pp. 810–819, 2016.

[98] F. Castro Sayas and R. N. Allan, "Generation availability assessment of wind farms," *IEE Proceedings - Generation, Transmission and Distribution*, vol. 143, no. 5, pp. 507–518, 1996.

[99] H. Kim, C. Singh, and A. Sprintson, "Simulation and estimation of reliability in a wind farm considering the wake effect," *IEEE Transactions on Sustainable Energy*, vol. 3, no. 2, pp. 274–282, 2012.

[100] B. Wang *et al.*, "An Analytical Approach to Evaluate the Reliability of Offshore Wind Power Plants Considering Environmental Impact," *IEEE Transactions on Sustainable Energy*, vol. 9, no. 1, pp. 249–260, 2018.

[101] A. S. Dobakhshari and M. Fotuhi-Firuzabad, "A reliability model of large wind farms for power system adequacy studies," *IEEE Transactions on Energy Conversion*, vol. 24, no. 3, pp. 792–801, 2009.

[102] R. Billinton, B. Karki, R. Karki, and G. Ramakrishna, "Unit commitment risk analysis of wind integrated power systems," *IEEE Transactions on Power Systems*, vol. 24, no. 2, pp. 930–939, 2009.

[103] C. Bouty, S. Schafhirt, L. Ziegler, and M. Muskulus, "Lifetime extension for large offshore wind farms: Is it enough to reassess fatigue for selected design positions?" in *14th Deep Sea Offshore Wind R&D Conference, EERA DeepWind'2017*, vol. 137, 2017, pp. 523–530.

[104] S. Ye, D. Zhou, and F. Blaabjerg, "Component-level reliability assessment of a direct-drive pmsg wind power converter considering long-term and short-term thermal cycles," in *2020 22nd European Conference on Power Electronics and Applications (EPE'20 ECCE Europe)*, 2020, pp. P.1–P.10.

[105] "Offshore wind data," Library Catalog: Ørsted.com. [Online]. Available: https://orsted.com/en/our-business/offshore-wind/wind-data

[106] R. Bayerer, T. Herrmann, T. Licht, J. Lutz, and M. Feller, "Model for power cycling lifetime of igbt modules - various factors influencing lifetime," in *5th International Conference on Integrated Power Electronics Systems*, 2008, pp. 1–6.

[107] R. Schnell, M. Bayer, and S. Geissmann, "Thermal design and temperature ratings of IGBT modules," ASEA Brown Boveri, Zurich, Switzerland, ABB Application Note, 5SYA 2093-00, 2011.

[108] A. Fatemi and L. Yang, "Cumulative fatigue damage and life prediction theories: a survey of the state of the art for homogeneous materials," *International Journal of Fatigue*, vol. 20, no. 1, pp. 9–34, 1998.

[109] J. Guo *et al.*, "Reliability Analysis of MMCs Considering Submodule Designs with Individual or Series-Operated IGBTs," *IEEE Transactions on Power Delivery*, vol. 32, no. 2, pp. 666–677, 2017.

[110] U. Choi, F. Blaabjerg, and K. Lee, "Study and Handling Methods of power IGBT Module Failures in Power Electronic Converter Systems," *IEEE Transactions on Power Electronics*, vol. 30, no. 5, pp. 2517–2533, 2015.

[111] J. Yu *et al.*, "Initial designs for angle-dc project: challenges converting existing ac cable and overhead line to dc operation," *CIRED - Open Access Proceedings Journal*, vol. 2017, no. 1, pp. 2374–2378, 2017.

[112] T. Joseph *et al.*, "Dynamic control of MVDC link embedded in distribution network:—Case study on ANGLE-DC," in *2017 IEEE Conference on Energy Internet and Energy System Integration*, 2017, pp. 1–6.

[113] J. Peralta, H. Saad, S. Dennetiere, J. Mahseredjian, and S. Nguefeu, "Detailed and Averaged Models for a 401-Level MMC–HVDC System," *IEEE Transactions on Power Delivery*, vol. 27, no. 3, pp. 1501–1508, 2012.

[114] J. Wylie, "Reliability analysis of modular multi-level converters for high and medium voltage applications," Ph.D. dissertation, Imperial College London, 2019.

[115] T. Joseph *et al.*, "Asset Management Strategies for Power Electronic Converters in Transmission Networks: Application to HVdc and FACTS Devices," *IEEE Access*, vol. 6, pp. 21 084–21 102, 2018.

[116] D. Rock, "Guidance on the offshore transmission owner licence for tender round 5 (TR5)," *Ofgem*, pp. 1–39, 2017.

[117] N. S. Dhaliwal *et al.*, "CIGRE WG B4.04: Converter transformer failure survey results from 2003 to 2012," CIGRE TB-617, Tech. Rep., 2015.

[118] Power semiconductors. Semiconductors Product Catalog 2020. [Online]. Available: https://new.abb.com/semiconductors

[119] Infineon, "Technical Information FZ1200r33he3," Infineon, Tech. Rep., 2013. [Online]. Available: https://www.infineon.com/dgdl/InfineonFZ1200R33HE3DSv0301EN.pdf?fileId=db3a304327b8975001283eeed2944021

[120] EPCOS, "B25750h2448k004 Details - TDK — Datasheets," TDK, Tech. Rep., 2013. [Online]. Available: https://www.datasheets.com/details/B25750H2448K004-TDK-54457966

[121] *PLECS- the Simulation Platform for Power Electronic Systems*, 4th ed., Plexim, Plexim, GmbH, Zurich,Switzerland, 2019.

[122] "Anholt Offshore Wind Farm," Accessed: Aug. 03, 2020. [Online]. Available: https://en.wikipedia.org/wiki/Anholt_Offshore_Wind_Farm

[123] Electronic Components. Mouser Electronics, United Kingdom. [Online]. Available: https://www.mouser.co.uk

[124] "Summer Outlook 2019," National Grid, UK, Tech. Rep., 2019. [Online]. Available: https://www.nationalgrid.com/document/111936

[125] H. Liu, M. S. A. Dahidah, J. Yu, R. T. Naayagi, and M. Armstrong, "Design and control of unidirectional dc–dc modular multilevel converter for offshore dc collection point: Theoretical analysis and experimental validation," *IEEE Transactions on Power Electronics*, vol. 34, no. 6, pp. 5191–5208, 2019.

[126] S. P. Engel, M. Stieneker, N. Soltau, S. Rabiee, H. Stagge, and R. W. De Doncker, "Comparison of the modular multilevel dc converter and the dual-active bridge converter for power conversion in hvdc and mvdc grids," *IEEE Transactions on Power Electronics*, vol. 30, no. 1, pp. 124–137, 2015.

[127] P. Lakshmanan, J. Guo, and J. Liang, "Energy curtailment of dc series–parallel connected offshore wind farms," *IET Renewable Power Generation*, vol. 12, no. 5, pp. 576–584, 2018.

[128] J. B. Leite, J. R. S. Mantovani, T. Dokic, Q. Yan, P.-C. Chen, and M. Kezunovic, "Resiliency assessment in distribution networks using gis-based predictive risk analytics," *IEEE Transactions on Power Systems*, vol. 34, no. 6, pp. 4249–4257, 2019.

[129] G. Abeynayake, T. Van Acker, D. Van Hertem, and J. Liang, "Analytical model for availability assessment of large-scale offshore wind farms including their collector system," *IEEE Transactions on Sustainable Energy*, pp. 1–1, 2021.

[130] M. Zhao, Z. Chen, and F. Blaabjerg, "Generation ratio availability assessment of electrical systems for offshore wind farms," *IEEE Transactions on Energy Conversion*, vol. 22, no. 3, pp. 755–763, 2007.

[131] "CATAPULT Offshore Renewable Energy," *ORE CATAPULT, UK*, 2019. [Online]. Available: https://guidetoanoffshorewind-farm.com/wind-farm-costs

[132] G. Stamatiou, "Techno-Economical Analysis of DC Collection Grid for Offshore Wind Parks," Master's thesis, University of Nottingham, Nottingham, UK, 2010.

[133] S. Lundberg, "Performance comparison of wind park configurations," Department of Electric Power Engineering, Chalmers University of Technology, Sweden, Tech. Rep., 2003.

[134] M. de Prada, L. Igualada, C. Corchero, O. Gomis-Bellmunt, and A. Sumper, "Hybrid ac-dc offshore wind power plant topology: Optimal design," *IEEE Transactions on Power Systems*, vol. 30, no. 4, pp. 1868–1876, 2015.

[135] "Ørsted Offshore Operational Data Sharing: Anholt and Westermost Rough LiDAR Data Documentation." [Online]. Available: https://orsted.com/en/our-business/offshore-wind/wind-data

[136] "MHI Vestas Offshore V164-9.5 MW." [Online]. Available: https://en.wind-turbine-models.com/turbines/1605-mhi-vestas-offshore-v164-9.5-mw

[137] "MHI Vestas Offshore V164-8.0 MW." [Online]. Available: https://en.wind-turbine-models.com/turbines/1419-mhi-vestas-offshore-v164-8.0-mw

[138] M. Saeki, I. Tobinaga, J. Sugino, and T. Shiraishi, "Development of 5-mw offshore wind turbine and 2-mw floating offshore wind turbine technology," *Hitachi Review*, vol. 63, pp. 414–421, 09 2014.

[139] G. Abeynayake, G. Li, T. Joseph, J. Liang, and W. Ming, "Reliability and cost-oriented analysis, comparison and selection of multi-level mvdc converters," *IEEE Transactions on Power Delivery*, pp. 1–1, 2021.

[140] S. Bala, J. Pan, D. Das, O. Apeldoorn, and S. Ebner, "Lowering failure rates and improving serviceability in offshore wind conversion-collection systems," in *2012 IEEE Power Electronics and Machines in Wind Applications*, 2012, pp. 1–7.

[141] A. Sannino, H. Breder, and E. K. Nielsen, "Reliability of collection grids for large offshore wind parks," in *2006 International Conference on Probabilistic Methods Applied to Power Systems*, 2006, pp. 1–6.

[142] O. Holmstrøm, "Survey of reliability of large offshore wind farms part 1: Reliability of state-of-the-art wind farms," Project Upwind, Tech. Rep., 2007.

[143] R. A. Howard, *Dynamic Probabilistic Systems: Volume I*, 2nd ed. Mineola, NY: Dover Publications, Inc., 1971.

[144] S. Meyn and R. Tweedie, "Markov Chains and Stochastic Stability," Cambridge University Press, 2009.

[145] B. Kerres, K. Fischer, and R. Madlener, "Economic evaluation of maintenance strategies for wind turbines: a stochastic analysis," *IET Renewable Power Generation*, vol. 9, no. 7, pp. 766–774, 2015.

[146] K. Fischer, F. Besnard, and L. Bertling, "Reliability-centered maintenance for wind turbines based on statistical analysis and practical experience," *IEEE Transactions on Energy Conversion*, vol. 27, no. 1, pp. 184–195, 2012.

[147] J. Carroll, A. McDonald, and D. McMillan, "Reliability comparison of wind turbines with DFIG and PMG drive trains," *IEEE Transactions on Energy Conversion*, vol. 30, no. 2, pp. 663–670, 2015.

[148] J. Carroll, A. McDonald, I. Dinwoodie, D. McMillan, M. Revie, and I. Lazakis, "Availability, operation and maintenance costs of offshore wind turbines with different drive train configurations," *Wind Energy*, vol. 20, pp. 361–378, 2017.

[149] J. J. B. Gill, "Forecasting underground electric cable faults using the Crow AMSAA model," *Asset Management & Maintenance Journal*, vol. 24, p. 40, 2011.

[150] O. Yevkin and V. Krivtsov, "Comparative analysis of optimal maintenance policies under general repair with underlying weibull distributions," *IEEE Transactions on Reliability*, vol. 62, no. 1, pp. 82–91, 2013.

[151] M. Buhari, V. Levi, and S. K. E. Awadallah, "Modelling of ageing distribution cable for replacement planning," *IEEE Transactions on Power Systems*, vol. 31, no. 5, pp. 3996–4004, 2016.

[152] Z. Tang, W. Zhou, J. Zhao, D. Wang, L. Zhang, H. Liu, Y. Yang, and C. Zhou, "Comparison of the weibull and the Crow-AMSAA Model in prediction of early cable joint failures," *IEEE Transactions on Power Delivery*, vol. 30, no. 6, pp. 2410–2418, 2015.

[153] R. Billinton and P. Alukal, "Availability analysis in a cable transmission system with repair restrictions," *IEEE Transactions on Power Systems*, vol. 3, no. 3, pp. 872–878, 1988.

[154] L. Cheng, H. Feng, Y. Chang, and C. Singh, "Reliability analysis of HTS cable systems," *IEEE Transactions on Power Delivery*, vol. 30, no. 3, pp. 1251–1259, 2015.

[155] A. Lisnianski, I. Frenkel, and Y. Ding, *Multi-State System Reliability Analysis and Optimization for Engineers and Industrial Managers.* London: Springer, 2010.

[156] J. Bezanson, A. Edelman, S. Karpinski, and V. B. Shah, "Julia: A fresh approach to numerical computing," *SIAM Review*, vol. 59, no. 1, pp. 65–98, 2017.

[157] O. Siirto, J. Vepsäläinen, A. Hämäläinen, and M. Loukkalahti, "Improving reliability by focusing on the quality and condition of medium-voltage cables and cable accessories," *CIRED - Open Access Proceedings Journal*, vol. 2017, no. 1, pp. 229–232, 2017.

[158] S. Lumbreras, A. Ramos, and P. Sánchez-Martin, "Offshore wind farm electrical design using a hybrid of ordinal optimization and mixed-integer programming," *Wind Energy*, vol. 18, no. 12, pp. 2241–2258, 2015.

[159] C. Smidt, "National Report: Denmark Status for 2017," Danish Utility Regulator, Denmark, Tech. Rep., 2018.

[160] J. Campos, T. Serebrisky, and A. Suárez-Alemán, "Time Goes By: Recent Developments on the Theory and Practice of the Discount Rate," Inter-American Development Bank, Tech. Rep., Sep. 2015.